ERDC/GSL TR-16-11

Geotechnical and Structures Laboratory

US Army Corps
of Engineers®
Engineer Research and
Development Center

ERDC
INNOVATIVE SOLUTIONS
for a safer, better world

Protocol for Cohesionless Sample Preparation for Physical Experimentation

Oliver-Denzil S. Taylor, Woodman W. Berry,
Katherine E. Winters, Wesley R. Rowland, Mark D. Antwine,
and Amy L. Cunningham

May 2016

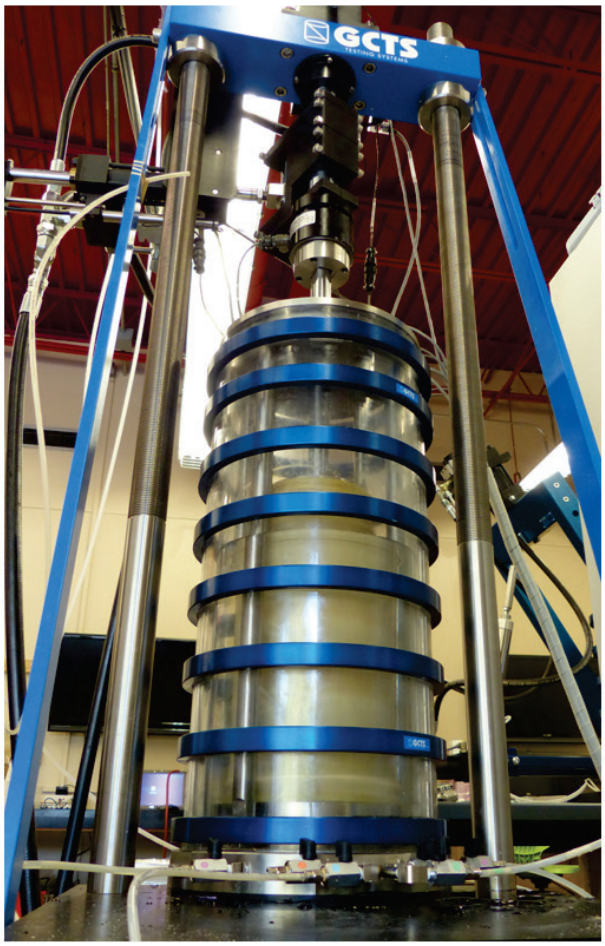

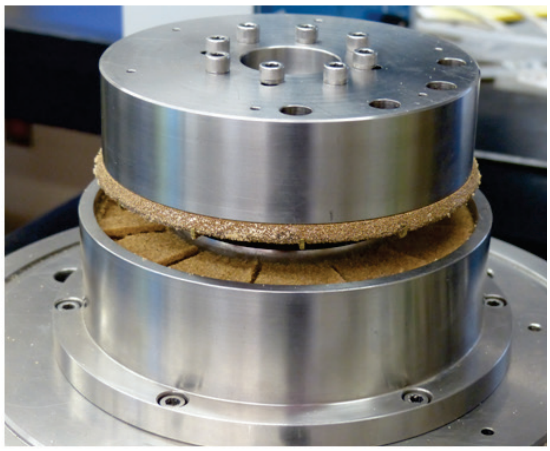

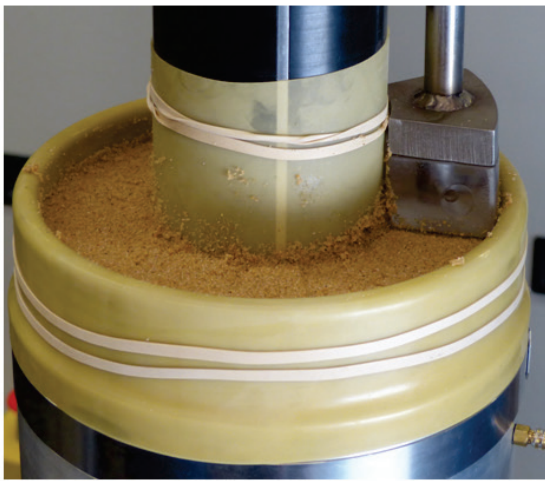

The U.S. Army Engineer Research and Development Center (ERDC) solves the nation's toughest engineering and environmental challenges. ERDC develops innovative solutions in civil and military engineering, geospatial sciences, water resources, and environmental sciences for the Army, the Department of Defense, civilian agencies, and our nation's public good. Find out more at www.erdc.usace.army.mil.

To search for other technical reports published by ERDC, visit the ERDC online library at http://acwc.sdp.sirsi.net/client/default.

ERDC/GSL TR-16-11
May 2016

Protocol for Cohesionless Sample Preparation for Physical Experimentation

Oliver-Denzil S. Taylor, Woodman W. Berry, Katherine E. Winters, Wesley R. Rowland, Mark D. Antwine, and Amy L. Cunningham

Geotechnical and Structures Laboratory
U.S. Army Engineer Research and Development Center
3909 Halls Ferry Road
Vicksburg, MS 39180-6199

Final report

Prepared for U.S. Army Corps of Engineers
Washington, DC 20314-1000

Abstract

The construction method and applied energy significantly influence sample behavior and strength characteristics; therefore, an energy-based sample reconstitution method is derived wherein uncertainties and laboratory scatter associated with soil fabric-behavior variance during sample preparation are mitigated. Samples of two different sands prepared using relative density methods resulted in different strengths at the point of failure; however, when prepared to the same normalized density, the same strength at the point of failure was observed. This suggests that normalized density could be a useful approach for laboratory investigation of cohesionless materials.

The procedure developed controls the three principal components of sample reconstitution, mass/type of material, quantity of water, and quantity/means of applied energy. All other properties, e.g., density, void ratio, etc., are products of sample preparation. Therefore, by controlling the three principal variables in sample preparation, high sample repeatability can be readily achieved wherein comparable analysis between different laboratory tests' results can be made by ensuring a comparable soil fabric prior to laboratory testing.

Contents

Figures and Tables

Figures

Tables

Preface

This study was conducted for the U.S. Army Corps of Engineers under the Integrated Protection Against Advanced Threats (IPAAT) program.

The work was performed by the Structural Engineering Branch (GSS) of the Geosciences and Structures Division (GS), U.S. Army Engineer Research and Development Center, Geotechnical and Structures Laboratory (ERDC-GSL). At the time of publication, Charles W. Ertle was Chief, CEERD-GSS; Dr. Amy Bednar was Acting Chief, CEERD-GS; and Dr. Michael D. Sharp, CEERD-GZT, was the Technical Director for Civil Works Infrastructure Research. The Deputy Director of ERDC-GSL was Dr. William P. Grogan, and the Director was Bartley P. Durst.

COL Bryan S. Green was the Commander of ERDC, and Dr. Jeffery P. Holland was the Director.

Unit Conversion Factors

English - Multiply	By	To Obtain - Metric
cubic feet	0.02831685	cubic meters
cubic inches	1.6387064 E-05	cubic meters
cubic yards	0.7645549	cubic meters
feet	0.3048	meters
pounds (force) per foot	14.59390	newtons per meter
pounds (force) per inch	175.1268	newtons per meter
pounds (mass)	0.45359237	kilograms
pounds (mass) per cubic foot	16.01846	kilograms per cubic meter
pounds (mass) per cubic inch	2.757990 E+04	kilograms per cubic meter
yards	0.9144	meters

1 Introduction

The focus of this research is to develop a standardized protocol for specimen preparation that will enable the use of soil strength curves based on expedient field classification testing (e.g., grain-size analyses) using a normalization approach to sample preparation that replaces the common relative density method of evaluating the strength of soils. This research is centered around using an equivalent energy to prepare consistent, highly repeatable test samples instead of relying on relative density methods. The following laboratory tests were used to compare the strength of cohesionless sands using the normalization approach to building partially saturated test specimens, i.e., Monotonic Triaxial (axial loading), Monotonic Simple Shear (shear strength), Ring Shear (anisotropic strength), and Hollow Core (isotropic strength).

The first order of influence in identifying similar cohesionless materials is grain size. While the sieve analysis verifies that the two test sands, SDA and SDB, are cohesionless materials and the grain-size distributions of the two sands are similar, there are enough physical property differences wherein density-based normalization does not yield comparable behavior (Taylor et al. 2012).

Presented herein is the research to show that two similar materials can obtain comparable continuum behavior in laboratory settings, thereby reducing the reliance on soil-specific sampling and testing. In addition, the concepts presented can be applied to the preparation and analysis of reconstituted test specimens using other cohesionless materials.

The generalized material strength curves developed from this research will make it possible to rapidly integrate indigenous (local) materials into force protection measures and produce cost savings analyses without the need for extensive laboratory testing, soil sampling, and/or engineered fill materials. Additionally, these curves provide a basis for expedient engineering designs and assessments as to the local soil capacity to withstand additional foundation loading from structural hardening and/or blast loadings.

1.1 Background

Extensive testing has concluded that specimen preparation has a significant impact on soil specimen test results for a variety of test conditions. Ladd (1974, 1977), Mulilis et al. (1977), and others determined the manner in which a laboratory test specimen is reconstituted can greatly influence the behavior of the material. Ladd (1977) attributed these differences due to differences in particle orientations and contact, differences in void ratio, and segregation of particles.

Mulilis et al. (1978) investigated cyclic triaxial strength of Monterey No. 0 sand with varying construction techniques and varying load forms. They found that cyclic strength of moist-rodded specimens was 38% to 58% greater than that of dry-rodded specimens, and an increase in relative density caused an increase in strength. The authors preferred moist tamping for closer density control.

Bradshaw and Baxter (2007) proposed a modified moist-tamping method for laboratory preparation of silty samples for liquefaction testing. Uniform density was achieved by varying the compactive energy applied to each layer during construction. Taylor (2011) showed that a blended (engineered) silt can be prepared in a standardized manner such that the engineered material behaves identically to three difference in-situ silts.

Recently, several studies have further explored sample preparation methods for non-cyclic testing in order to ensure that laboratory-prepared specimens accurately represent in-service conditions. Sandrekarimi and Olsen (2012) studied ring-shear tests on three sands prepared using moist tamping and air pluviation. They found a wide variation in initial behavior, but little difference in critical-state behavior. Wanatowski and Chu (2008) compared moist-tamped and water-sedimented sand in plane-strain conditions, noting that under drained conditions, moist-tamped specimens behaved more contractively although both types reached the same failure line. Huang et al. (2015) conducted triaxial testing on drained and undrained loose and medium dense sands at 10-kPa and 5-kPa confining pressures. They concluded that loose sands under low pressures behave similarly to dense sands under conventional confining pressures.

Throughout the literature, it is clear that sample preparation methods significantly impact testing results and that clear, consistent, repeatable preparation methods are essential in order to yield accurate results.

1.2 Overview

The purpose of this research is to show that two similar materials can obtain comparable continuum behavior, thereby reducing the reliance on soil-specific sampling and testing. The purpose of this work is to show that energy and reconstitution saturation, referred to herein as S_R, are the governing criteria for sample preparation and that two similar soil types reconstituted with the same energy and saturation have the same continuum behavior.

1.2.1 Chapter 2 Material Index Testing

Chapter 2 begins with an explanation of relative density, which relies on calculations of minimum and maximum void ratio and relative compaction, which compares field compaction to a laboratory maximum density. Gradation charts for the two materials used in this study (SDA and SDB) are presented; both are poorly graded sands (SP) with a specific gravity of 2.70. The standard Proctor hammer caused punching shear failure when used to compact this soil, so a new hammer was developed that allowed the hammer base, rammer weight, and drop height to be adjusted as needed to effectively compact the soil. We then review the calculation of compactive energy based on rammer weight, drop height, blows per layer, number of layers, and volume of the specimen. The hammer must be moved in an even pattern around the specimen in order to ensure even compaction. As the energy calculation is dependent on the volume of the compacted material, achieving the target volume is critical. Finally, sample compaction curves for SDA at 200 kJ/m^3 and SDB at 800 kJ/m^3 are presented.

1.2.2 Chapter 3 Modified Sample Preparation Procedure for Cohesionless Soils

Chapter 3 addresses modified sample preparation procedures for cohesionless soils using a 152-mm (nominal 6-in.) diameter, 300-mm (nominal 12-in.) tall triaxial test specimen. First, the reconstitution saturation, Sr, was chosen as 24%, dryer than both the optimal saturations of SDA and SDB but wetter than the moisture contents at which bulking was observed. Normalized densities were then calculated based on the work with silt in Taylor et al. (2012). The sample preparation protocol is then created, specifying the amounts of dry soil and water to mix, the

number of layers in which to build the specimen, blows per layer, rammer weight, drop height, and diameter of hammer base.

1.2.3 Chapter 4 Adjustments for Specimen Geometry

Chapter 4 covers adjustments to specimen preparation procedures for each of the different apparatuses, including adjustments for non-circular compaction hammers. Since the energy applied to the soil at any compaction effort is a function of the manner to which it is applied, the ratio of the coverage area of the application instrument, and the spatial area of the material to which the energy is being applied, corrections to energy calculations are required using an adjustment factor. For samples constructed in one layer, the adjustment factor, ψ, is a function of the circumference of the hammer edges that are in contact with the rigid mold. The higher the ψ, the less the equivalent energy has to be adjusted. In other words, for the lower compactive energies, the reflective energy is much less than with the higher compactive energies.

1.2.4 Chapter 5 Testing Apparatus Description

Chapter 5 contains descriptions of each testing apparatus used for this research and photographs of the laboratory equipment, namely the triaxial testing, simple shear, ring shear, and hollow-core testing devices. Triaxial testing for this study was performed using the USTX-2000 and the HCA-150 devices manufactured by GCTS. Specimens were then subject to an axial strain of 0.25% per minute and confining pressure of 100 kPa, and the maximum deviator stress was recorded. Simple shear testing was performed using the GCTS Simple Shear System SSH-100. Specimens were subject to a shear strain of 0.25% per minute and confining pressure of 100 kPa. The shear stress corresponding to 3.50% shear strain was used as the failure stress. Ring shear testing was performed using the GCTS Residual-Ring Shear System SRS-150 in order to measure the peak torsional strength. Normal loads were applied via the top plate. Hollow Core testing for this study was performed using the HCA-150 Dynamic Hollow Cylinder Testing (HCA) System by GCTS. Specimens were tested in torsion with confining pressure of 100 kPa, and the torsional shear strength was recorded.

1.2.5 Chapter 6 Laboratory Testing Results and Observations

Chapter 6 presents results from laboratory testing of SDA and SDB for triaxial shear (ICD_{TX}), simple shear (ICD_{SS}), hollow core isotropic torsional consolidation and shear (ICD_{HC}), monotonic ring shear (ACD_{RS}), and cyclic ring shear ($ACD_{CYC,RS}$) tests. For ICD_{TX} testing SDA and SDB show a strong correlation; however, there is no tangible increase in peak strength of either SDA or SDB past 1150 kJ/m^3 of compactive effort. This suggests that there exists an ultimate fabric strength of these SP sands and that energy applied in excess of this limit is unnecessary, resulting in an unstable soil continuum.

The ACD_{RS} results show both SDA and SDB normalized to within +/- 5 kPa of each other for a given target energy. Additionally, irrespective of compactive effort the torsional strength of these sands are within +/- 10 kPa indicating that the torsional or shear resistance of SP material is more defined by the confining pressure than the energy applied or internal fabric. Each $ACD_{CYC,RS}$ test sample performed nearly identically, confirming that the protocol presented herein is applicable to both monotonic and cyclic loading investigations.

ICD_{HC} tests were conducted on SDA and SDB using a compactive effort of 200 kJ/m^3 via the normalized density approach and behaved nearly identical in all cases both in terms of peak strength and stress-strain behavior. ICD_{SS} results are comparable to the ICD_{HC} tests in terms of both behavior (strain-softening) and peak shear strength.

1.2.6 Chapter 7 Conclusions

Chapter 7 begins with a summary of findings; namely, that the data presented herein show that two similar materials can obtain comparable continuum behavior in laboratory settings when constructed following normalized density/relative energy procedures. This reduces reliance on soil-specific sampling and testing. In addition, the concepts presented can be applied to the preparation and analysis of reconstituted test specimens using other cohesionless materials. Chapter 7 also contains a summary of steps needed to construct a sample following the methods presented in this report.

1.2.7 Chapter 8 References

Chapter 8 contains the references cited within this technical report.

1.2.8 Appendices

The Appendices contain a listing of non-standard terminology and test results for each of the tests referenced in this report.

2 Material Index Testing

2.1 Relative density and relative compaction

Relative density and void ratios have been used to compare materials and specimens in several previous works addressing sample preparation methods (DeGregorio 1990; Sandrekarimi and Olson 2012). Relative density originally was approximated by field penetration resistance (Sowers and Sowers 1951). Today, relative density represents the void ratio of the specimen relative to maximum and minimum void ratios, as shown in Equation 1 and expressed as a percentage.

$$D_r = \frac{e_{max} - e}{e_{max} - e_{min}} x100 \quad (1)$$

Densities are then approximately classified as very loose for D_r less than 15%, loose for D_r 15% to 35%, medium dense for D_r 35% to 65%, dense for D_r 65% to 85%, and very dense for D_r values above 85% (Holtz et al. 2011). The maximum void ratio of the material is determined by wet or air pluviation while the minimum void ratio is determined by vibratory compaction (ASTM D4254 and ASTM D4253, respectively). However, actual sample preparation may use yet another method, e.g., dry rodding, moist tamping, etc.

Relative compaction, however, is simply the ratio of actual field dry density to maximum dry density determined in the laboratory, often using Proctor or modified Proctor procedures. Practically, this value varies between 80% and 100%. A value of about 95% is typically indicated in field construction specifications (Holtz et al. 2011).

Neither method takes into account the method for achieving a specified density, and, as previously discussed, different methods of energy application yield different soil fabric structures and therefore different loading behaviors (Mulilis et al. 1978).

2.2 Physical properties

To illustrate the importance of a standardized sample preparation method, experimentation on two different cohesionless sands, SDA and SDB, was

performed. SDA is a washed uniform, medium-to-fine beach sand, and SDB is a more well-graded sand (with respect to SDA) of the same mineralogy. The grain-size distributions were completed in accordance with ASTMC136/C136M-14. The grain-size distribution plot in Figure 1 shows 70-90% of the material is between 0.25 and 0.85 mm in diameter.

Figure 1. Grain-size distribution of SDA and SDB.

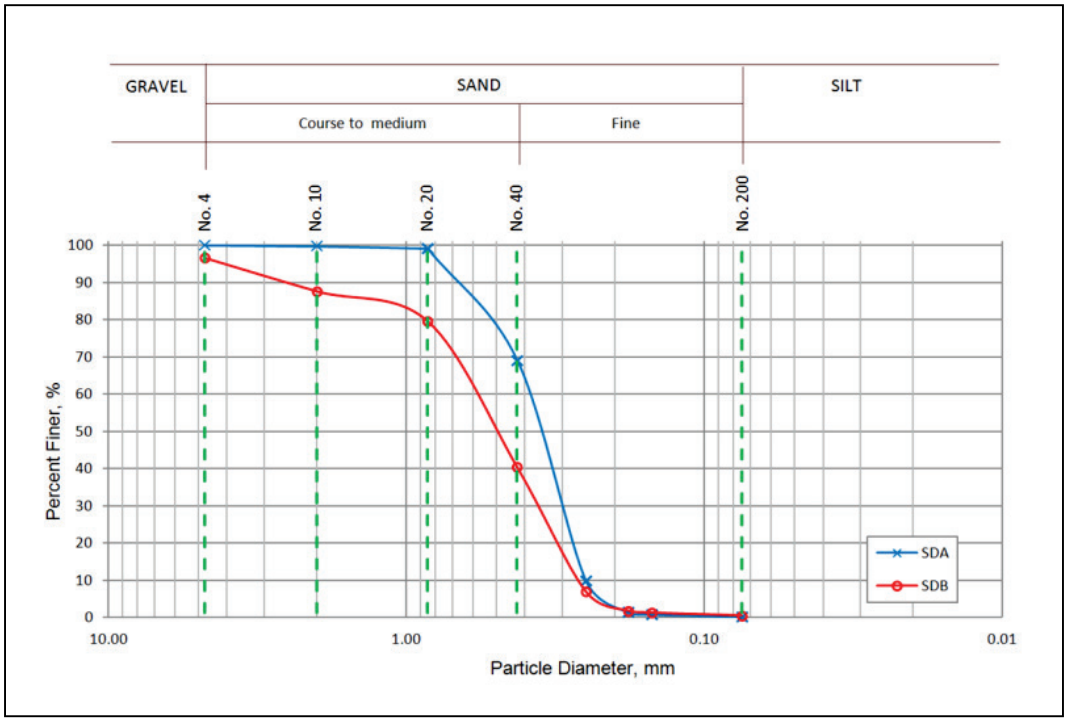

The Coefficient of Uniformity, C_u, is calculated as the grain diameter corresponding to 60-percent passing divided by the grain diameter corresponding to 10-percent passing.

$$C_u = \frac{D_{60}}{D_{10}} \tag{2}$$

A material comprised of all one grain size would have a C_u value of 1. Poorly graded soils, such as beach sands, have C_u values around 2 or 3. It is possible to have C_u values well into the hundreds for soils with a very wide range of grain sizes, such as a clay material that includes boulders (Holtz et al. 2011). To be considered a well-graded, a sand must have a C_u value greater than 6.

The Coefficient of Curvature, C_c, relates to the shape of the grain-size distribution curve by also considering the grain diameter corresponding to 30% passing.

$$C_c = \frac{D_{30}^2}{D_{10} D_{60}} \quad (3)$$

For well-graded sand, the C_c value must be greater than 1 and less than 3, which helps to identify gap-graded soils or soils where a small range of particle sizes dominate.

The Coefficients of Uniformity of SDA and SDB are 1.52 and 2.20, respectively. These small values show the dominance of the No. 40 and No. 60 sieves in the grain-size distributions. The Coefficients of Curvature for SDA and SDB are 1.12 and 0.84, respectively. Based on these results, and the determination that more than 50% of each soil passes the No. 4 sieve but less than 5% passes the No. 200 sieve, both soils can be classified as SP, or poorly graded sands, in accordance with the Unified Soil Classification System (USCS; ASTM D2487-11).

Specific gravity is the unitless ratio of the unit weight of the soil solids to the unit weight of water (1 g/cm^3). Typical soil unit weights are between 2.60 to 2.75. For SDA and SDB, the specific gravity is 2.70.

2.3 Problem with standard compaction testing for cohesionless soils

The ASTM *Standard Test Methods for Laboratory Compaction Characteristics of Soil Using Modified Effort* (ASTM D1557-12e1) defines the maximum dry unit weight as being obtained with a compactive effort of 2700 kJ/m^3. Initial compaction tests for SDA and SDB were completed in accordance with ASTM D1557-12e1 using the 152-mm diameter mold and the 44.5-N rammer to determine the optimal moisture content and the maximum dry densities for each material.

The standard 44.5-N Proctor rammer, which drops from a height of 457.2 mm, was found to cause punching shear failure instead of material compaction for the cohesionless sands (Figure 2). Figure 2A shows sand that had been moderately tamped in a single layer prior to dropping the Proctor hammer (as opposed to dropping the Proctor hammer on a loose,

un-compacted sand base) to show the magnitude of the shearing caused by the Proctor hammer (Figure 2B). Such shearing causes the development of shear bands within the sample continuum, which will alter the soil fabric resulting in non-repeatable or highly variable behavior even if sample properties, e.g., density, void ratio, etc., are similar. To reduce the fabric variability and eliminate punching shear, it was necessary to develop a modified hammer that applies the same compactive energy (2707 kJ/m^3) without inducing punching shear or micro-failure planes within the sample fabric. Thus, very dense cohesionless samples can be readily achieved without altering the moist-tamping method of energy delivery, e.g., changing to a vibratory source.

Figure 2. Punching shear failure in cohesionless sands.

(A) (B)

2.4 Modified compaction hammer

The Proctor hammer was modified with a larger striking surface (95 mm diameter vs. 50.8 mm) to spread the energy over a larger area of the specimen to reducing punching shear (Figure 3). Additionally, the striking face is separate from the falling weight and remains in contact with the surface of the specimen as the weight is raised, unlike the standard compaction hammer with a weight that is raised and dropped directly onto the surface of the specimen. The height at which the weight falls can be adjusted by securing a compression ring around the rod. The weight is allowed to free-fall onto the strike plate, and the energy is transferred through the hammer base into the soil. The amount of energy applied to

the sample with each drop can be adjusted based on the height at which the weight is dropped. There is some energy loss within the energy transfer from the strike plate to the soil but is relatively minor and considered as negligible.

Figure 3. Compaction hammer design.

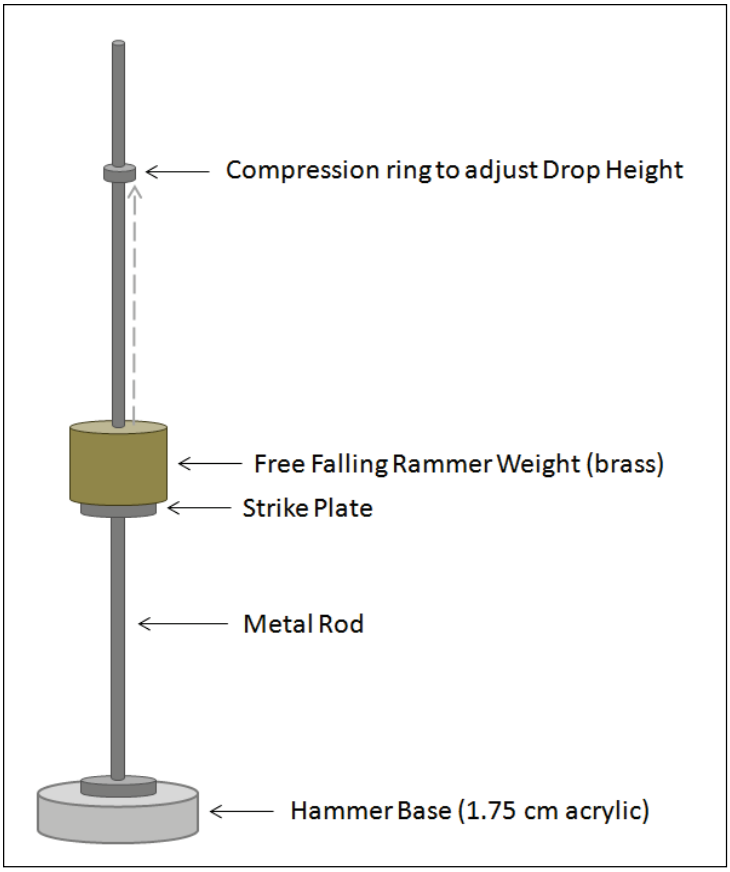

By modifying the standard Proctor hammer, fine- through coarse-grained soil specimens are constructed through identical means of energy application. Thus, differences in behavior are not by-products of preparation.

2.5 Calculating target compactive effort

The test method outlined in ASTM D1557-12e1 is used to determine values of optimum water content and modified maximum dry unit weight using a single compactive effort, 2707 kJ/m^3. For this study, however, compaction curves for a range of compactive efforts were developed, starting at 2707 kJ/m^3 and going as low as 50 kJ/m^3. Developing compaction curves from samples created using various compactive efforts allows a relationship between density and energy to be established (Peck et al. 1953).

The target energy using a 95-mm-diameter hammer base for a 152-mm-diameter mold follows the form.

$$E = \frac{W_h \; h \; b \; N}{V} \tag{4}$$

where

W_h = weight of the hammer, kN
h = the drop height of the weight, m
b = the number of blows per layer
N = the number of layers
V = the target volume of the specimen, m^3

The required energy for each of the compaction tests was obtained by varying the number of blows per layer, rammer weight, and the drop height. Because the diameter of the hammer base affects the energy concentration applied to the sample (Section 5.1 Developing *a protocol for sample preparation*), a 95-mm-diameter hammer base was used for all compaction tests, thereby establishing a reference energy for variances in sample/equipment dimensions. In accordance with ASTM D1557-12e1, each specimen is molded into five layers using the standard 15-cm (nominal) diameter Proctor mold.

By fixing the number of layers, an iterative process of calculating the appropriate combination of blows per layer, weight, and drop height is conducted to eliminate the development of internal shear bands and punching failures (Figure 4). As values for the hammer weight, blows per layer, and drop height are entered into the spreadsheet, the resulting compactive effort, or work per unit volume of soil, is calculated and displayed at the bottom of the worksheet. The values for blows per layer and exact drop height can be adjusted until the target compactive effort is obtained.

Generally, heavier weights are chosen to achieve the larger compactive energies without an excessive number of blows required per layer. To verify consistent results in this study, some compaction tests at specific energies were duplicated using different weights to obtain the same compactive energy. Once a target energy and hammer weight has been selected, the two remaining variables that must be determined iteratively are the blows per layer and the drop height.

Figure 4. Energy-controlled modified Proctor tests for (a) SDA at 200 kJ/m³ compactive effort and (b) SDB at 2700 kJ/m³ compactive effort.

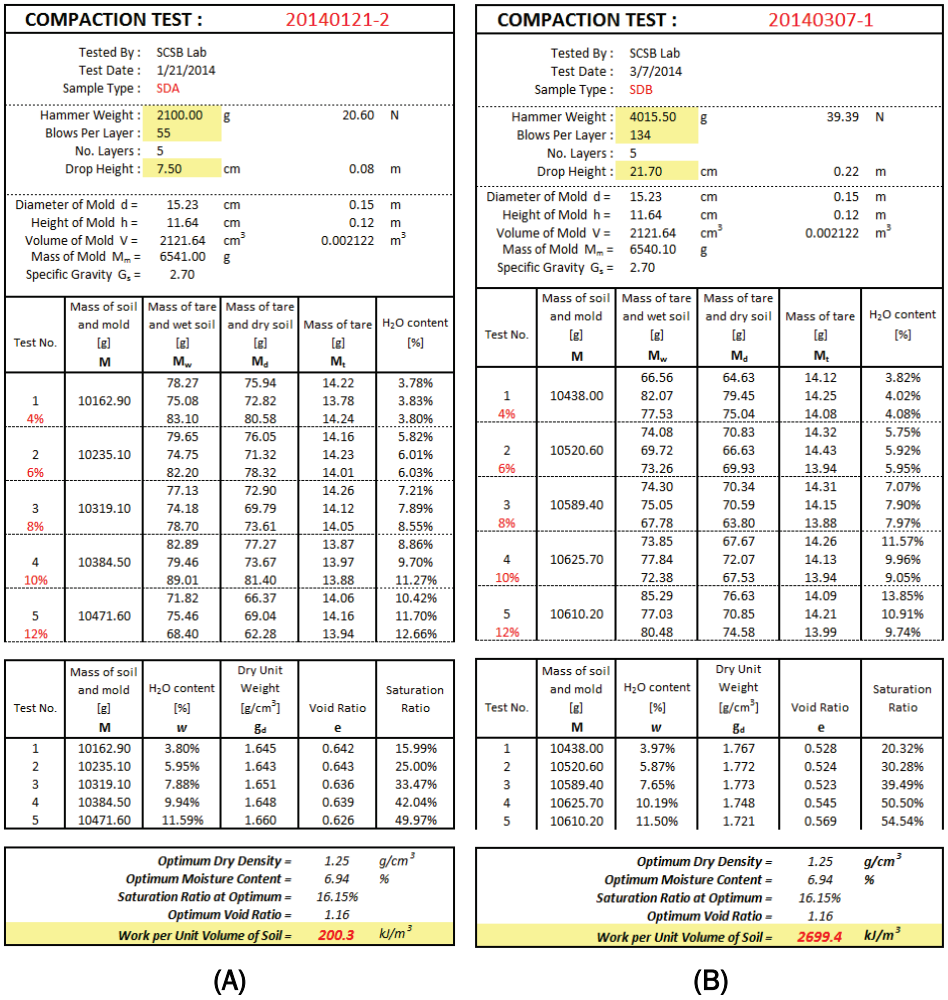

COMPACTION TEST : 20140121-2

Tested By : SCSB Lab
Test Date : 1/21/2014
Sample Type : SDA

Hammer Weight :	2100.00	g	20.60	N
Blows Per Layer :	55			
No. Layers :	5			
Drop Height :	7.50	cm	0.08	m

Diameter of Mold d =	15.23	cm	0.15	m
Height of Mold h =	11.64	cm	0.12	m
Volume of Mold V =	2121.64	cm^3	0.002122	m^3
Mass of Mold M_m =	6541.00	g		
Specific Gravity G_s =	2.70			

Test No.	Mass of soil and mold [g] M	Mass of tare and wet soil [g] M_w	Mass of tare and dry soil [g] M_d	Mass of tare [g] M_t	H_2O content [%]
		78.27	75.94	14.22	3.78%
1	10162.90	75.08	72.82	13.78	3.83%
4%		83.10	80.58	14.24	3.80%
		79.65	76.05	14.16	5.82%
2	10235.10	74.75	71.32	14.23	6.01%
6%		82.20	78.32	14.01	6.03%
		77.13	72.90	14.26	7.21%
3	10319.10	74.18	69.79	14.12	7.89%
8%		78.70	73.61	14.05	8.55%
		82.89	77.27	13.87	8.86%
4	10384.50	79.46	73.67	13.97	9.70%
10%		89.01	81.40	13.88	11.27%
		71.82	66.37	14.06	10.42%
5	10471.60	75.46	69.04	14.16	11.70%
12%		68.40	62.28	13.94	12.66%

Test No.	Mass of soil and mold [g] M	H_2O content [%] w	Dry Unit Weight [g/cm^3] g_d	Void Ratio e	Saturation Ratio
1	10162.90	3.80%	1.645	0.642	15.99%
2	10235.10	5.95%	1.643	0.643	25.00%
3	10319.10	7.88%	1.651	0.636	33.47%
4	10384.50	9.94%	1.648	0.639	42.04%
5	10471.60	11.59%	1.660	0.626	49.97%

Optimum Dry Density =	*1.25*	*g/cm^3*
Optimum Moisture Content =	*6.94*	*%*
Saturation Ratio at Optimum =	*16.15%*	
Optimum Void Ratio =	*1.16*	
Work per Unit Volume of Soil =	*200.3*	*kJ/m^3*

(A)

COMPACTION TEST : 20140307-1

Tested By : SCSB Lab
Test Date : 3/7/2014
Sample Type : SDB

Hammer Weight :	4015.50	g	39.39	N
Blows Per Layer :	134			
No. Layers :	5			
Drop Height :	21.70	cm	0.22	m

Diameter of Mold d =	15.23	cm	0.15	m
Height of Mold h =	11.64	cm	0.12	m
Volume of Mold V =	2121.64	cm^3	0.002122	m^3
Mass of Mold M_m =	6540.10	g		
Specific Gravity G_s =	2.70			

Test No.	Mass of soil and mold [g] M	Mass of tare and wet soil [g] M_w	Mass of tare and dry soil [g] M_d	Mass of tare [g] M_t	H_2O content [%]
		66.56	64.63	14.12	3.82%
1	10438.00	82.07	79.45	14.25	4.02%
4%		77.53	75.04	14.08	4.08%
		74.08	70.83	14.32	5.75%
2	10520.60	69.72	66.63	14.43	5.92%
6%		73.26	69.93	13.94	5.95%
		74.30	70.34	14.31	7.07%
3	10589.40	75.05	70.59	14.15	7.90%
8%		67.78	63.80	13.88	7.97%
		73.85	67.67	14.26	11.57%
4	10625.70	77.84	72.07	14.13	9.96%
10%		72.38	67.53	13.94	9.05%
		85.29	76.63	14.09	13.85%
5	10610.20	77.03	70.85	14.21	10.91%
12%		80.48	74.58	13.99	9.74%

Test No.	Mass of soil and mold [g] M	H_2O content [%] w	Dry Unit Weight [g/cm^3] g_d	Void Ratio e	Saturation Ratio
1	10438.00	3.97%	1.767	0.528	20.32%
2	10520.60	5.87%	1.772	0.524	30.28%
3	10589.40	7.65%	1.773	0.523	39.49%
4	10625.70	10.19%	1.748	0.545	50.50%
5	10610.20	11.50%	1.721	0.569	54.54%

Optimum Dry Density =	*1.25*	*g/cm^3*
Optimum Moisture Content =	*6.94*	*%*
Saturation Ratio at Optimum =	*16.15%*	
Optimum Void Ratio =	*1.16*	
Work per Unit Volume of Soil =	*2699.4*	*kJ/m^3*

(B)

The drop height of the rammer weight should stay as low as possible to achieve the desired range of compactive energies but also high enough to disperse the energy entirely through the layer. The maximum drop heights used for the 2100.0-g and 4015.5-g weights were 18.5 cm and 21.7 cm, respectively. These limits were chosen to avoid punching shear, bulking, or generation of shear bands, as determined by observation. For higher energies, larger weights may be chosen to minimize the number of drops required. As can be seen in Figure 4b, 134 blows per layer of the 4015.5-g weight dropped from 21.7 cm delivered the requisite 2707 kJ/m³ compactive energy. In contrast, for the 200 kJ/m³ energy sample shown in Figure 4A, only 55 blows per layer from a 2100.0 g hammer from just 7.5 cm above the sample were required.

In order to achieve adequate distribution of compactive effort over the specimen area, the rammer weight should be dropped on the specimen at least 10 times per layer. Figure 5 shows the blow pattern for the minimum number of drops per layer. For the initial round, Figure 5a, the blow pattern should be in a crisscross pattern to prevent uneven distribution of material throughout each layer and to maintain a level layers throughout the construction of the specimen. Subsequent rounds should be offset, as shown in Figure 5b. Finally, Figure 5c shows the resulting coverage after multiple rounds.

Figure 5. Blow pattern for minimum number of drops per layer.

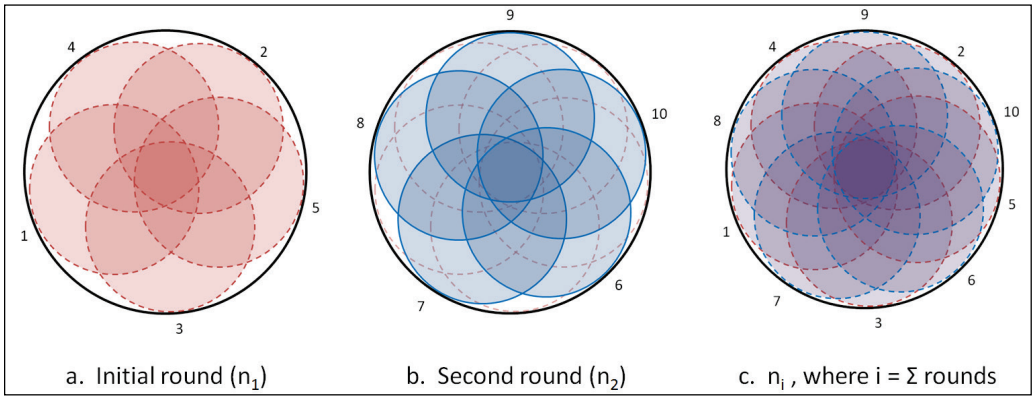

For the smaller energy tests, the drop heights will have to be adjusted to ensure that the number of drops per layer is no less than 10, always making at least two revolutions around each layer in the specimen. Higher-energy tests require more blows per layer. Approximately 300 blows per layer are required to achieve for 2700 kJ/m^3 while preventing punching shear failures when using the 2100 g weight.

2.6 Achieving target volume

Following compaction of the fifth layer, the specimen must be trimmed to create a top that is even with the mold. While it is acceptable to trim small amounts of excess material (for Standard and Modified Proctor compaction, ASTM allows up to 6 mm to be scraped off [ASTM D698-12e2 and ASTM D1557-12e1]), this practice should be minimized as much as possible. The procedure herein allows for more strict tolerances of allowable error over current ASTM standards by reducing the allowable error of +/-5% of target to +/-2% of target. The target energy applied to the specimen is calculated based on the mold volume. However, this energy is applied over the entire volume during compaction, which is the volume of the mold plus the

volume of the material scraped away. Removing some portion of this volume when scraping the top smooth can significantly impact the compactive energy calculations. For example:

> A mold with a 7.07-cm diameter and 10.22-cm height was filled with soil in three layers for a target compactive effort of 803 kJ/m^3. The amount of soil required was overestimated, so the final height was 11.10 cm or 8.8 mm above the target. Standard procedure would be to scrape off the excess soil and report the resulting density at target compactive effort of 803 kJ/m^3. However, by using the actual volume in the calculations, the real compactive effort applied to the sample was 740 kJ/m^3, only 92% of the target compactive effort.
>
> Had the sample been 6 mm above the target height, the limit for ASTM standard and modified Proctor compaction procedures, 759 kJ/m^3 of compactive effort would have been applied, or only 94.5% of the target. This is well below the 98% lower acceptable error achieved through the procedure outlined in this technical report.

Calculating the actual compactive effort by measuring precise volumes for each compaction test will yield the most accurate results. For analysis purposes, it is often desirable to conduct multiple tests at the same compactive effort. Therefore, filling the compaction mold to a consistent volume is critical.

To achieve greater accuracy in filling the compaction mold, it can be helpful to mark the inside of the mold with a permanent marker line at each target layer height. For example, to fill a mold in five layers, mark the mold at locations evenly spaced over the total height, then estimate the amount of soil needed to fill the first layer, weigh the soil added, and compact the first layer. Compare the actual height to the marked line. If the soil is below the first line, then increase the amount of soil added to the second layer. If the first layer is above the marked line, then decrease the amount of soil added to the second layer. Repeat this process with each additional layer. Ideally, this method will result in a final compacted sample within +/-2% of the target height. If the sample is between 98% and 100% of the target, a small amount of soil can be added and gently pressed into place to fill the mold. If the sample is 100% to 102% of the target height, the excess can be scraped off. If the sample is outside the

target height by more than +/- 2%, the sample should be discarded and a new sample constructed.

2.7 Compaction curves

Energy-controlled modified Proctor compaction tests were conducted using energies varying from 50–2700 kJ/m^3, each using moisture contents of 4%, 6%, 8%, 10%, and 12%. The relationship of dry density to moisture content was plotted to establish the compaction curve for each compaction test. Figure 6 and Figure 7 show two examples of the compaction curves. See Appendix B for the complete set of compaction data.

Figure 6. Compaction curve: SDA, energy = 199.8 kJ/m^3, optimal moisture content = 7.95%, and maximum dry density = 1.658 g/cm^3.

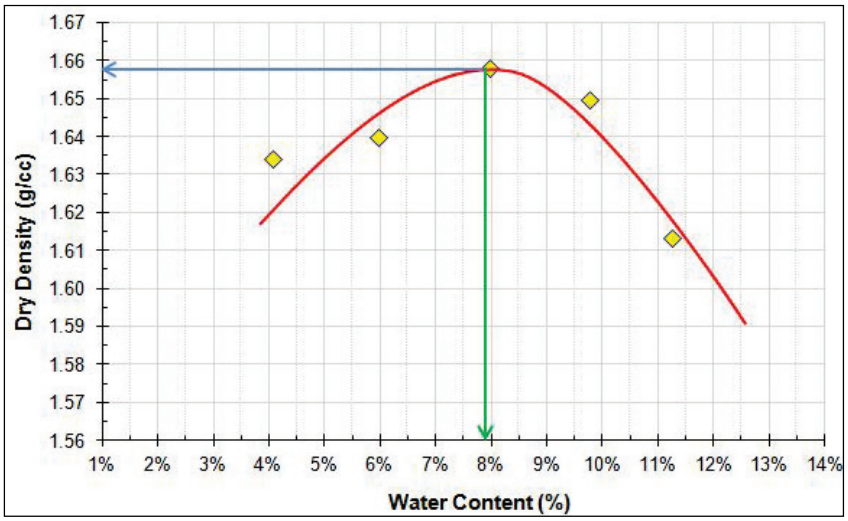

Figure 7. Compaction curve: SDB, energy = 800.6 kJ/m^3, optimal moisture content = 7.70%, and maximum dry density = 1.835 g/cm^3.

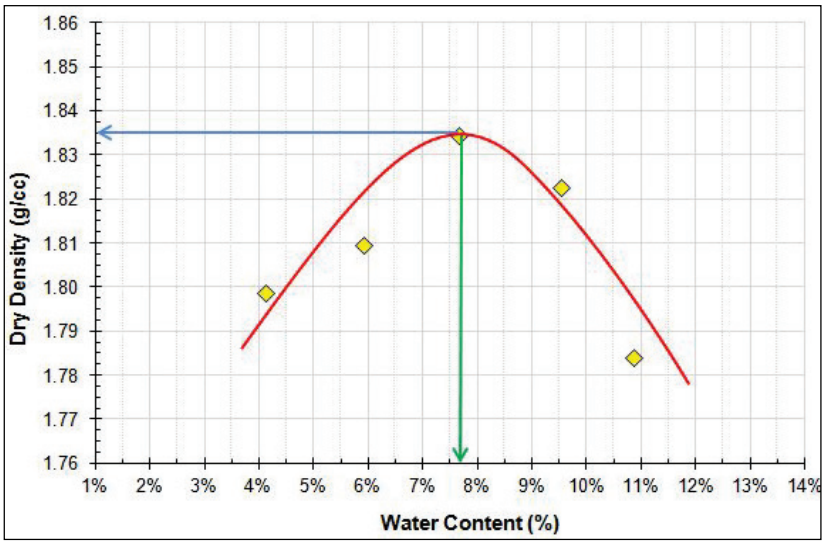

The optimal moisture content was obtained from the peak point of the compaction curve (shown with green arrows in Figures 6 and 7). The maximum dry density obtained from the compaction curves (shown with blue arrows in Figures 6 and 7) correspond with the optimal moisture content. The optimal moisture content (ω_{opt}) and maximum dry density ($\rho_{d,max}$) obtained from each compaction test, for both SDA and SDB, are listed in Table 1, columns 7 and 8. The optimal saturation at the point of maximum dry density for each compaction curve was calculated averaging 34% and 42% for SDA and SDB, respectively (Table 1, column 9).

Table 1. Summary of compaction data for SDA and SDB.

1	2	3	4	5	6	7	8	9	10	11	12
Material / Test No.	Hammer Weight grams	Blows per Layer	No. Layers	Drop Height cm	Energy kJ/m³	ω @ ρ_{opt} %	ρ_{opt} g/cc	S @ ρ_{opt} %	ρ_d @ S_R g/cc	ω @ S_R %	ρ_N %
SDA - 1	2100.0	19	5	5.62	**51.8**	7.50	1.588	28.9%	**1.585**	6.25%	0.916
SDA - 2	2100.0	34	5	6.00	**99.0**	7.75	1.636	32.2%	**1.631**	5.83%	0.942
SDA - 3	4015.5	19	5	5.62	**99.1**	7.80	1.632	32.0%	**1.627**	5.86%	0.940
SDA - 4	2100.0	55	5	7.50	**200.3**	7.85	1.651	33.4%	**1.646**	5.69%	0.951
SDA - 5	4015.5	36	5	6.00	**200.5**	7.75	1.663	33.6%	**1.661**	5.56%	0.960
SDA - 6	2100.0	50	5	15.00	**364.1**	7.50	1.670	32.8%	**1.658**	5.59%	0.958
SDA - 7	2100.0	54	5	15.25	**399.8**	7.00	1.688	31.5%	**1.686**	5.35%	0.974
SDA - 8	2100.0	103	5	8.00	**400.1**	7.75	1.696	35.3%	**1.686**	5.35%	0.974
SDA - 9	2100.0	90	5	18.30	**799.6**	7.25	1.701	33.3%	**1.693**	5.29%	0.978
SDA - 10	2100.0	122	5	13.50	**799.6**	8.40	1.704	38.8%	**1.689**	5.32%	0.976
SDA - 11	4015.5	77	5	11.20	**800.6**	8.25	1.700	37.9%	**1.678**	5.41%	0.969
SDA - 12	4015.5	90	5	19.15	**1600.0**	8.75	1.713	41.0%	**1.692**	5.30%	0.977
SDA - 13	2100.0	206	5	16.00	**1600.2**	7.25	1.710	33.8%	**1.695**	5.27%	0.979
SDA - 14	2100.0	180	5	18.50	**1616.7**	7.00	1.715	32.9%	**1.711**	5.14%	0.988
SDA - 15	4015.5	134	5	21.70	**2699.4**	6.80	1.776	35.3%	**1.762**	4.73%	1.018
SDB - 1	2100.0	34	5	6.00	**99.0**	7.75	1.770	39.8%	**1.748**	4.85%	0.964
SDB - 2	4015.5	19	5	5.62	**99.1**	7.75	1.775	40.2%	**1.749**	4.84%	0.965
SDB - 3	2100.0	55	5	7.50	**200.3**	7.45	1.787	39.4%	**1.763**	4.73%	0.972
SDB - 4	2100.0	103	5	8.00	**400.1**	7.55	1.816	41.9%	**1.759**	4.76%	0.970
SDB - 5	4015.5	56	5	7.70	**400.3**	7.50	1.798	40.3%	**1.750**	4.83%	0.965
SDB - 6	2100.0	122	5	13.50	**799.6**	7.50	1.815	41.5%	**1.791**	4.51%	0.988
SDB - 7	4015.5	77	5	11.20	**800.6**	7.70	1.833	43.9%	**1.790**	4.52%	0.987
SDB - 8	4015.5	90	5	19.15	**1600.0**	7.90	1.845	44.0%	**1.811**	4.36%	0.999
SDB - 9	2100.0	206	5	16.00	**1600.2**	7.75	1.852	45.7%	**1.798**	4.46%	0.992
SDB - 10	2100.0	300	5	18.50	**2694.5**	8.00	1.847	46.8%	**1.818**	4.31%	1.003

3 Modified Sample Preparation Procedure for Cohesionless Soils

3.1 Determining the reconstituted saturation

While ASTM D1557-12e1 is used to determine the optimal saturation, natural materials are not at optimal saturation; they are at a reduced saturation percentage. Previous research (Bradshaw and Baxter 2007; Taylor 2011; Taylor et al. 2012) hypothesizes that in situ conditions are approximately 71% of optimum. This value is the subject of continued research and is irrelevant to the protocol presented herein. However, it is of importance when determining the in situ fabric of the material for laboratory testing. The purpose of this work is to show that energy and reconstituted saturation, referred to herein as S_R, are the governing criteria for sample preparation and that two similar soil types reconstituted with the same energy and saturation have the same continuum behavior. Thus, an S_R of 24% was chosen for this dataset.

The two example compaction curves shown in Figure 8 are the results from the SDA and SDB materials compacted using a compactive effort of 400 kJ/m^3. Also shown in Figure 8 are the contours of constant saturation that appear linear; however, they are actually curved over a larger range of compactive energies. The S_R chosen for testing should be on the dry side (left) of optimum as the wet side (right) side of the continuum is governed by the internal water and not the solid material. If water governs the continuum on the wet side of optimum, no unique relationship exists between energy, density, and water content.

To select a single degree of saturation to use for testing two or more materials, it is important to ensure that the reconstituted saturation is on the dry side of the smallest optimum saturation of all test materials. For the two test materials in this study, the optimum saturations are 34% and 42% for SDA and SDB, respectively. Therefore, a degree of saturation less than 34% is needed to ensure the reconstituted saturation for both materials remained on the dry side of optimum. It is also equally important to select a reconstituted saturation that falls on the wet side of observed bulking. This lower limit for reconstitution is determined from compaction curves at the water content where bulking is observed. In this study, the bulking limit for SDA was observed at a water content of 4%.

Figure 8. Saturation contours for SDA and SDB with compactive energy of 400 kJ/m³.

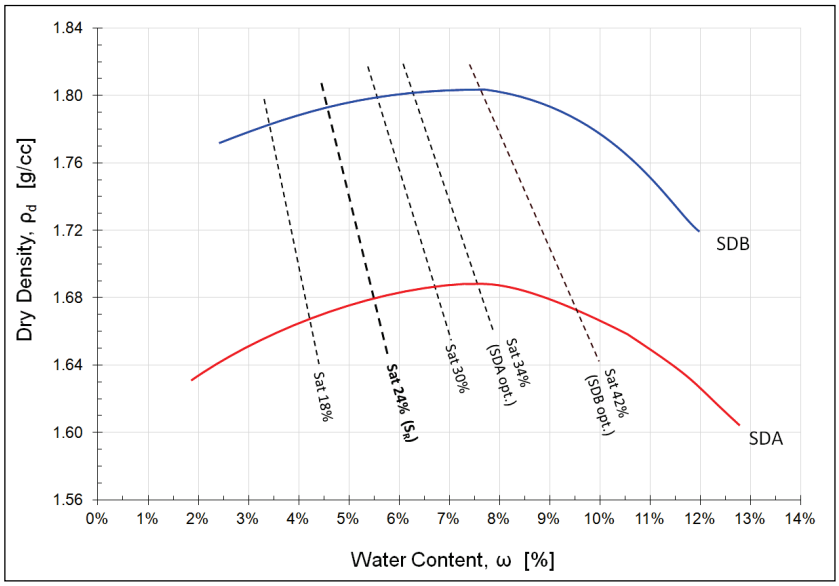

Figure 9 highlights the range of saturations (yellow region) that will yield specimens for both SDA and SDB that meet the aforementioned criteria. The S_R value selected for the tests in this study was 24%, corresponding to water contents of 5.5% and 4.6% for SDA and SDB, respectively. These water contents are on the dry side of the optimum saturation for each material and on the wet side of observed bulking (see Figure 9).

Figure 9. Range of testable reconstituted saturations (S_R) for SDA and SDB.

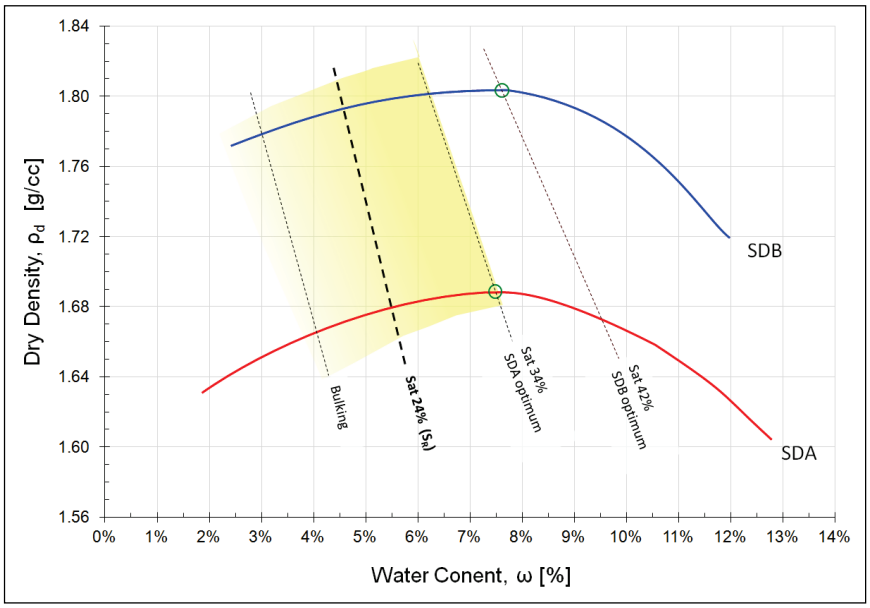

In order to show the sensitivity of S_R to the behavior of the sand, a series of triaxial tests were conducted on materials at 18% and 30% saturation in addition to the selected S_R of 24%. Test specimens were built using multiple compactive energies ranging from 200 to 1150 kJ/m^3. Figure 10 shows the deviator stress at failure, σ_d, for the SDB material for each saturation at a given energy. Figure 10 illustrates the variation of σ_d for any given energy is approximately 20 kPa from 18% to 30% saturation, or +/- 10 kPa from the 24% saturation line. The variation in saturation between 18% to 24% or 24% to 30% equates to a water content change of +/- 25%. However, tighter tolerances are achievable as described herein and, as such, the allowable water content error is +/-3%. This tolerance provides a greater confidence of consistency and repeatability in test specimen behavior with minimal epistemic uncertainty. Therefore, the deviation of the continuum behavior from the mean is significantly reduced and is predominately a function of aleatory uncertainty and instrument sensitivity.

Figure 10. Sensitivity of reconstituted specimen to saturation (SDB).

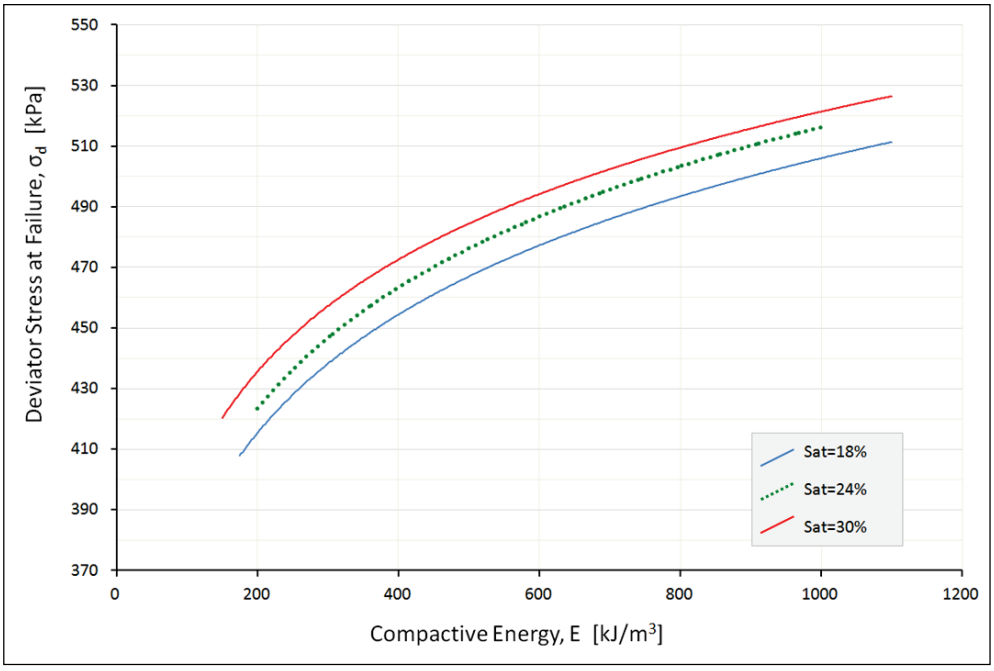

To further illustrate the confidence and repeatability of laboratory testing using a specified reconstituted saturation, Figure 11 shows the water content tolerances maintained for the SDA material using a target reconstituted saturation of 24% relative to that of +/-25% water content tolerances. For example, an SDB sample reconstituted with a compactive energy of 200 kJ/m^3 and a saturation of 24% requires a water content of 4.90%. In

order for this specimen to meet the +/- 3% tolerance, the water content is required to be between 4.76 and 5.04%. A specimen reconstituted to achieve 18% or 30% saturation, using the same material and compactive energy, requires a water content of 3.68% and 5.98%, respectively. Comparing Figure 11 with Figure 10, it can be concluded that a large change in water content results in a small change in peak strength, i.e., +/- 25% change in water content results in +/- 10 kPa in peak strength. These small variations in soil strength become critically important in investigations of soil behavior in low to zero confining pressure environments. Maintaining a strict +/- 3% tolerance in the water content, which is easily attainable in the laboratory, significantly reduces the standard deviation from the mean in terms of continuum strength and behavior. This yields a reduction in the standard deviation from the mean strength, thereby reducing uncertainty and increasing repeatability in reconstituted specimens.

Figure 11. Allowable saturation error limits for sample reconstitution (SDB).

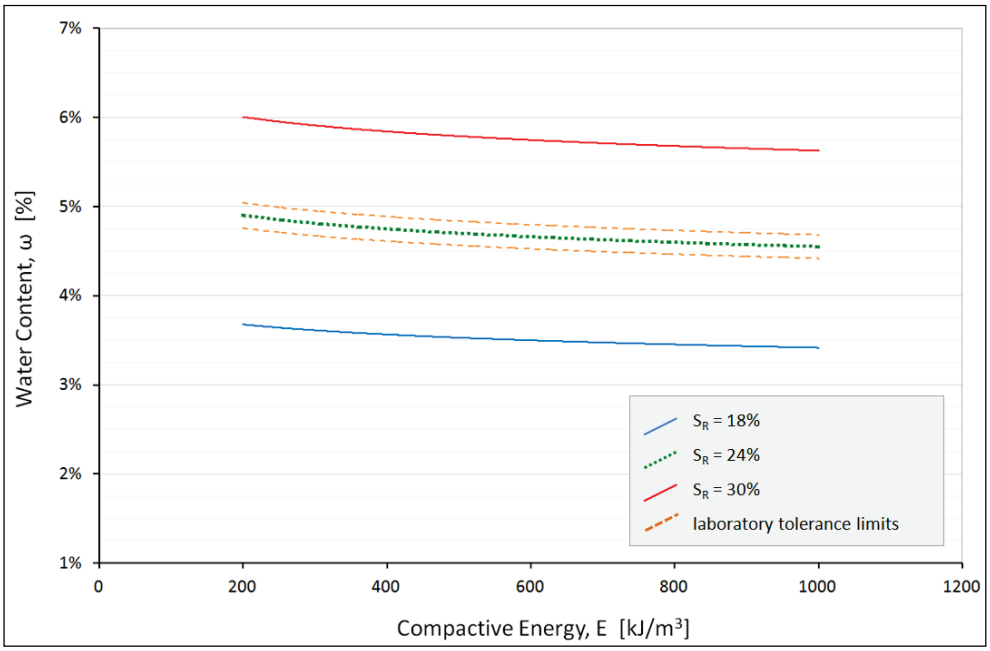

3.2 Normalized density

Typically, samples are reconstituted to equivalent relative densities as determined by a percentage of the void ratio. However, this does not account for the method by which the sample was constructed; sample reconstitution method has been shown to predominantly influence the sample behavior (Mulilis et al. 1978). Therefore, to accurately compare two different materials, consideration must be made to the method by which the sample is constructed (Chapter 4), and the normalization method used

to account for variability in physical properties between the sample material, e.g., mineralogy, grain size, etc. This section outlines the method for normalizing the density of cohesionless soils for the purpose of comparing the behavior of soils with similar gradations.

Normalized density is an important concept when considering (a) relative behavior of two or more materials with similar gradations, (b) determining the behavior of soil C based on soil A and B that had been tested in the laboratory, (c) estimating the behavior of an unavailable soil with that of a soil that had been tested in the laboratory, i.e., development of a proxy soil from which behavior can be derived, and (d) a means of sample preparation to investigate soil fabric effects.

Where the ASTM D-1557 test procedures are designed to produce a maximum dry unit weight when subjecting the soil to a total compactive effort of 2707 kJ/m^3, this study's intent is to prove the theory that, to the dry side of optimum, there exists a unique relationship between saturation and energy that, for a constant saturation, only one compactive energy-saturation combination will yield a specific density or soil fabric.

Taylor et al. (2012) proposed a new normalization concept termed *normalized density* wherein a standard compaction test, 2707 kJ/m^3 of compactive effort, is conducted to determine the modified maximum dry density, $\rho_{d\,max.}$ This modified maximum dry density is the density at a specific degree of saturation and is used to normalize the reconstituted sample's dry density, ρ_d, at the same constant degree of saturation (in this study S=24%). This new normalized quantity, called Normalized Density, ρ_N, is expressed as

$$\rho_N = \frac{\rho_d}{\rho_{d\,max}} \tag{5}$$

According to Taylor et al. (2012), using this normalization approach yields a stronger correlation between density and tamping energy irrespective of the materials tested for a constant degree of reconstituted saturation.

To further elaborate on the steps to complete this normalization process, Figure 12 shows a sample compaction curve developed using SDA material and constructed with 200 kJ/m^3 of compactive effort (test SDA-4 from Table 1). From this curve, the ρ_d corresponding to a saturation of 24% was determined.

Figure 12. Sample compaction curve for SDA using 200 kJ/m³ of compactive effort.

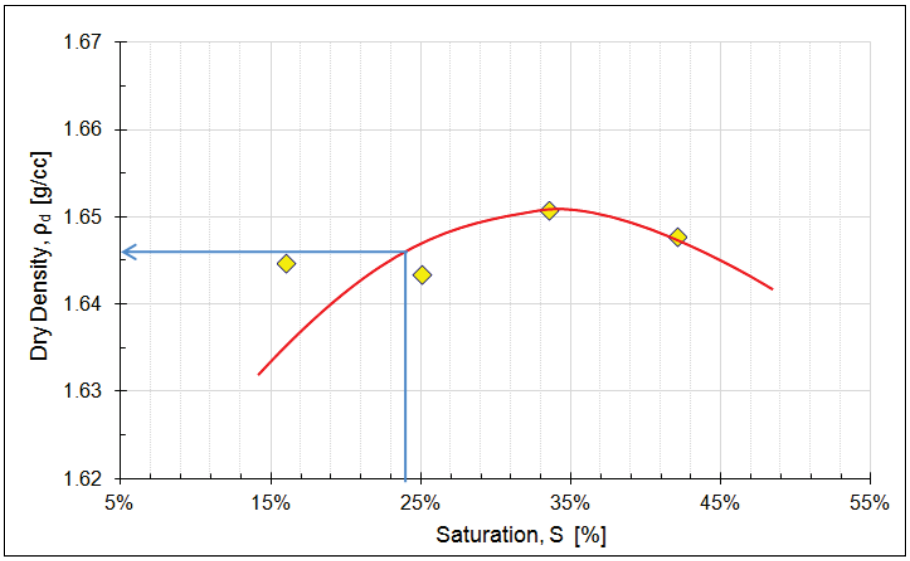

A total of 25 compaction curves, similar to Figure 12, were developed for the SDA and SDB materials. These compaction tests were completed using a range of compactive efforts from 200 to 2700 kJ/m³ (see Table 1). A plot of ρ_d vs. energy, E, was then developed from the suite of compaction tests (Figure 13). Figure 13 illustrates that there is a strong logarithmic relationship (R^2=0.86) between E and ρ_d even over small ranges of dry densities. Note that SDA has a larger range of potential dry densities (1.57 g/cm³ to 1.76 g/cm³) than SDB (1.75 g/cm³ to 1.82 g/cm³).

Figure 13. Relationship of energy to dry density for SDA and SDB.

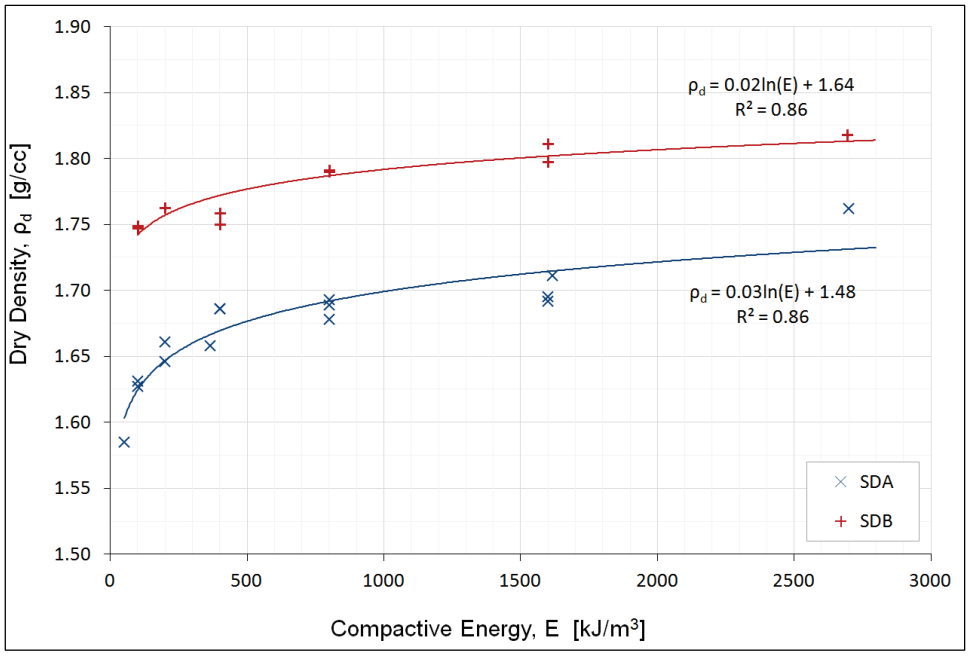

This relationship is used to calculate the dry density of the material for a given energy, or provide the energy required to produce a given density for materials similar to SDA and SDB at a reconstituted degree of saturation of 24%. It is critical to note that reconstituted saturation is different from in-situ saturation or tested saturation, because the reconstituted saturation controls the internal fabric of specimen. A specimen that is reconstituted at a saturation of 24% can then be allowed to dry out or gain moisture to a desired testing saturation without it changing the specimen's internal structure. The reconstituted saturation (the degree of saturation of the material when the specimen is being constructed) and the compactive effort (energy) applied to the material when the specimen is built have a first order influence on the continuum behavior.

Using Equations 6 and 7 developed from the logarithmic trend lines for SDA and SDB (Figure 13), dry density (ρ_d) is correlated to energy as

$$\textbf{SDA}: \rho_d = 0.03 \ln(E) + 1.48 \tag{6}$$

$$\textbf{SDB}: \rho_d = 0.02 \ln(E) + 1.64 \tag{7}$$

Using Equations 6 and 7, $\rho_{d\,max}$ for SDA and SDB is found using a standard Proctor test's compaction energy of 2707 kJ/m^3. This produces a $\rho_{d\,max}$ of 1.73 and 1.81 for SDA and SDB, respectively. This calculated density, $\rho_{d\,max}$, is the density a compaction test would provide a user in the field, relating this normalization approach to the modified Proctor test. In Equation 5, ρ_d is divided by $\rho_{d\,max}$, calculated from Equations 6 or 7, thus normalizing the range of potential sample densities (Figure 14).

Therefore, from the normalization of the dry density for SDA and SDB at a reconstituted saturation of 24%, the normalized dry density, Equation 8, becomes

$$\rho_N = 0.02 \ln(E) + 0.87 \tag{8}$$

Figure 15 presents a flow chart outlining the procedures for normalizing cohesionless soils. Note that this procedure can be eliminated if a particular material is within the gradation range (Figure 1) of other previously normalized soils. In this case Equation 8 can be used directly.

Figure 14. Normalization of SDA and SDB with respect to compactive energy.

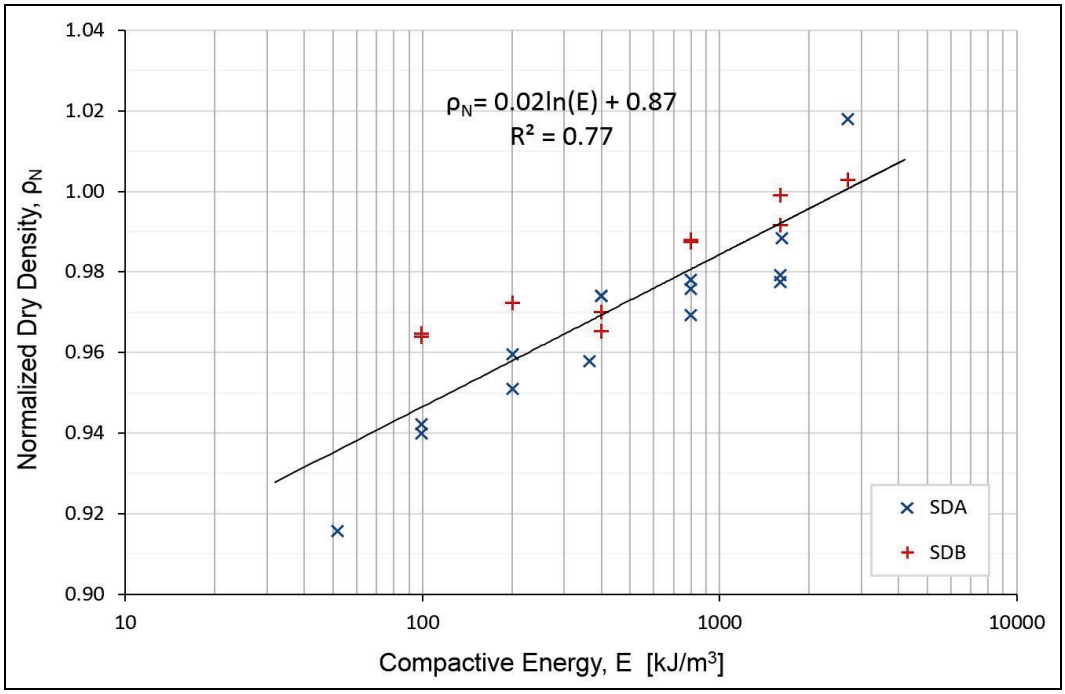

Figure 15. Schematic of normalized density method.

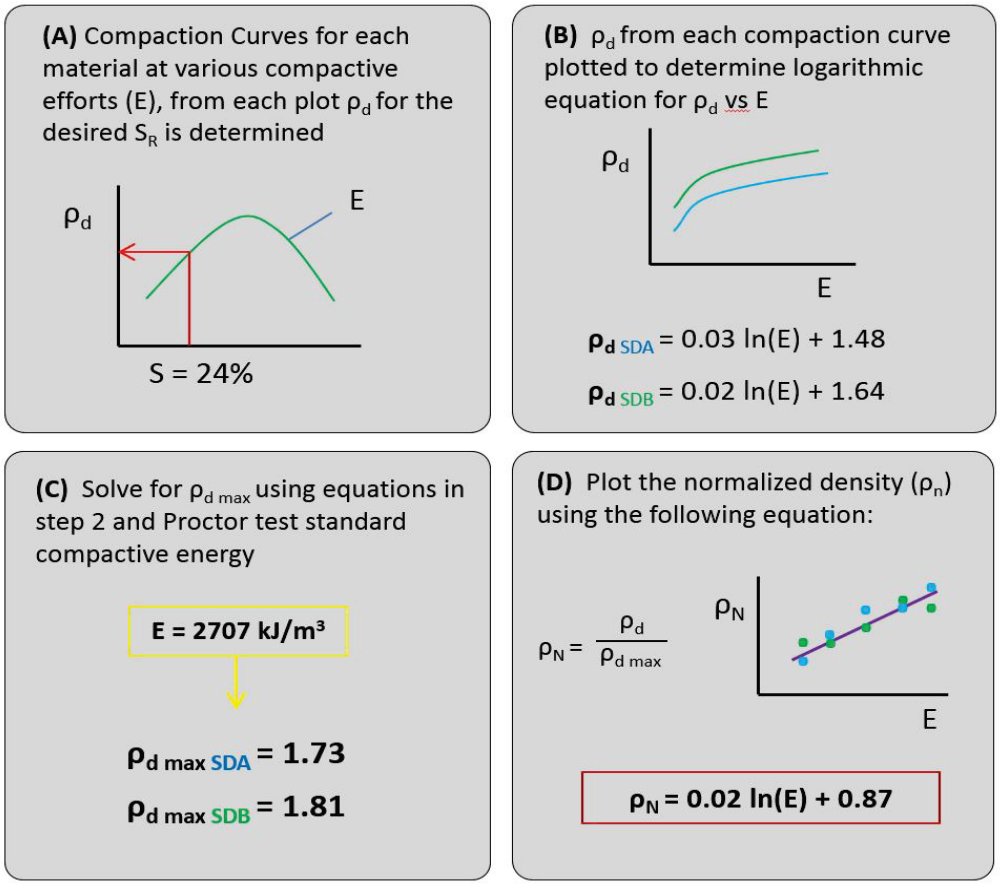

Figure 14 illustrates that, for a given S_R, e.g., 24%, cohesionless materials of similar gradation normalize. Using this normalization approach, the behavior of any two (or more) cohesionless materials with a similar gradation and USCS classification can be compared. For an example, if soil C is within the same gradation range as soil A and B, then soils A and B can be used as a proxy to test the behavior of C without ever testing C in the laboratory. This is most useful if soil C is unattainable or insufficient quantities of Soil C are available for laboratory testing.

3.3 Developing the protocol for sample preparation

All laboratory samples herein are modified moist tamped (MMT) similar to Bradshaw and Baxter (2007). The benefit of the MMT approach to sample reconstitution is maintaining a uniform compactive effort throughout the sample. The method herein controls the tamping energy applied to each layer and the reconstitution saturations, allowing density, void ratio, etc., to be by-products of the sample reconstitution.

The controlling parameters in sample reconstitution are (a) the applied compactive energy and (b) the degree of saturation prior to reconstitution efforts. All other physical phase relationships, i.e., density, void ratio, permeability, etc., are by-products of (a) and (b) (Taylor et al. 2012). In order to have a testing procedure that is consistent, repeatable, and epistemic variability in sample preparation, a protocol must be developed for how the water is added to the sand and how the moist sand is then reconstituted. Herein, the protocol is presented in theory and is entered in a spreadsheet to aid with sample construction and to calculate exact amounts of de-aired water and oven-dried material at a specified S_R.

The target energy is calculated based on the weight of the rammer, number of layers, and number of blows per layer. A “dummy” sample should be constructed to ensure no bulking or punching shear failures are observed during sample construction. If the “dummy” sample does not meet the specification criteria, or if failure bands, internal weaknesses, etc., are observed during reconstitution, then the rammer weight, drop height, and/or number of blows per layer must be adjusted accordingly. The revised protocol is then verified by an additional “dummy” specimen.

The amount of sand required is calculated based on the volume of the mold, the amount of energy being applied to the sample, the number of layers in the sample, the reconstituted saturation, and the dry density of

the material. For single soil investigations, the normalized density approach described in the previous section is not required in the dry density calculations shown throughout this section. It is only for multiple soil analyses that the normalized density from Figure 14 is required.

Initial laboratory testing of SDA and SDB was completed using a specimen with a height and diameter of 300 mm and 152 mm, respectively. Figure 16 illustrates example calculations for the 300-mm specimen. The complexity of the testing protocol is dependent on the testing regime. Before the actual calculations are discussed, focus will be given to the user defined variables that must be considered when developing an appropriate protocol.

Figure 16. Sample preparation worksheet layout.

Layer No	E_n	Drop Height mm	Volume per layer	Mass Add g
1	0.000532	25.76	0.000276	511.12
2	0.000535	25.89	0.000276	511.12
3	0.000538	26.03	0.000276	511.12
4	0.000540	26.16	0.000276	511.12
5	0.000543	26.29	0.000276	511.12
6	0.000546	26.42	0.000276	511.12
7	0.000549	26.55	0.000276	511.12
8	0.000551	26.69	0.000276	511.12
9	0.000554	26.82	0.000276	511.12
10	0.000557	26.95	0.000276	511.12
11	0.000560	27.08	0.000276	511.12
12	0.000562	27.22	0.000276	511.12
13	0.000565	27.35	0.000276	511.12
14	0.000568	27.48	0.000276	511.12
15	0.000570	27.61	0.000276	511.12
16	0.000573	27.75	0.000276	511.12
17	0.000576	27.88	0.000276	511.12
18	0.000579	28.01	0.000276	511.12
19	0.000581	28.14	0.000276	511.12
20	0.000584	28.27	0.000276	511.12

Energy	200.0	kJ/m3		
Sample Height	0.303	m	303	mm
Sample Dia	0.1524	m	152.4	mm
Water Content	4.70%			
Dry Density	1.766	g/cc		
E_d	0.000553	kJ/layer/blow		
Bulk Density	1.85	g/cc		
Rammer Weight	2106	g		
# blows/layer	100	Saturation	0.24	
# of layers	20			
μ	0.046973			

Normalized Eq :	$\rho_n = \rho_{d\,max}$ (a ln(E)+b)
$\rho_{d\,max}$ SDA :	1.73
$\rho_{d\,max}$ SDB :	1.81
a :	0.02
b :	0.87

Target Energy (kJ/m³)=	200.0
W % =	4.70%
Material :	SDB
Amount of Sand (g) =	12,000
Amount of Water to add to Sand (g) =	563.68
Rammer Weight (g) :	2106
Diameter of Hammer Base (mm) :	9.5
Drops per layer =	100

3.3.1 Number of layers in a sample

The size of a specimen will primarily dictate the number of layers required in a specimen. Vertical force applied by the hammer does not propagate solely in the vertical direction; neither does the force remain constant throughout the soil profile. Instead, the force spreads and lessens with depth. Because the same compactive energy does not translate to the full depth, it is important to compact tall samples in layers. If a tall sample was compacted in a single layer, the resulting specimen would be much denser at the top (near the compaction hammer) than at the bottom (away from the compaction hammer).

For larger samples, more layers will be required to ensure a consistent density throughout the specimen. Layers that are too thick will result in a non-uniform soil fabric continuum. Additionally, the number of layers used in sample construction will reduce the potential for internal failure, or "weak zones," which can artificially produce a failure that is not dependent on soil behavior. Further, the number of layers can either increase the required energy per blow (increase compaction through the layer and into the layer below), or decrease the required energy per blow (prevent punching shear from compaction hammer). There is also a consideration for layers that are too thin, resulting in the compactive effort that is being applied to the top layer passing down to lower layers. For this reason, choosing an appropriate number of layers directly relates to the rammer drop height (see Section 3.3.4 *Drop height*).

The number of layers and the thickness of the layers should end up with the exact target height without the need to scrape material from the top, thereby reducing the total compactive effort applied to the sample as discussed in Section 2.6. The allowable error for final sample volume used in this study is +/-2%.

3.3.2 Number of blows per layer

In order to achieve uniform density, the rammer should be dropped on the specimen a minimum of 10 times per layer along a specific blow pattern (Figure 5). For the initial round, the blow pattern should be in a crisscross pattern to prevent uneven distribution of material throughout each layer and to maintain level layers throughout the construction of the specimen. Creating a sample with a level top (without scraping the top of the sample

and disturbing the internal fabric) ensures the normal forces that are applied to the sample are distributed evenly.

3.3.3 Rammer weight

The rammer weight is determined based on the energy requirement. The transfer of the compactive energy throughout the sample depends on the material properties, the size of the hammer base, the rammer weight, and the boundary conditions of the compaction mold. For compaction tests, rammer weights of 4015.5 grams and 2107.0 grams were used. If the weight is too heavy, it can easily generate internal shear bands/failure planes within the specimen (Figure 17a) or cause punching shear (Figure 17b). The weight must be sufficient to compact through the entire layer, light enough as to not eject material upon strike, but heavy enough as to create uniform compaction throughout the layer. This is critically important at low (dry) or high (wet) water contents. A larger weight can be used to minimize the drop height (Section 3.3.4 *Drop Height)* or the number of blows required, provided that failure potentials (Figure 17) are not observed at any point in the sample construction process.

Figure 17. Types of failure: (a) local failure, (b) punching shear failure.

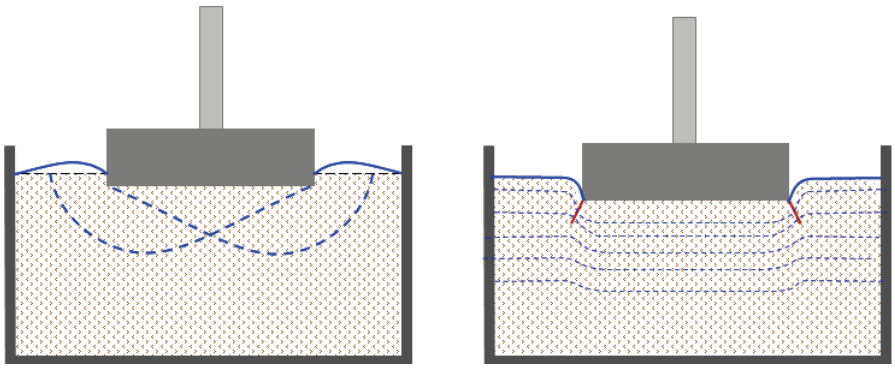

3.3.4 Drop height

The rammer drop height should be sufficient to fully compact the layer but prevent punching shear or generation of internal shear bands (Figure 17). A minimum rammer drop height should be observed to ensure there is enough energy transmission for undercompaction. When higher energies are desired, a balance between the drop height and the drop weight must be considered to prevent shearing of the specimen (Figure 17). Therefore, the rammer drop height should be the shortest possible with emphasis

placed on altering other energy factors, e.g., hammer weight, blow per layer, etc., to achieve different compactive energies.

3.3.5 Diameter of hammer base

The diameter of the hammer base and its relationship to the diameter of the specimen is a critical component in creating a repeatable and consistent continuum throughout the specimen and in determining the actual compactive effort applied to the specimen. The ASTM Standard Modified Proctor test's hammer-to-specimen ratio, or HSR, is 95 mm/152 mm, and the amount of energy the Proctor Hammer applies (2707 kJ/m^3) has been used as a basis, or reference energy, E_R, for determining the amount of energy being applied with other HSRs, referred to herein as equivalent energy, E_{eq}. This idea of equivalent energy is explained in more detail in Section 3.4.

In addition to equivalent energy, another consideration when using other HSRs (other than 95 mm/152 mm) is how the energy is dispersed through the sample. The dispersion of energy across the hammer base directly influences the energy concentration applied to the specimen. The larger base will have smaller stresses applied across a larger area of the sample that decreases with depth (Figure 18a). A smaller base will have larger stresses over a smaller area of the sample thereby propagating further underlying sample layers (Figure 18b). Therefore, it is essential to have a large enough base that you don't shear the sample, and a small enough base that the energy is dispersed all the way through the layer. Too small however will create columns of dense material across the sample and leave other void areas that remain uncompacted.

The diameter of the hammer base must be a minimum of half the specimen diameter to keep from shearing the sample and to ensure that sufficient overlap between blows is achieved. It is also recommended that the hammer base be no larger than 75% of the sample mold diameter; any larger can cause binding, energy transfer loss along the mold edge, or air pressure resistance reducing stress and energy transfer. For 150-mm or larger diameter molds, the hammer base will likely need to be significantly smaller than 75% of the sample diameter in order to reach the required energy, as larger bases require more weight or increased number of blows to reach equivalent energies, keeping in mind the hammer diameter must be at least half the width of the specimen.

Figure 18. Energy distribution relative to hammer size.

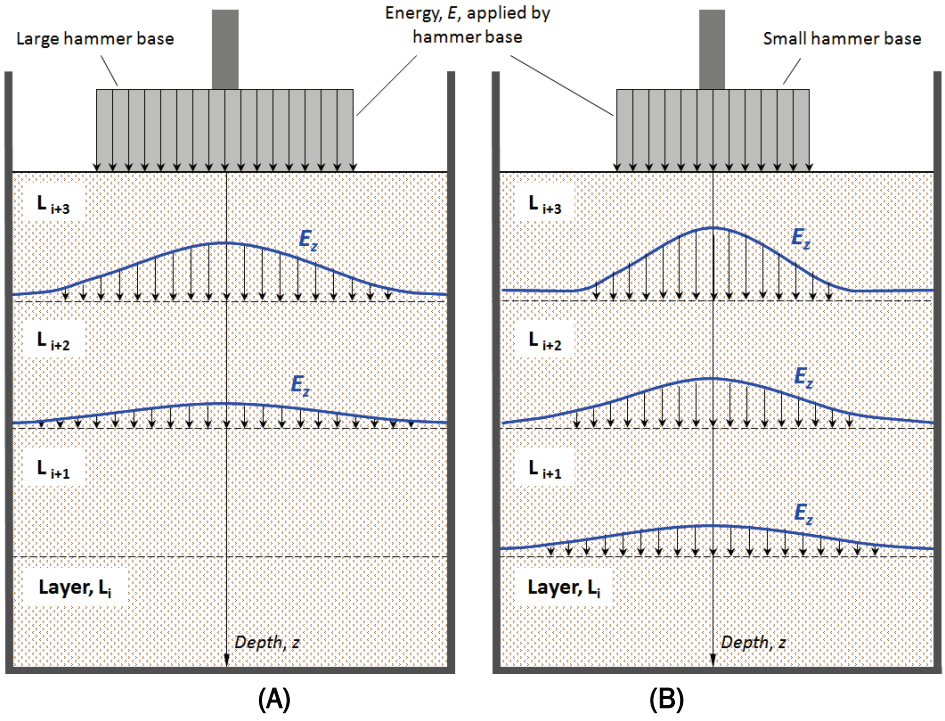

3.4 Equivalent energy, E_{eq}

It is important when comparing behavior of laboratory reconstituted specimens that the resultant density of the specimen is achieved in the same manner. Just having a similar density does not mean the behavior will be the same. For example, one sample that was vibrated will have a different behavior than one that reached the same density through dry tamping (Mulilis et al. 1978). Similarly, a sample that was created using a target energy of 200 kJ/m^3 and a 95-mm base will perform differently than reconstituted sample using a 50-mm base at the same 200 kJ/m^3 energy due to energy dispersion.

Determining the amount of energy applied to a specimen involves considering the hammer-to-sample ratio, HSR. This research is based on energy calculations of the ASTM Standard Modified Proctor Test, a hammer base (95 mm in diameter), and the standard 6-in. Proctor mold (152 mm inside diameter) to determine a standard E_R for all other HSRs. For any HSR, matching that used in the Modified Proctor test energy is simply calculated using Equation 4. E_R is not important if samples are created using the 95/152 HSR or if different size molds and hammers are

not being used to compare behavior. To calculate the energy being applied for any other HSR, E_{eq} is calculated as

$$E_{eq} = E_R \frac{A_{RH} / A_{RS}}{A_H / A_S} \tag{9}$$

where A_{RH} is the area of the reference hammer base, A_{RS} is the area of the reference specimen, A_H is the area of the hammer base, and A_S is the area of the specimen.

3.5 Material preparation calculations

The volume of the specimen is used to calculate an approximate amount of moist sand required to build the specimen. The target height of the specimen is inflated 1% for determining the amount of material required. This is to account for some loss during the sample reconstitution and also to allow for enough excess material for moisture content verification.

The water content, cell H5 in Figure 16, is calculated based on the desired reconstitution saturation (for this study, S_R=24%).

$$\omega = \frac{S_r \left(\rho_w - \rho_d\right)}{\rho_w \ \rho_d} \tag{10}$$

where S_r is reconstituted saturation, ρ_w is the density of water, and ρ_d is the dry density of the soil.

When two or more cohesionless materials with similar gradations and USCS classifications are being compared, the normalized density should be used (Equation 8). If the sample reconstitution is for a single material analysis, the dry density determined from the proctor test at a specific S_R should be used. For this study, the dry density, cell H6 in Figure 16, for SDA and SDB is calculated by multiplying $\rho_{d\,max}$ by Equation 8. The material dry density based on the normalization curve of Equation 8 for SDA and SDB are

$$\rho_{n\,SDA} = 1.73\,(0.02\,\ln(E) + 0.87) \tag{11}$$

$$\rho_{n\,SDB} = 1.81\,(0.02\,\ln(E) + 0.87) \tag{12}$$

The amount of energy applied per single hammer drop, E_d, cell H7 in Figure 16, is calculated as

$$E_d = E_R \frac{V}{b\,N} \tag{13}$$

where V is the target volume of the sample, b is the number of blows per layer, and N is the total number of layers. In order to determine the energy required for each layer, the appropriate number of layers for the size specimen must be determined (see Section 3.3.1).

The left side of the sample preparation worksheet in Figure 16 contains the calculations for each individual layer of the sample. The energy, drop height, volume of material, and mass of material for each layer is carefully controlled for each layer to ensure the repeatability of the resultant soil fabric and strength characteristics.

In order to obtain the desired compactive energy for the entire sample, the total applied energy must be divided between the designated number of layers by incorporating μ, yielding an equivalent 1% density under-compaction uniform density (Ladd 1978). This undercompactive energy is calculated per hammer drop for each unique layer using a 7.7% under-compactive energy requirement. The tamping energy per drop, adjusted for undercompaction, for the n^{th}-layer, E_n, column B in Figure 16, is calculated as

$$E_n = E_d(1-\mu) + (n+1)\frac{2E_d\mu}{N-1} \tag{14}$$

where μ is percent energy undercompaction (decimal form), N is the total number of compactive layers, and E_d is the energy applied per single hammer drop. The drop height for the n^{th}-layer, h_n, column C in Figure 16, is calculated by

$$h_n = \frac{E_n}{m_R\, g} \tag{15}$$

where m_R is the mass of the rammer, and g is the gravitational acceleration.

The volume of material per layer, V_L, column D in Figure 16, is based simply on the total volume of the specimen divided by the number of layers. The mass of material to add per layer, m_L, column E in Figure 16, is a function of the bulk density, ρ, cell H8 in Figure 16, and the target water content, ω (Equation 10). Bulk density is calculated by

$$\rho = \rho_n (1 + \omega) \tag{16}$$

where ρ_n is calculated using the normalization curve equations, Equations 11 and 12. The mass of material to add per layer, m_L, is calculated based on ρ and the volume of material per layer, V_L:.

$$m_L = V_L \rho \tag{17}$$

4 Adjustments for Specimen Geometry

4.1 Hammer to sample ratio, HSR

The diameter of the hammer base directly influences the energy concentration applied to the specimen. The smaller the hammer base, the more energy that will be transferred to the specimen beneath the footprint of the hammer base. A larger hammer base transfers the energy over more surface area but does not transfer the energy as deep into the specimen. The ASTM Standard Modified Proctor test (ASTM D698) uses a hammer with a 95-mm-diameter base and a specimen that is 6 in. (152.4 mm) in diameter. The energy applied by this size hammer to this specimen is considered the standard for compactive effort. For this reason, hammer bases and/or specimens that vary from these diameters require an adjustment for the energy associated with its compactive effort. Refer to Section 3.4 when adjustments are required due to hammer or sample diameters that vary from outlined in the ASTM Standard Modified Proctor Test.

4.2 Correction for non-cylindrical solid specimen

Non-cylindrical solid samples, e.g., ring shear, hollow core, etc. (Figure 19), require an adjustment to the E_{eq} associated with the compaction hammer for such specimen. This adjustment factor, ψ, is required for non-cylindrical samples being compacted with a non-cylindrical hammer base to account for the energy reflection from the sides of the rigid mold.

Figure 19. Energy transfer (a) circular solid samples (b) circular hollow samples.

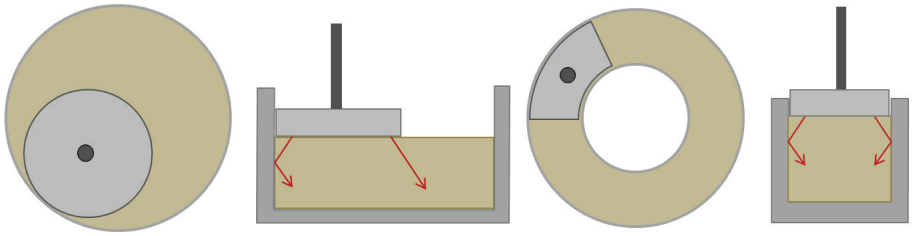

The ψ for a triaxial sample is assumed to be equal to 1 and is therefore the reference sample for non-cylindrical sample adjustments. As applied energy increases, ψ decreases because more of the energy is reflected back into the sample with the higher energies. This is due to the higher energies reflecting back from the sides of the mold. When smaller energies are

applied, less energy is reflected back into the sample, therefore creating less reflective energy than with higher energy samples. When the energy that is being reflected back into the sample is not accounted for, it results in a specimen that is denser than intended, thus the need for the ψ adjustment factor.

$\mathbb{C}$ is the circumference percentage that is in contact with the rigid mold and is calculated as

$$\mathbb{C} = \frac{C_m}{C_h} \tag{18}$$

where C_m is the circumference in contact with the rigid mold and C_h is the total hammer base circumference. The hammer used for compaction for ring shear tests has a total circumference of 180 mm. The portion of the ring shear hammer circumference that is in contact with the rigid mold is 127 mm. Using Equation 18, $\mathbb{C}$ for the ring shear is equal to 70%. The $\mathbb{C}$ for the 95/152 HSR is used as the Reference Circumference Percentage, $\mathbb{C}_R$, but the exact circumference of the hammer that is actually in contact with the mold is unknown.

The ψ for the ring shear hammer is a ratio of $\mathbb{C}$ and $\mathbb{C}_R$.

$$\psi = \frac{\mathbb{C}_R}{\mathbb{C}} \tag{19}$$

The corrected energy, E_ψ, then becomes

$$E_\psi = \psi E_{eq} \tag{20}$$

An iterative process was completed to determine exactly what the $\mathbb{C}$ for the 95/152 HSR was. Ring shear specimens were reconstituted using both SDA and SDB material with compactive energies ranging from 200 to 2700 kJ/m^3. For each material and compactive energy combination, a series of iterations were completed varying the $\mathbb{C}$ from 0.5 to 7.0%. The final height of the specimens were measured and, if the height was within +/-2%, the $\mathbb{C}$ was considered acceptable. For each passing height, the ψ was calculated (Equation 19) for the associated $\mathbb{C}$. These specimens resulting in a final height with the target allowable error were plotted (Figure 20).

Figure 20. Analysis of ψ.

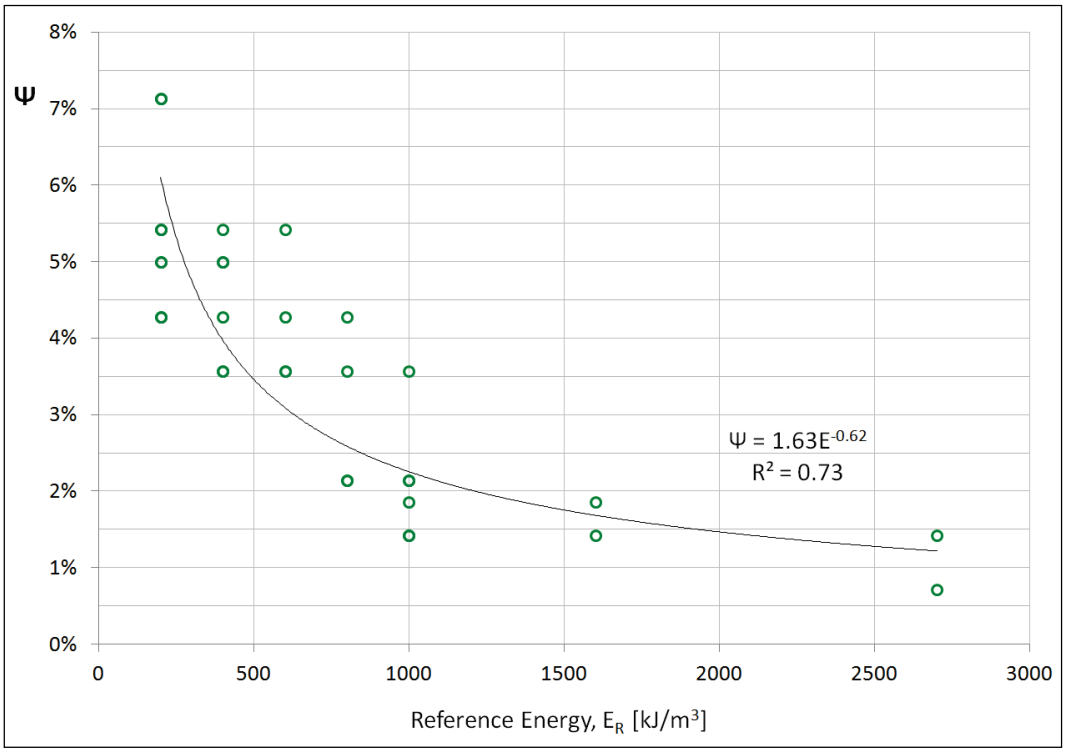

A power trendline was fit to the data to determine an equation for ψ (R^2 = 0.73). The higher the ψ, the less the equivalent energy has to be adjusted. In other words, for the lower compactive energies, the reflective energy is much less than with the higher compactive energies.

5 Testing Apparatus Description

5.1 Triaxial

Triaxial testing for this study was performed using the USTX-2000 (Figure 21a), and the HCA-150 (Figure 21b) devices manufactured by GCTS. Specimens with a 152.5-mm diameter and 300-mm height were tested on the HCA-150, and 71.1-mm-diameter by 145-mm-tall specimens were tested on the USTX-2000. For both devices, an anisotropic confining pressure of 100 kPa was applied. Specimens were then subject to an axial strain of 0.25% per minute, and the maximum deviator stress was recorded. Standard triaxial testing procedures for isotropically consolidated drained specimens, ICD_{TX}, are in ASTM D7181-11.

Figure 21. (a) GCTS USTX-2000 triaxial testing device for samples up to 70-mm diameter; (b) GCTS HCA-150 triaxial setup for samples up to 150-mm diameter.

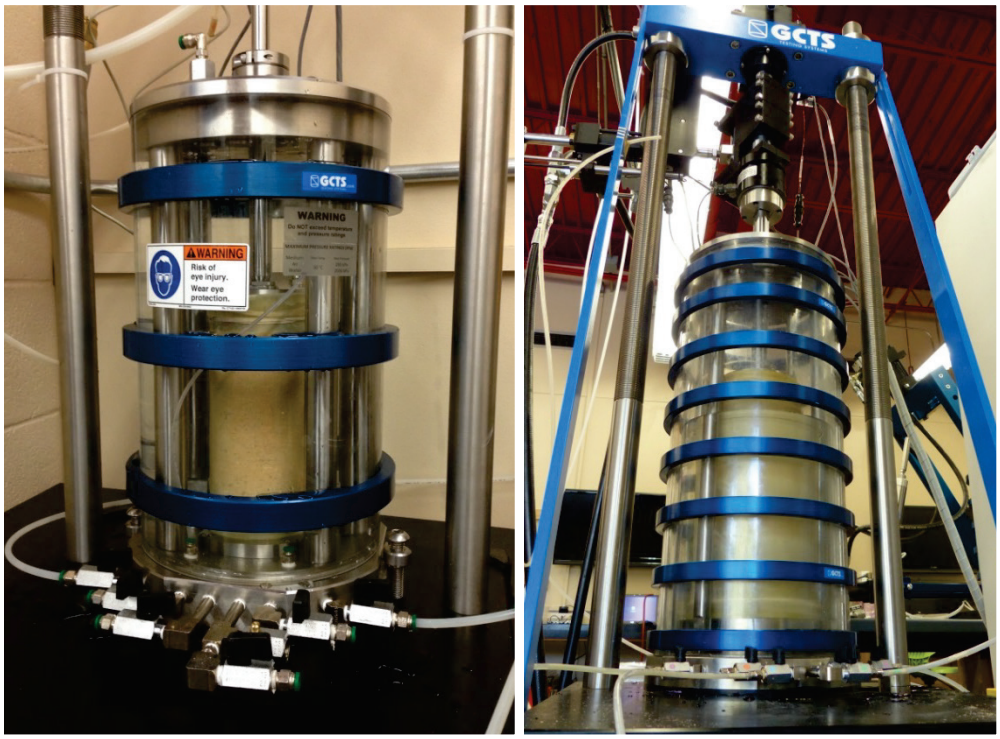

(a) (b)

5.2 Simple shear

Simple shear testing was performed with the GCTS Simple Shear System SSH-100 (Figure 22). Specimens measured 72.9 mm in diameter and 34.0 mm in height. An isotropic confining pressure of 100 kPa was applied

under drained conditions, ICD_{SS}. Specimens were then subject to a shear strain of 0.25% per minute. Neither SDA nor SDB exhibited strain-hardening behavior, and failure was defined at a shear strain of 3.50%.

Figure 22. GCTS SSH-100 simple shear testing device.

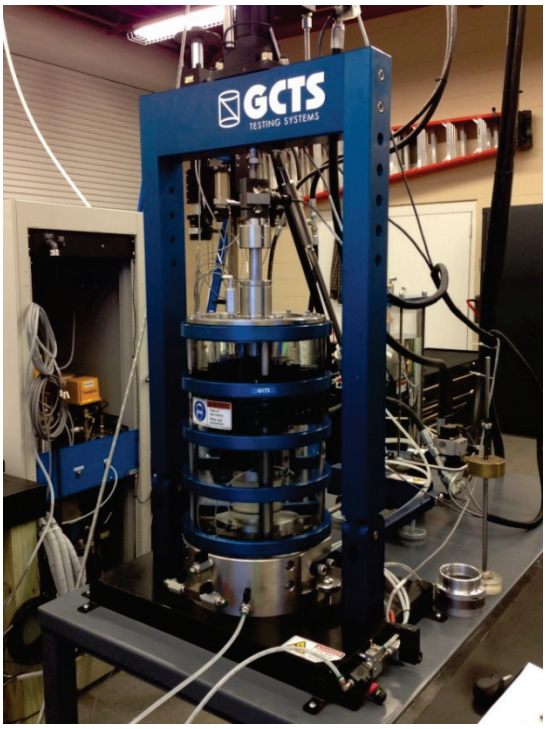

5.3 Ring shear

Ring shear testing was performed using the GCTS Residual-Ring Shear System SRS-150 for the torsional shear strength of soils. The ring shear apparatus is typically used to measure residual strength of continuously sheared soils, but for this work, only the peak strength for given test conditions was recorded. Ring shear specimens have an interior diameter of 96.5 mm, outer diameter of 152.3 m, and height of 25 mm. This system uses a rigid cylinder sample holder instead of a membrane like the other GCTS systems, so isotropic confining pressures could not be applied. Normal loads were applied by the top plate. Therefore, all tests were anisotropic confined drained where the degree of anisotropy was determined from K_O-conditions with varying applied normal stresses. Samples were then torsionally sheared monotonically, ACD_{RS}, and cyclically, $ACD_{CYC,RS}$. The apparatus with a specimen after testing and lifting the top plate is shown in Figure 23.

Figure 23. GCTS SRS-150 residual-ring shear system.

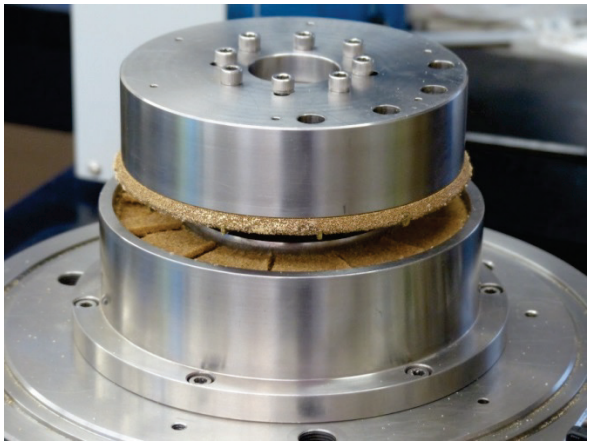

5.4 Hollow core

Hollow core testing for this study was performed using the HCA-150 Dynamic Hollow Cylinder Testing (HCA) System by GCTS. This apparatus (Figure 24) can be modified to run triaxial or hollow-core specimens. Hollow-core testing allows for the application of external and internal cell pressure. Specimens were isotropically consolidated, ICD_{HC}, drained, and tested in torsion. The torsional shear strength was recorded. Hollow-core specimens had an interior diameter of 76.2 mm, outer diameter of 152.5 mm, and height of 300 mm.

Figure 24. Hollow-core specimen during construction.

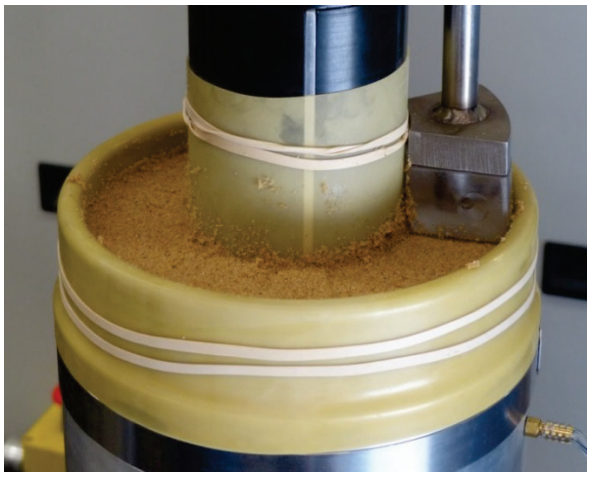

6 Laboratory Testing Results and Observations

The results presented herein are for samples prepared at S_R of 24% for sands SDA and SDB. Both materials were normalized (Section 3.2) for comparison and subjected to ICD_{TX}, ICD_{SS}, ICD_{HC}, ACD_{RS}, and $ACD_{CYC,RS}$ tests (Section 5) with individual results in the Appendix.

6.1 Triaxial testing

ICD_{TX} tests were performed using fully automated triaxial equipment manufactured by GCTS Testing Systems. The cell and pore pressures were controlled by flow pumps, and the axial loads were applied using a hydraulic actuator. Each of the materials was tested at confining stresses of 50 and 100 kPa. The deviator stress at failure, σ_d, was determined as the peak stress. The maximum deviator stress from all tests are shown in Figure 25. Individual test results are in Appendix B.

Figure 25. Strength curves for SDA and SDB with confining pressures of 50 and 100 kPa.

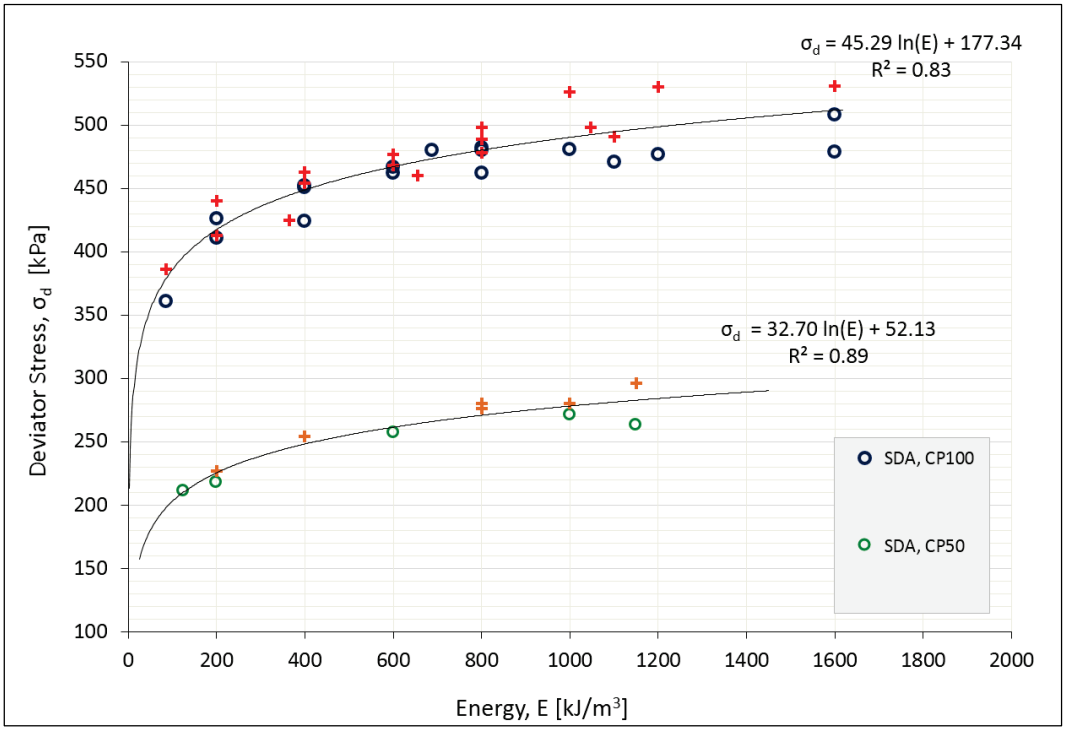

For higher compactive energies (>1000 kJ/m³), there is an increased variability in peak deviator stress despite a strong normalization correlation (R^2 = 0.83). A closer examination (Figure 26) illustrates that this variability occurs where the logarithmic relationship of dry density to energy becomes asymptotic (Figure 13) and where exponentially more energy is required to achieve negligible increases in dry density. Thus, Figure 26 shows that there is no tangible increase in peak strength of either SDA or SDB beyond 1000 kJ/m³ of compactive effort. This suggests that there exists an ultimate fabric strength of these SP sands (500 kPa at 100 kPa confining pressure and 1000 kJ/m³ compactive effort) and that energy applied in excess of this limit is unnecessary resulting in a unstable soil continuum, i.e., a continuum that would not exist in situ. Therefore, the correlation of energy to soil strength, limited by 1000 kJ/m³, yields a stronger relationship (R^2 = 0.88) and is recommended for any data interpretation or strength calculations.

Figure 26. Strength curve for SDA and SDB at a confining pressure of 100 kPa.

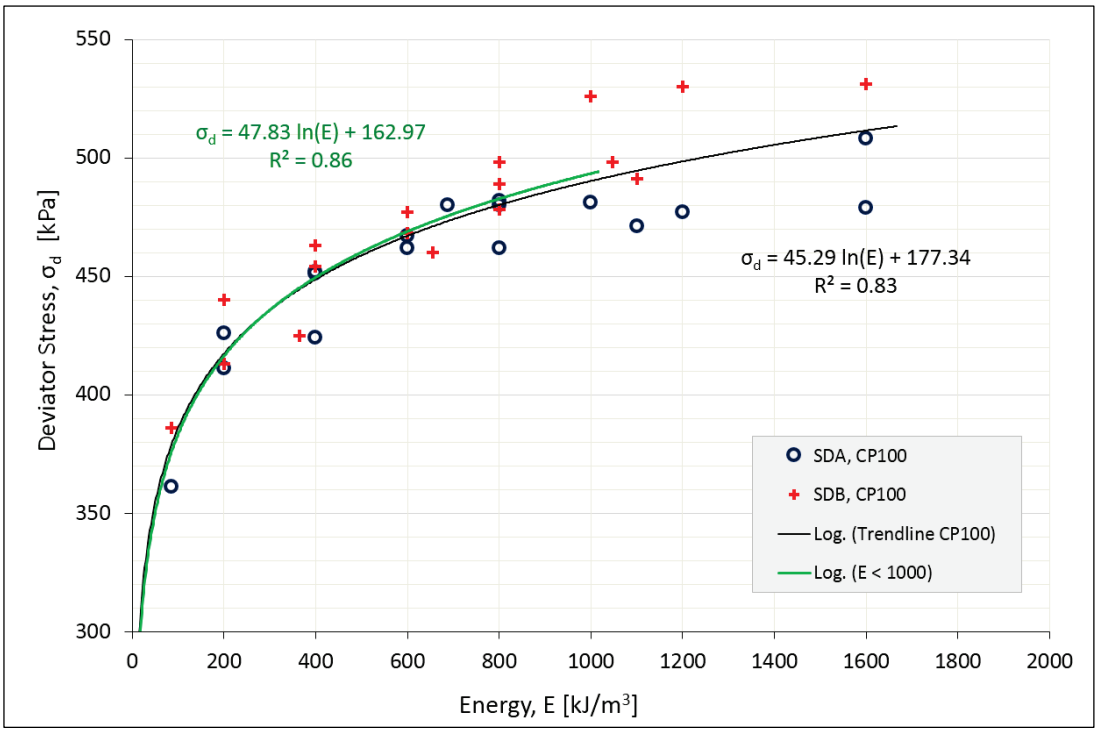

6.2 Ring shear testing

The ACD_{RS} results are shown in Figure 27, wherein both SDA and SDB are normalized to within +/- 5 kPa of each other for a given target energy (see Appendix C for individual test results). Additionally, irrespective of compactive effort, the torsional strength of these sands are within

+/- 10 kPa, indicating that the torsional or shear resistance of SP material is more defined by the confining pressure than the energy applied or internal fabric. Further, Figure 27 illustrates that the strain corresponding to the peak strength (shown in time on Figure 27) is the same and independent of sample type (SDA or SDB) and energy.

Figure 27. Shear stress curves for SDA and SDB at a confining pressure of 150 kPa, reconstituted with compaction efforts of 200, 400, and 600 kJ/m³.

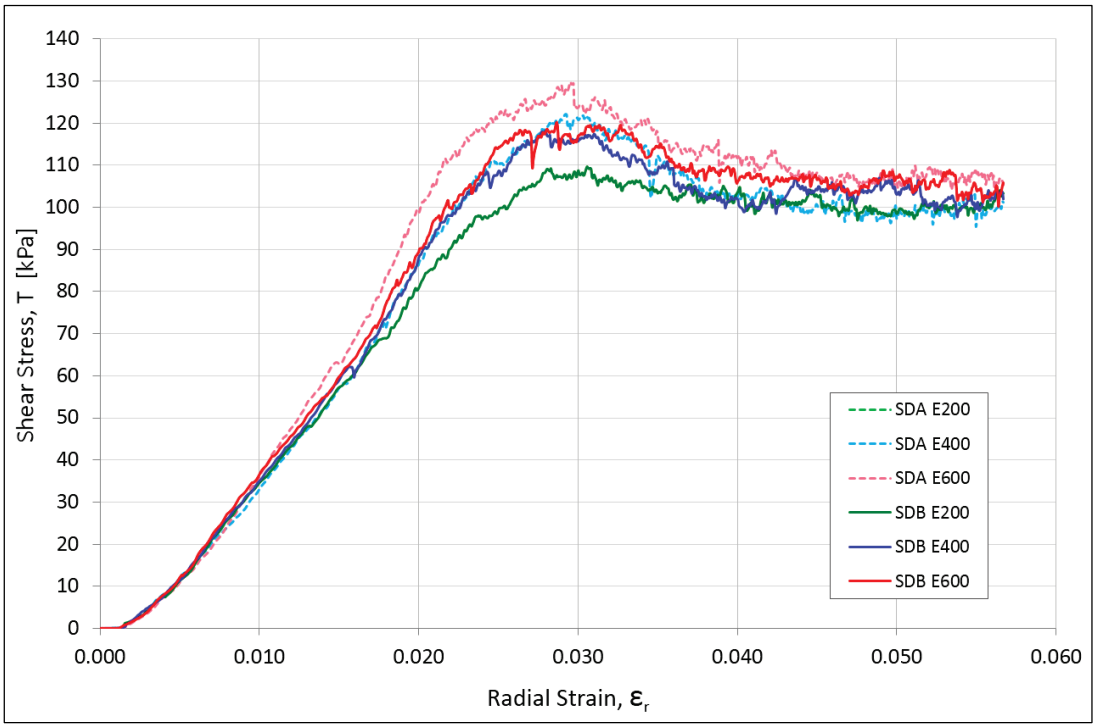

To investigate sample reconstitution repeatability in respect to cyclic loading, SDA was tested $ACD_{CYC,RS}$ (see Figure 28). Note that each test is offset by 1 deg of angular rotation for illustrative purposes; see Appendix C for individual test results. From Figure 28, it is observed that each test sample performed almost identically and that the protocol presented herein is applicable to both monotonic and cyclic loading investigations.

Figure 28. Hysteresis curves for SDA reconstituted at compactive efforts of 600, 800, and 1150 kJ/m³ (normalized and offset for viewing purposes).

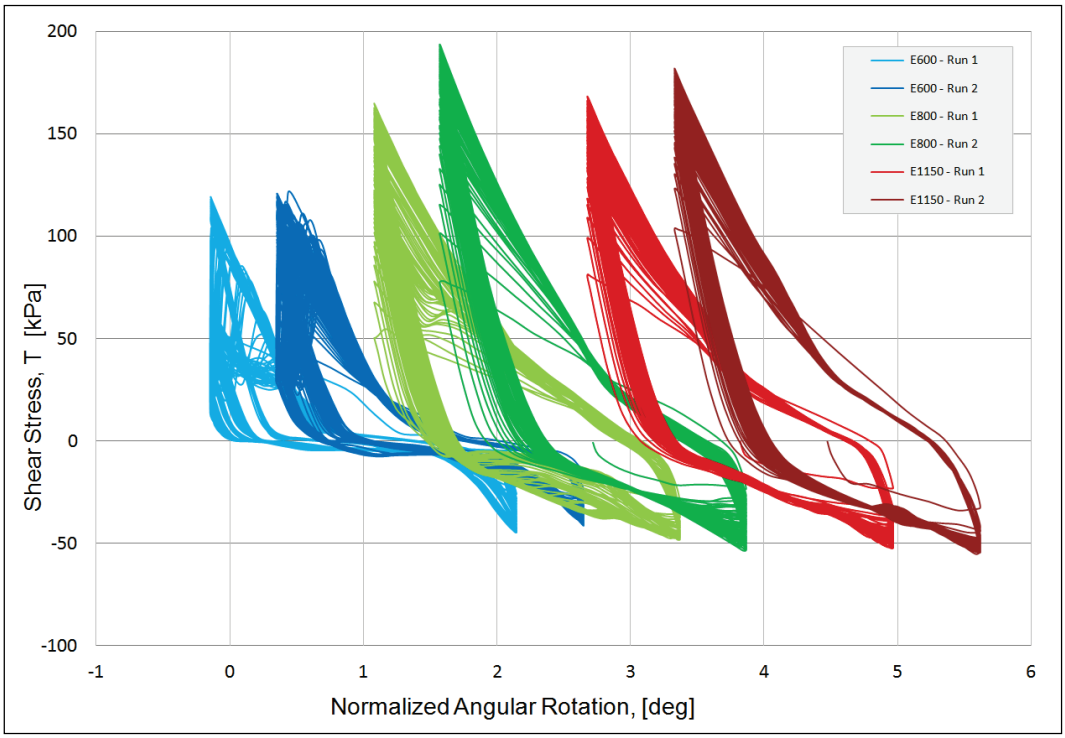

6.3 Hollow-core testing

ICD_{HC} tests were conducted on SDA and SDB over a range of compactive efforts from 200 to 1000 kJ/m³ via the normalized density approach. Each test specimen behaved almost identically in all cases both in terms of peak strength and stress-strain behavior (Figure 29). Individual test results are in Appendix D. The behavior of the same continuum sample under isotropic torsional loading conditions (Figure 29) exhibits strain-hardening behavior while under anisotropic conditions there is distinct strain-softening behavior (Figure 27). The isotropic torsional strength is approximately 63% of that from the anisotropic condition.

Figure 29. Hollow-core test stress-strain curves for SDA and SDB at a confining pressure of 100 kPa. Each depicted line represents the best fit for three tests at each soil-energy combination in the legend.

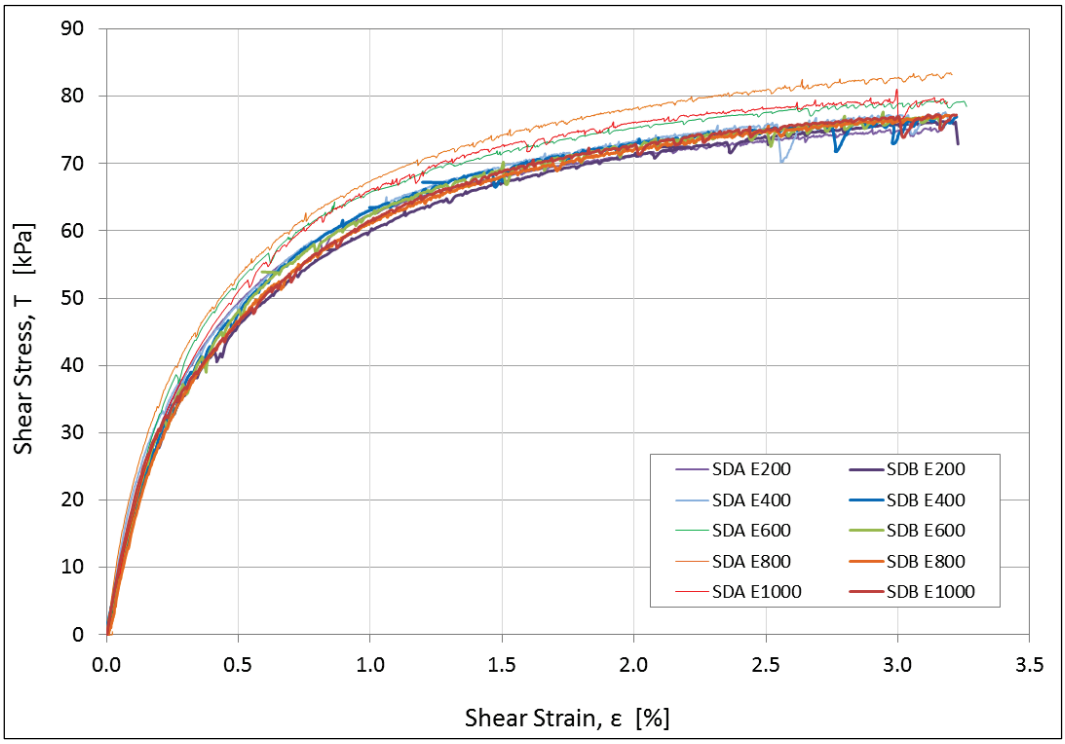

6.4 Simple shear testing

ICDSS tests were conducted on SDA and SDB over a range of compactive efforts equivalent to those of the ICDTX tests and normalized by the normalized density approach (Figure 30). Individual test results are in Appendix E. The results are comparable to the ICDHC tests in terms of both behavior (strain-softening) and peak shear strength. Similar to the ACDRS results, the range of peak shear strength is within +/- 15 kPa irrespective of compaction effort further evidencing that the shear resistance of these materials is not a function of the internal fabric but rather the applied confining pressures.

Figure 30. Simple shear test stress-strain curves for SDA and SDB at a confining pressure of 100 kPa and reconstituted with compaction efforts of 200, 400, 600, 800, and 1000 kJ/m³.

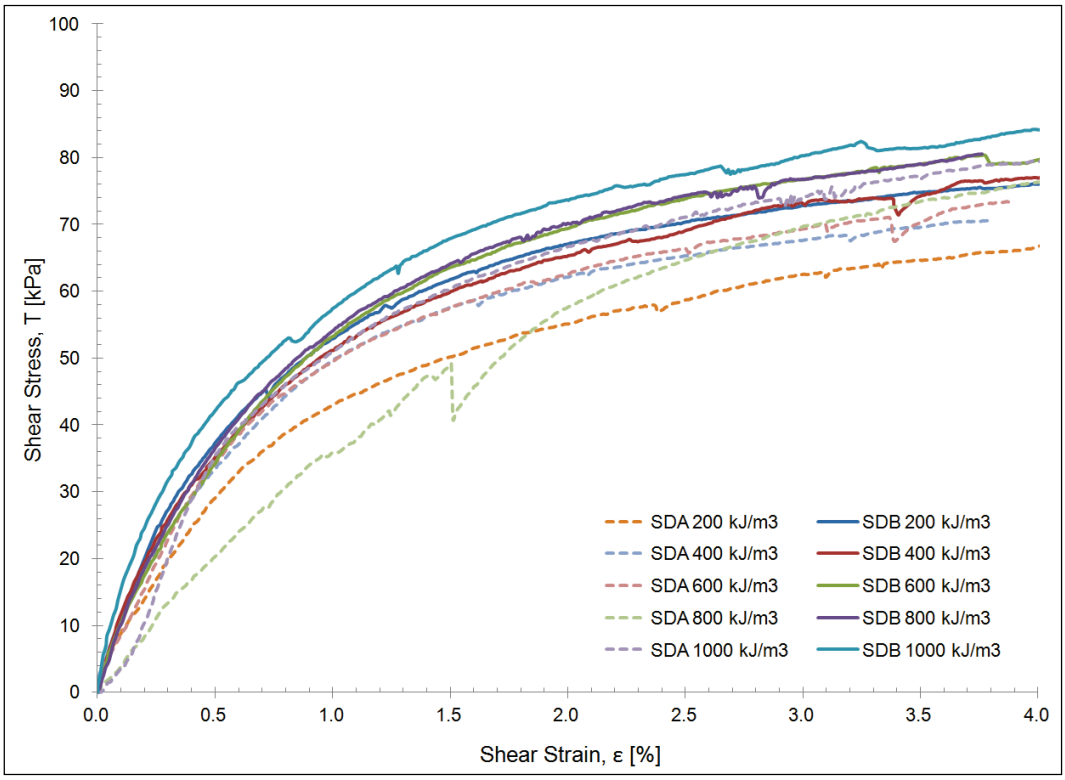

7 Conclusions

7.1 Summary of findings

The focus of this research was to develop a standardized protocol for specimen preparation that will enable the use of soil strength curves based on expedient field classification testing (e.g., grain-size analyses) using a normalization approach to sample preparation that replaces the common relative density method for evaluating the strength of soils. This research was centered around using an equivalent energy to prepare consistent, highly repeatable test samples instead of relying on relative density methods.

The data presented herein show that two similar materials can obtain comparable continuum behavior in laboratory settings when sample construction follows normalized density/relative energy procedures. This reduces reliance on soil-specific sampling and testing. In addition, the concepts presented can be applied to the preparation and analysis of reconstituted test specimens using other cohesionless materials.

With respect to the shear strength of the material, the internal fabric strength appears to have a minimal influence on the shear resistance. The range of peak resistance varies by approximately +/- 10 kPa torsionally to +/- 80 kPa axially over a range of compactive efforts of 200 to 1150 kJ/m^3 at the same confining pressures. The global shear behavior of the fabric changes from strain hardening to strain softening for isotropic and anisotropic conditions, respectively.

Continuation of this work will result in generalized material strength curves that will make it possible to rapidly integrate indigenous (local) materials into force protection measures and produce cost savings analyses without the need for extensive laboratory testing, soil sampling, and/or engineered fill materials. Specifically, the findings will allow engineers to reduce performance factors for LRFD analysis/designs by significantly reducing epistemic uncertainty and variability in determination of peak strength and stress/strain behavior in cohesionless soils. These generalized material strength curves will also provide a basis for expedient engineering designs and assessments as to the local soil capacity. Finally, the broadest impact of this work is that the methods

outlined herein will increase repeatability and confidence in laboratory testing and critically important investigations of soil behavior in low to zero confining pressure environments.

7.2 Condensed sample preparation procedure

The following is the condensed protocol for cohesionless sample preparation. Each step is referenced to an appropriate section in this report for further detail. As noted in the report, all steps may not be required depending on material or testing protocol. However, all steps need to be considered prior to sample reconstitution.

1. Determine the grain-size distribution of the test materials. (Section 2.2)
2. Develop compaction curves for the test materials by conducting ASTM Standard Modified Proctor Tests. (Sections 2.4-2.7)
3. Choose a target reconstituted saturation. (Section 3.1)
4. Normalize the dry density of the test materials based on the target saturation. (Section 3.2)
5. Determine number of layers in the specimen, number of blows per layer, rammer weight and drop height, and size of hammer base. (Section 3.3)
6. Calculate the equivalent energy (when required) for the hammer-to-sample ratio, HSR. (Section 3.4)
7. Make adjustments to the equivalent energy when testing non-cylindrical solid specimens. (Section 4.2)
8. Calculate (1) the amount of water to mix with the oven-dried material to obtain the desired S_R, (2) the amount of material to add per layer, and (3) the tamping energy per drop, adjusted for undercompaction. (Section 3.5)
9. Mix the test material and water, following strictly the calculated amounts of each. Allow appropriate time for saturation uniformity post batch preparation. Batch material must be sealed in an airtight container to prevent moisture loss.
10. Build the reconstituted test specimen following strictly the amount of material calculated per layer and the rammer drop heights required to achieve the target compactive effort. Note that all other sample properties, void ratio, permeability, density, etc., are byproducts of the energy-based compaction protocol.

References

ASTM C136/C136M-14. 2014. Standard test method for sieve analysis of fine and coarse aggregates. In *Annual book of ASTM standards*. West Conshohocken, PA: ASTM International.

ASTM D698-12e2. 2012. Standard test methods for laboratory compaction characteristics of soil using standard effort (12,400 ft-lbf/ft^3 [600 kN-m/m^3]). In *Annual book of ASTM standards*. West Conshohocken, PA: ASTM International.

ASTM D1557-12e1. 2012. Standard test methods for laboratory compaction characteristics of soil using modified effort (56,000 ft-lbf/ft^3 [2,700 kN-m/m^3]). In *Annual book of ASTM standards*. West Conshohocken, PA: ASTM International.

ASTM D2487-11. 2011. Standard practice for classification of soils for engineering purposes (Unified Soil Classification System). In *Annual book of ASTM standards*. West Conshohocken, PA: ASTM International.

ASTM D4253-14. 2014. Standard test methods for maximum index density and unit weight of soils using a vibratory table. In *Annual book of ASTM standards*. West Conshohocken, PA: ASTM International.

ASTM D4254-14. 2014. Standard test methods for minimum index density and unit weight of soils and calculation of relative density. In *Annual book of ASTM standards*. West Conshohocken, PA: ASTM International.

ASTM D7181-11. 2011. Standard test method for consolidated drained triaxial compression test for soils. In *Annual book of ASTM standards*. West Conshohocken, PA: ASTM International.

Bradshaw, A., and C. Baxter. 2007. Sample preparation of silts for liquefaction testing. *Geotechnical Testing Journal* 30:324-332.

DeGregorio, V. B. 1990. Loading systems, sample preparation, and liquefaction. *Journal of Geotechnical Engineering* 116:805-821.

Holtz, R. D., W. D. Kovacs, and T. C. Sheehan. 2011. *An introduction to geotechnical engineering*. Upper Saddle River, NJ: Pearson.

Huang, Y., H. L. Cheng, T. Osada, A. Hosoya, and A. Zhang. 2015. Mechanical behavior of clean sand at low confining pressure: Verification with element and model tests. *Journal of Geotechnical and Geoenvironmental Engineering* 141.

Ladd, R. S. 1974. Specimen preparation and liquefaction of sands. *Journal of the Geotechnical Engineering Division* 100:1180-1184.

Ladd, R. S. 1977. Specimen preparation and cyclic stability of sands. *Journal of the Geotechnical Engineering Division* 103:535-547.

Ladd, R. S. 1978. Preparing test specimens using undercompaction. *Geotechnical Testing Journal* 1:16-23.

Mulilis, J. P., H. B. Seed, and C. K. Chan. 1977. Effects of sample preparation on sand liquefaction. *Journal of the Geotechnical Engineering Division* 103:91-108.

Mulilis, J. P., F. C. Townsend, and R. C. Horz. 1978. Triaxial testing techniques and sand liquefaction. In *Dynamic geotechnical testing*. ASTM STP 654. West Conshohocken, PA: ASTM International.

Peck, R. B., W. E. Hanson, and T. H. Thornburn. 1953. *Foundation engineering*. New York, NY: John Wiley & Sons.

Sandrekarimi, A., and S. M. Olson. 2012. Effect of sample-preparation method on critical-state behavior of sands. *Geotechnical Testing Journal* 35:1-12.

Sowers, G. B., and G. F. Sowers. 1951. *Introductory soil mechanics and foundations*. New York, NY: Macmillan.

Taylor, O. S. 2011. Use of an energy-based liquefaction approach to predicting deformation in silts due to pile driving. PhD diss., University of Rhode Island.

Taylor, O. S., C. D. Baxter, A. S. Bradshaw, and A. C. Morales. 2012. New density normalization approach for evaluation of the cyclic resistance of silts. In *GeoCongress 2012, 25-29 March, Oakland, California,* 809-818.

Wanatowski, D., and J. Chu. 2008. Effect of specimen preparation method on the stress-strain behavior of sand in plane-strain compression tests. *Geotechnical Testing Journal* 31:1-13.

Appendix A: Terminology

Area of the reference hammer base, A_{RH} - The area of a 95-mm-diameter compaction hammer base (7088 mm^2).

Area of the reference specimen, A_{RS} - The area of a 152-mm-diameter specimen (18,146 mm^2).

Area of the hammer base, A_H - The area of the compaction hammer base being used for the sample reconstitution.

Blow, b – Refers to a single drop of the rammer weight on the compaction hammer, transferring the resultant energy to the specimen.

Coefficient of Curvature, C_c – The grain-size distribution shape parameter based on D_{10}, D_{30}, and D_{60}.

Coefficient of Uniformity, C_u — The grain-size distribution shape parameter based on D_{60} and D_{10}.

Dry density, ρ_d (g/cm^3) – The ratio of the mass of the solid phase of the soil to its total volume.

Density of water, ρ_w – The mass per unit volume of water (1 g/cm^3).

Drop height, h - The height at which the rammer free falls, starting from the compression ring secured around the rod to the strike plate. This distance is adjusted depending on the amount of energy to be applied per drop.

Energy, E (kJ/m^3) – Amount of compactive effort per unit volume imparted on a specimen by the compaction hammer.

Equivalent Energy, E_{eq} – A relative compactive effort per unit volume as compared to the hammer/specimen diameter ratio of an ASTM Standard Modified Proctor test.

Hammer – The tool used to apply the compactive energy to the specimen; consists of a free-falling weight connected to a rod that has a cylindrical acrylic base.

Hammer Base – The acrylic plate attached to the bottom of the compaction hammer where the energy is imparted to the specimen.

HSR – Hammer to Sample Ratio, the ratio of the hammer base area to sample area. The reference HSR for this study is 0.39 calculated by π 0.25 (95 mm)^2/ π 0.25 (152.4 mm)^2.

Mass per layer, m_L (g) – The amount of material required to add a single layer when building a reconstituted specimen.

Mass of rammer, m_R (g) – The mass of the hammer's free falling weight.

Maximum dry density, $\rho_{d,max}$ (g/cm^3) – The dry density of a material obtained from a Modified Proctor compaction test using 2707 kJ/m^3 of compactive effort.

Moisture content, ω (%) – The weight of water divided by weight of dry solids.

Normalized density, ρ_N (unitless) – The ratio of a material's density and maximum dry density.

Number of layers, N – The number of layers in the specimen.

Optimal dry density, ρ_{opt} (g/cm^3) – The maximum dry density at a given energy determined from a compaction curve.

Optimal moisture content, ω_{opt} (%) – The moisture content corresponding to the maximum dry density determined from a compaction curve.

Rammer – the free-falling weight of the compaction hammer; as the weight falls to the strike plate, the energy is transferred through the hammer base into the soil.

Reconstitution Saturation, S_R – The saturation required during sample reconstitution to achieve the desired soil fabric.

Reference Energy, E_R – The energy applied to a specimen using a 95mm/152mm hammer to sample ratio (HSR).

Relative Density, D_r (%) – Compares the void ratio of a given sample to the maximum and minimum void ratios of that material.

Saturation, S – Refers to the ratio of the volume of water to the volume of voids in the sample.

Testing Saturation – The saturation of the sample specimen at the point of testing, e.g., consolidation and shear.

Void ratio, e (unit-less) – The volume of voids divided by the volume of solids

Volume, V (m^3) – The target volume of the specimen.

Volume of layer, V_L (m^3) – The volume of a single layer in a reconstituted specimen.

Appendix B: Triaxial Test Data

Test No.	ENERGY	HEIGHT		DRY DENSITY			AT FAILURE					
				Target	Actual	% Error	σ_d	CP	U_w	ε_a	ε_r	ε_v
	kJ/m3	Final	% of Target	ρ_d , g/cc	ρ_d , g/cc	%	kPa	kPa	kPa	%	%	%
SDA TX1	85	305.36	101.8%	1.650	1.615	2.1%	361	101	1	2.127	0.006	-0.304
SDA TX2	200	295.30	98.4%	1.650	1.654	-0.2%	426	104	4	2.365	0.004	-0.349
SDA TX3	200	297.60	99.2%	1.650	1.641	0.5%	411	105	5	2.588	0.003	-0.341
SDA TX4	400	294.55	98.2%	1.663	1.672	-0.5%	452	100	0	2.580	0.004	-0.170
SDA TX5	400	297.29	99.1%	1.669	1.678	-0.5%	424	100	0	2.232	-0.003	-0.261
SDA TX6	400	295.62	98.5%	1.669	1.685	-1.0%	451	100	0	2.544	-0.003	-0.305
SDA TX7	600	296.96	99.0%	1.679	1.675	0.2%	467	101	1	3.066	0.004	-0.148
SDA TX8	600	296.15	98.7%	1.680	1.696	-1.0%	462	100	0	2.179	-0.004	-0.355
SDA TX9	687	297.85	99.3%	1.706	1.708	-0.1%	480	100	0	2.154	0.002	-0.448
SDA TX10	800	296.23	98.7%	1.687	1.704	-1.0%	482	100	0	2.567	0.007	-0.493
SDA TX11	800	294.90	98.3%	1.687	1.712	-1.5%	480	100	0	2.627	-0.001	0.135
SDA TX12	800	296.16	98.7%	1.687	1.709	-1.3%	462	101	0	2.624	-0.002	-0.426
SDA TX13	1000	295.54	98.5%	1.693	1.715	-1.3%	481	100	0	2.864	0.000	-0.389
SDA TX14	1100	295.87	98.6%	1.696	1.712	-0.9%	471	100	0	2.627	-0.004	-0.405
SDA TX15	1200	296.60	98.9%	1.698	1.713	-0.9%	477	100	0	2.578	0.004	-0.381
SDA TX16	1600	298.33	99.4%	1.706	1.711	-0.3%	479	101	1	2.578	0.006	-0.569
SDA TX17	1600	297.19	99.1%	1.706	1.717	-0.6%	508	101	1	2.390	0.004	-0.173
SDB TX1	85	301.08	100.4%	1.744	1.736	0.5%	386	100	0	1.609	0.000	0.060
SDB TX2	200	297.29	99.1%	1.744	1.757	-0.7%	413	100	0	2.126	0.001	-0.186
SDB TX3	200	296.11	98.7%	1.744	1.761	-1.0%	440	101	1	2.444	-0.005	-0.156
SDB TX4	364	301.85	100.6%	1.803	1.790	0.7%	425	100	0	1.928	0.003	0.000
SDB TX5	400	295.21	98.4%	1.765	1.781	-0.9%	463	100	0	2.111	-0.003	-0.271
SDB TX6	400	297.41	99.1%	1.764	1.776	-0.7%	454	100	0	2.061	-0.006	-0.172
SDB TX7	600	299.81	99.9%	1.777	1.774	0.2%	477	100	0	2.165	0.003	-0.339
SDB TX8	600	298.07	99.4%	1.777	1.783	-0.3%	468	100	0	2.041	0.000	-0.214
SDB TX9	655	296.07	98.7%	1.790	1.810	-1.1%	460	100	0	1.545	0.001	-0.164
SDB TX10	800	296.14	98.7%	1.784	1.800	-0.9%	478	100	0	2.154	-0.002	-0.192
SDB TX11	800	295.59	98.5%	1.784	1.804	-1.1%	489	100	0	2.155	-0.008	-0.384
SDB TX12	800	296.15	98.7%	1.784	1.801	-1.0%	498	100	0	2.275	0.010	-0.231
SDB TX13	1000	295.27	98.4%	1.790	1.816	-1.5%	526	100	0	2.207	0.001	-0.182
SDB TX14	1048	295.77	98.6%	1.791	1.814	-1.3%	498	100	0	2.184	-0.002	-0.306
SDB TX15	1100	296.29	98.8%	1.793	1.813	-1.1%	491	100	0	1.934	-0.001	-0.237
SDB TX16	1200	295.76	98.6%	1.795	1.820	-1.4%	530	100	0	2.101	-0.005	-0.361
SDB TX17	1600	296.13	98.7%	1.803	1.821	-1.0%	531	100	0	2.136	0.004	-0.339

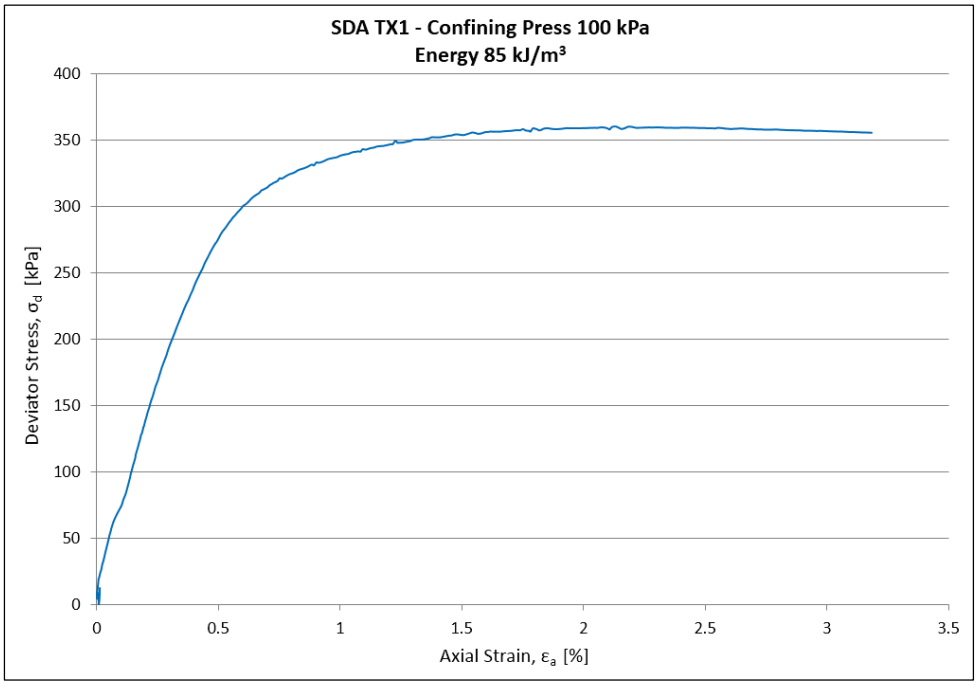

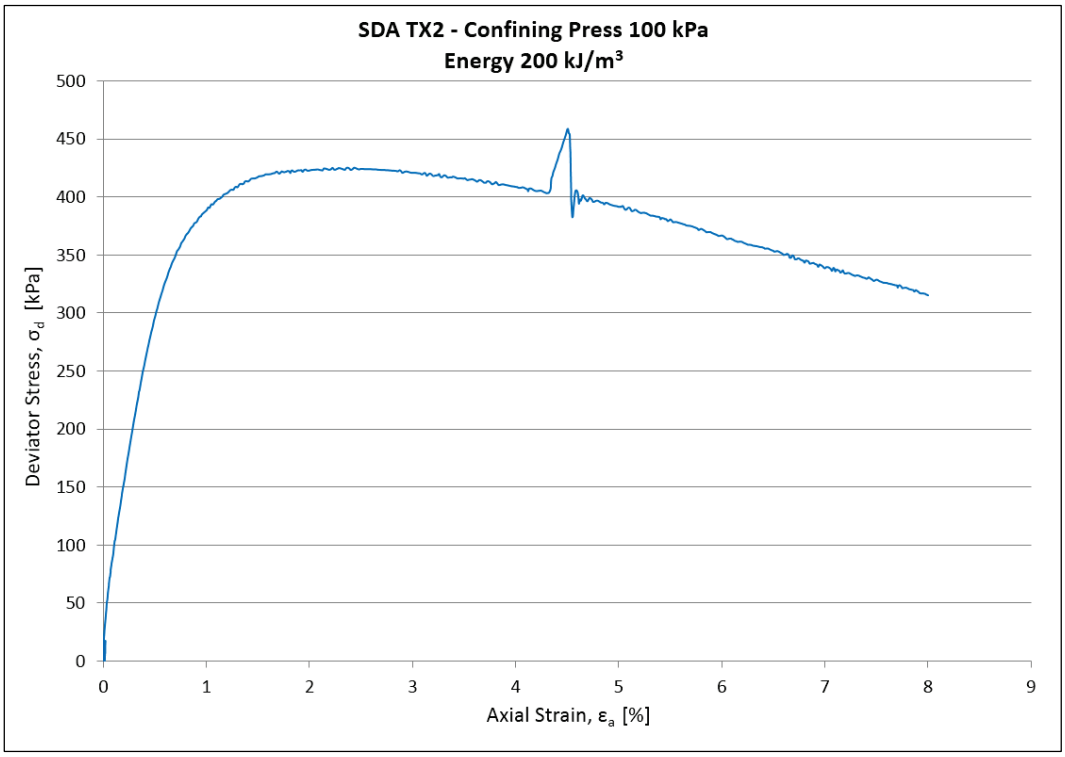
SDA TX2 - Confining Press 100 kPa
Energy 200 kJ/m³
Deviator Stress, σd [kPa]
Axial Strain, εa [%]
0
50
100
150
200
250
300
350
400
450
500
0
1
2
3
4
5
6
7
8
9

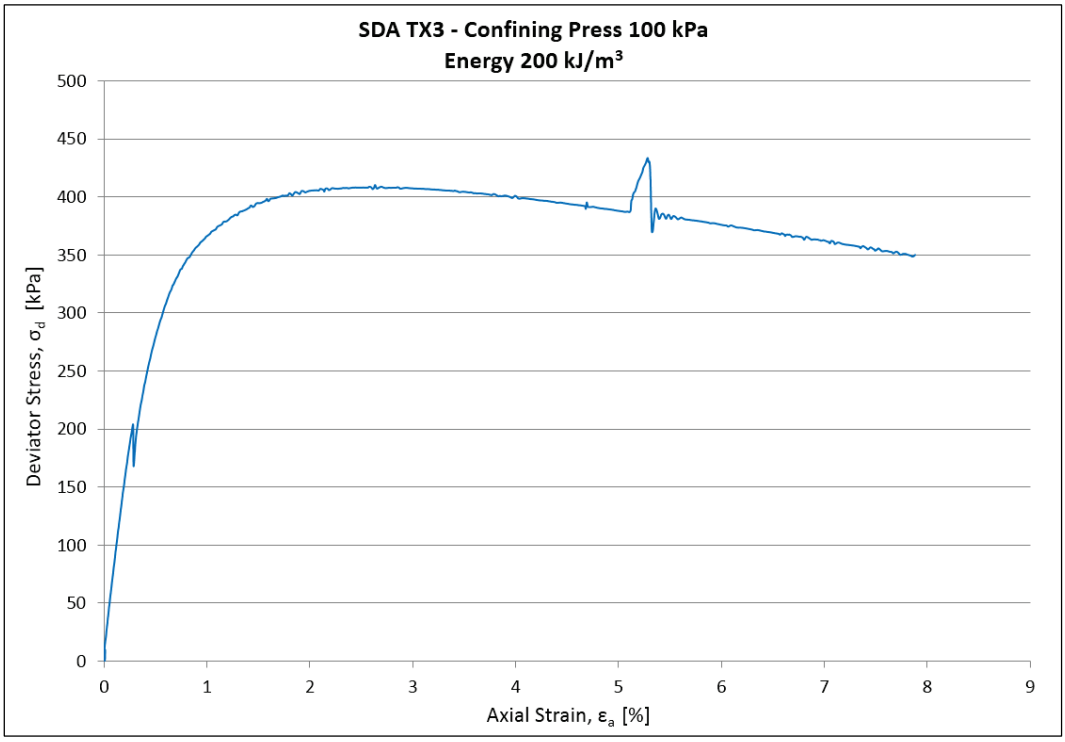
SDA TX3 - Confining Press 100 kPa
Energy 200 kJ/m³
Deviator Stress, σd [kPa]
Axial Strain, εa [%]
0
50
100
150
200
250
300
350
400
450
500
0
1
2
3
4
5
6
7
8
9

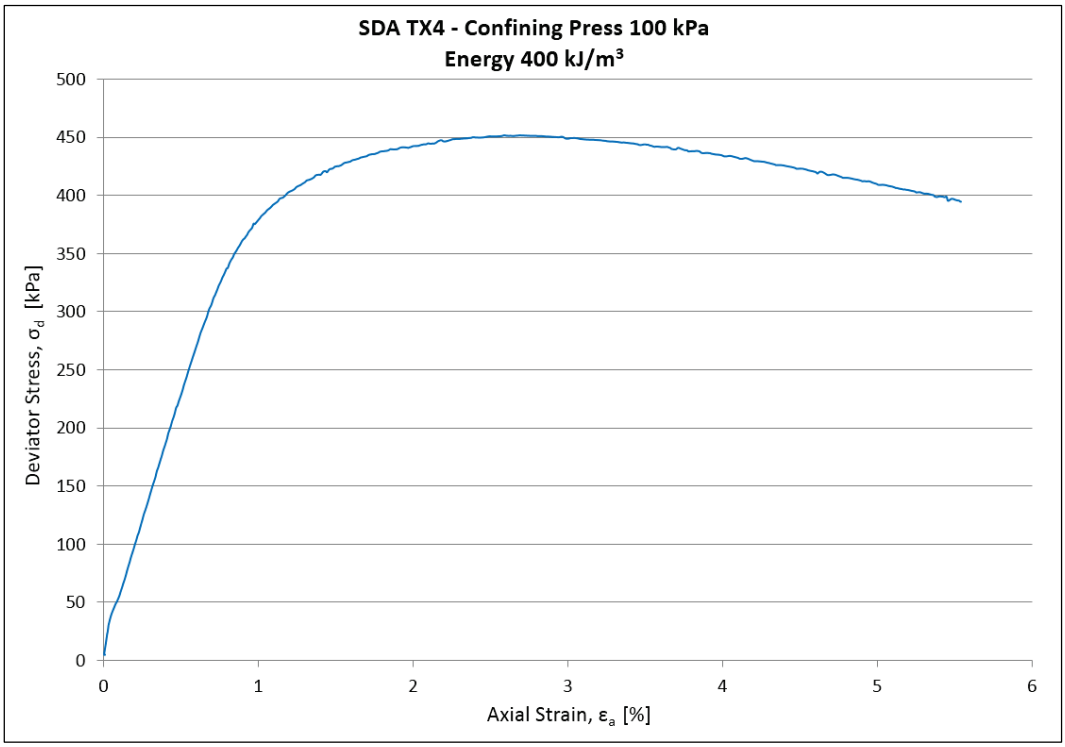
SDA TX4 - Confining Press 100 kPa
Energy 400 kJ/m³
Deviator Stress, σd [kPa]
0
50
100
150
200
250
300
350
400
450
500
0
1
2
3
4
5
6
Axial Strain, εa [%]

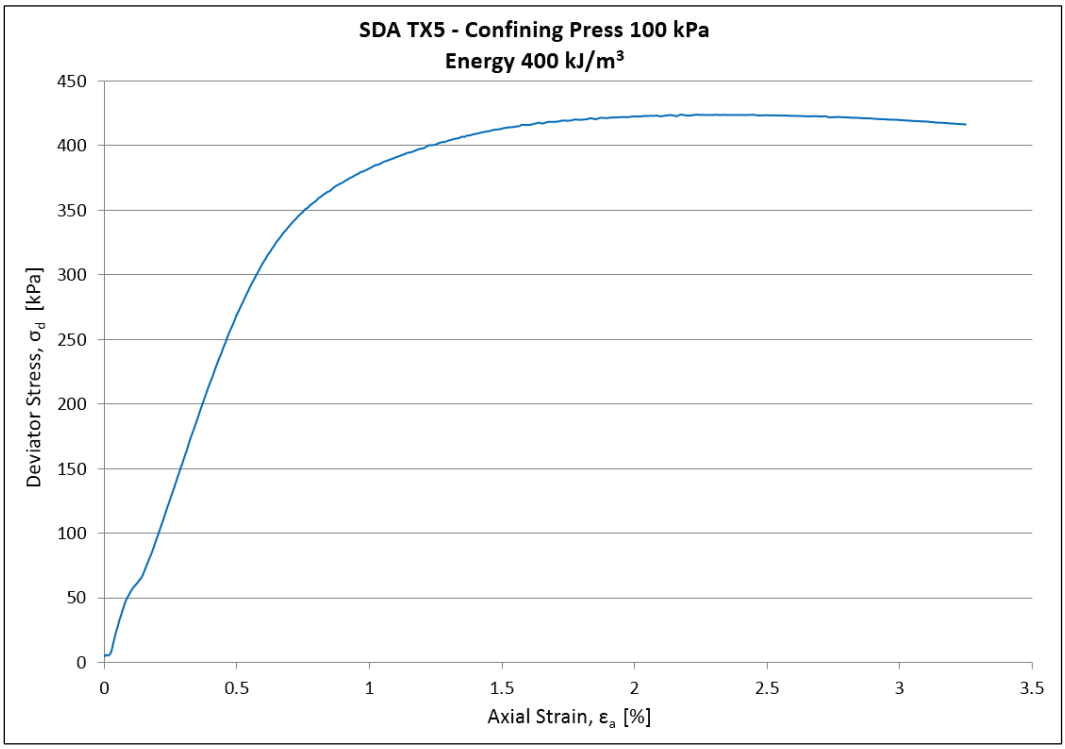
SDA TX5 - Confining Press 100 kPa
Energy 400 kJ/m³
Deviator Stress, σd [kPa]
0
50
100
150
200
250
300
350
400
450
0
0.5
1
1.5
2
2.5
3
3.5
Axial Strain, εa [%]

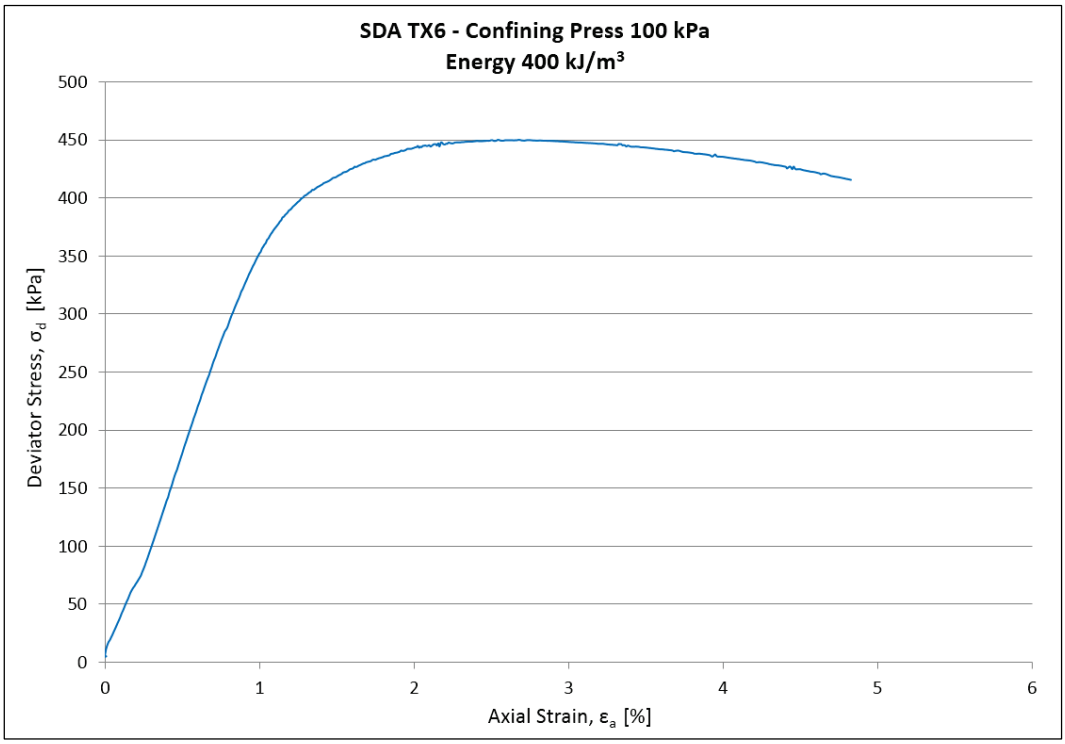
SDA TX6 - Confining Press 100 kPa
Energy 400 kJ/m³
Deviator Stress, σd [kPa]
0
50
100
150
200
250
300
350
400
450
500
0
1
2
3
4
5
6
Axial Strain, εa [%]

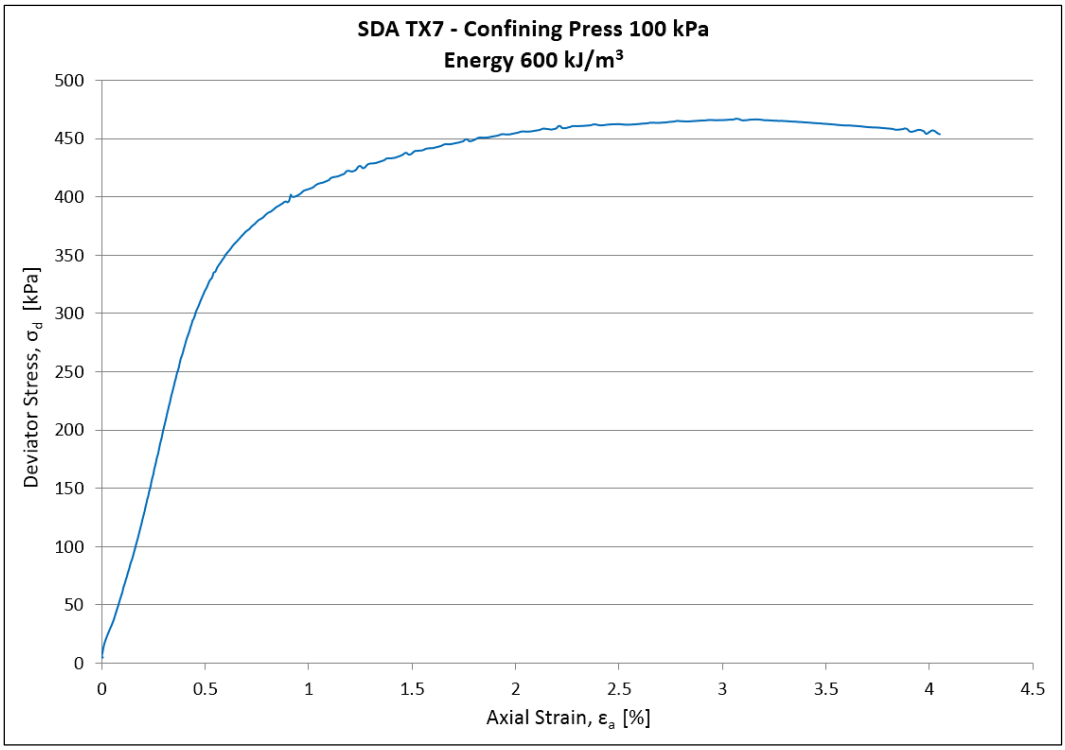
SDA TX7 - Confining Press 100 kPa
Energy 600 kJ/m³
Deviator Stress, σd [kPa]
0
50
100
150
200
250
300
350
400
450
500
0
0.5
1
1.5
2
2.5
3
3.5
4
4.5
Axial Strain, εa [%]

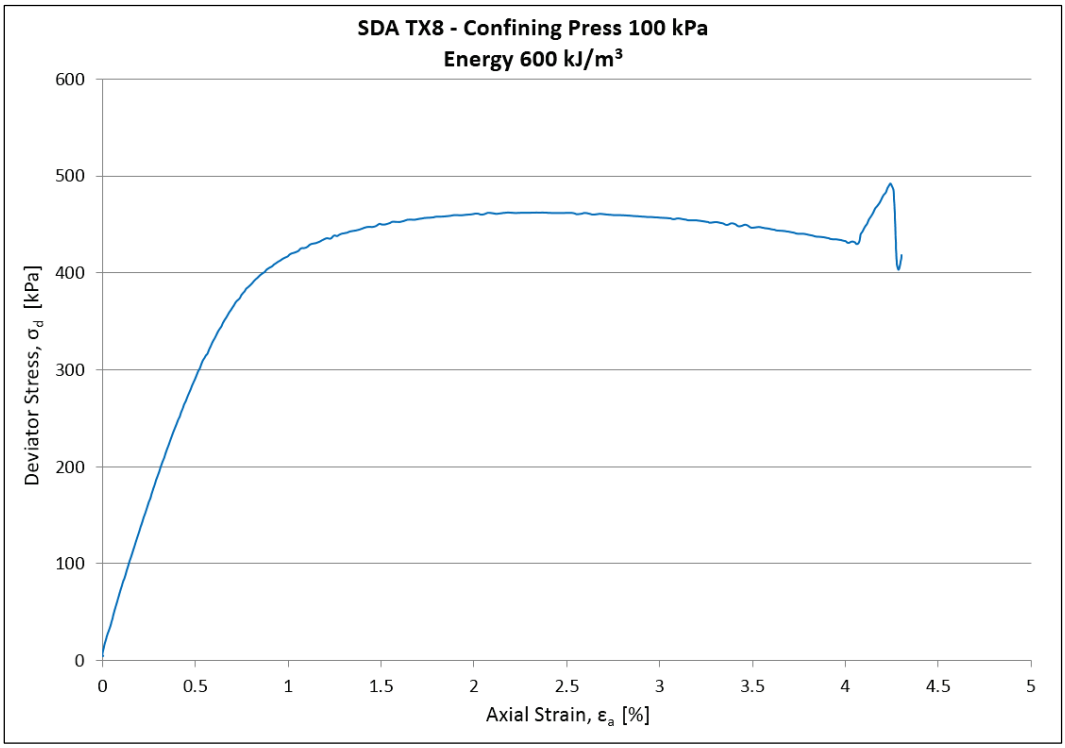
SDA TX8 - Confining Press 100 kPa
Energy 600 kJ/m³
Deviator Stress, σd [kPa]
600
500
400
300
200
100
0
0
0.5
1
1.5
2
2.5
3
3.5
4
4.5
5
Axial Strain, εa [%]

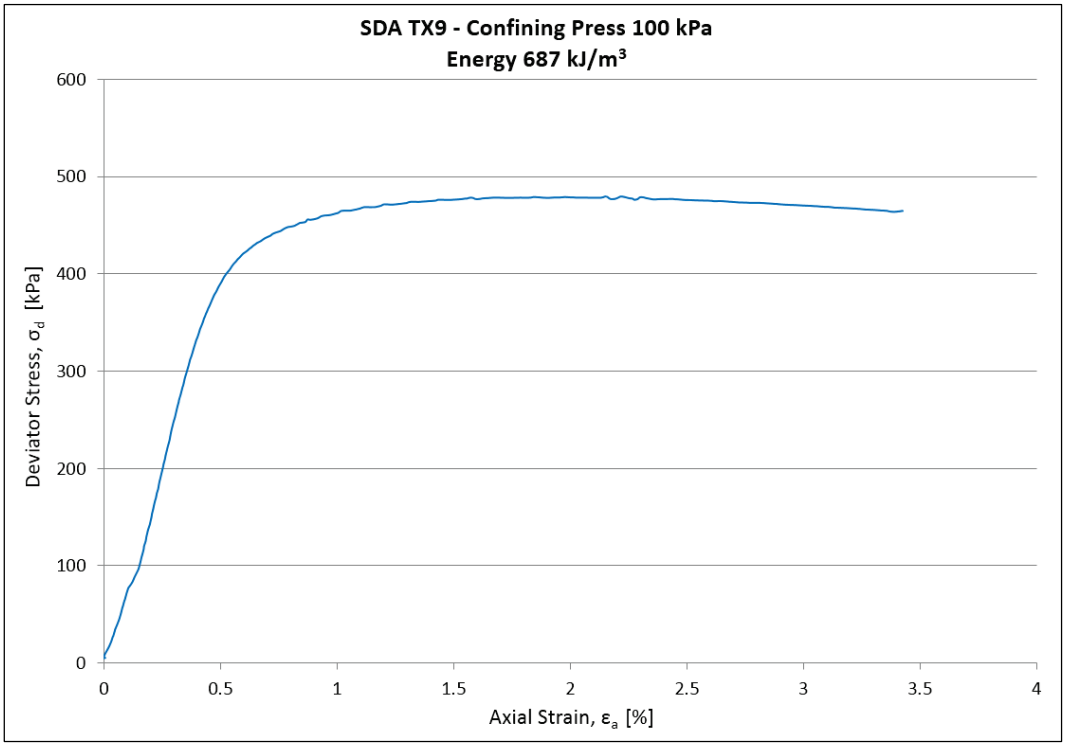
SDA TX9 - Confining Press 100 kPa
Energy 687 kJ/m³
Deviator Stress, σd [kPa]
600
500
400
300
200
100
0
0
0.5
1
1.5
2
2.5
3
3.5
4
Axial Strain, εa [%]

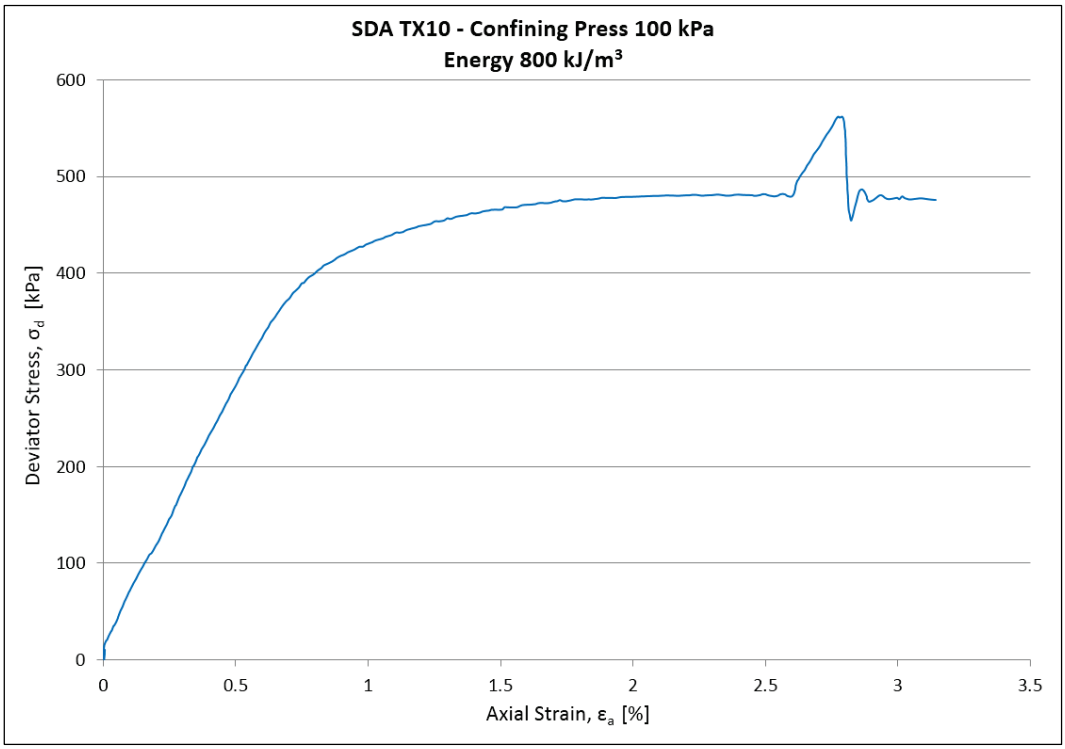
SDA TX10 - Confining Press 100 kPa
Energy 800 kJ/m³
Deviator Stress, σd [kPa]
Axial Strain, εa [%]
0
100
200
300
400
500
600
0
0.5
1
1.5
2
2.5
3
3.5

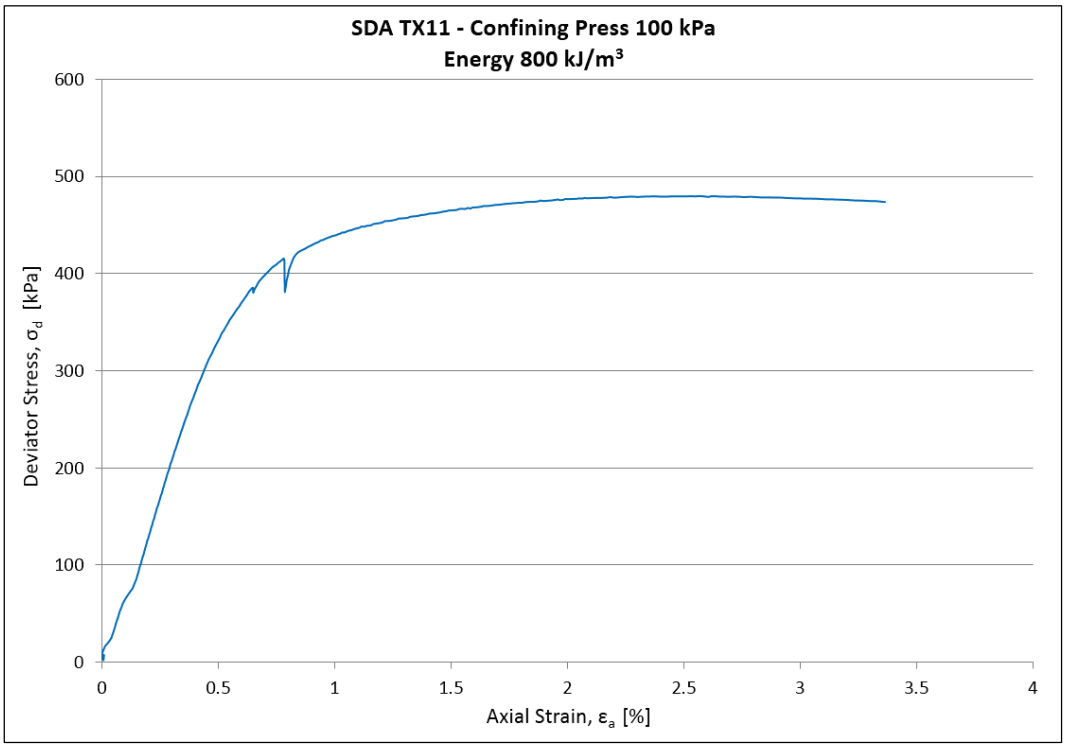
SDA TX11 - Confining Press 100 kPa
Energy 800 kJ/m³
Deviator Stress, σd [kPa]
Axial Strain, εa [%]
0
100
200
300
400
500
600
0
0.5
1
1.5
2
2.5
3
3.5
4

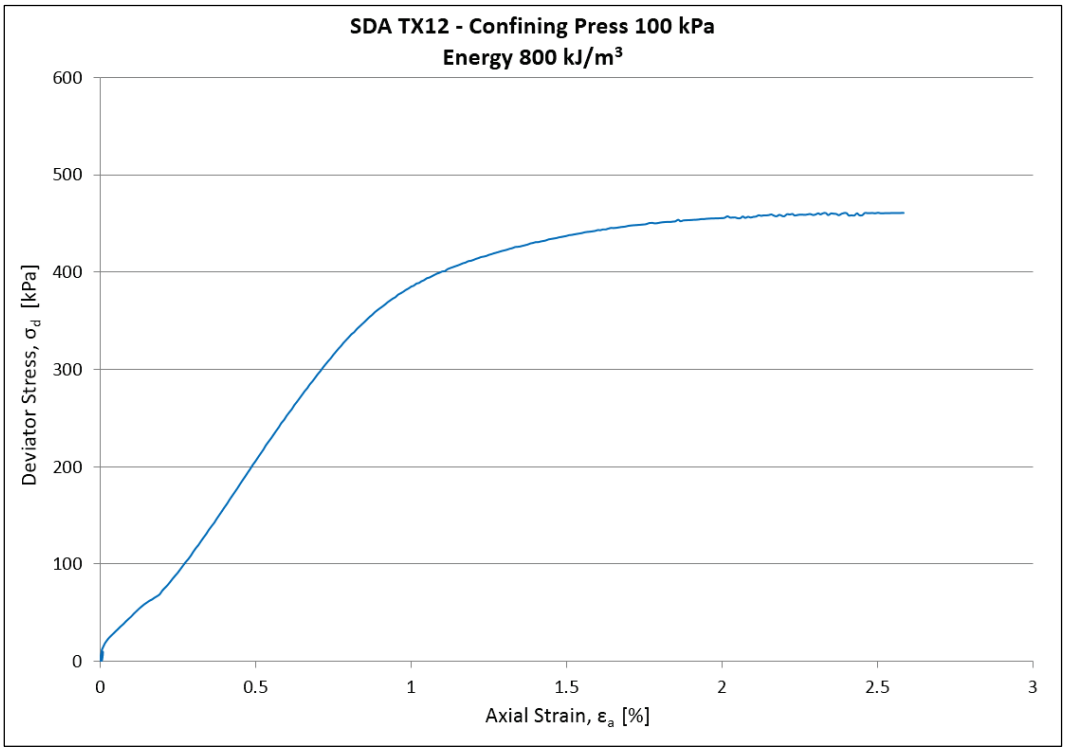
SDA TX12 - Confining Press 100 kPa
Energy 800 kJ/m³
Deviator Stress, σd [kPa]
600
500
400
300
200
100
0
0
0.5
1
1.5
2
2.5
3
Axial Strain, εa [%]

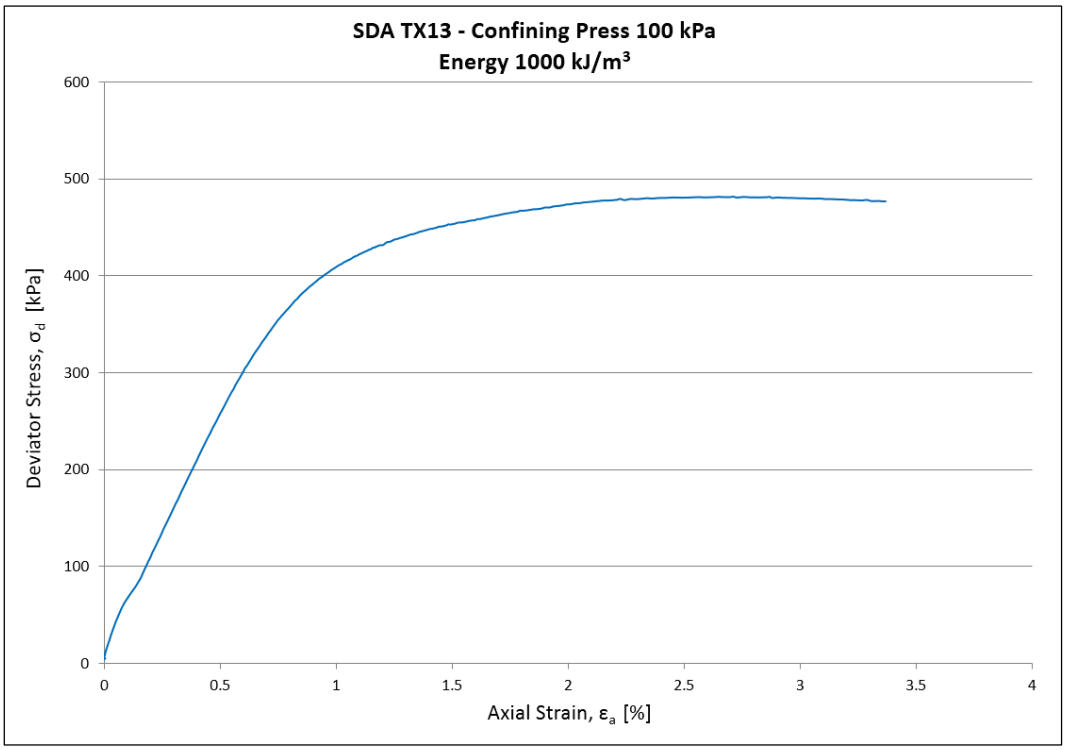
SDA TX13 - Confining Press 100 kPa
Energy 1000 kJ/m³
Deviator Stress, σd [kPa]
600
500
400
300
200
100
0
0
0.5
1
1.5
2
2.5
3
3.5
4
Axial Strain, εa [%]

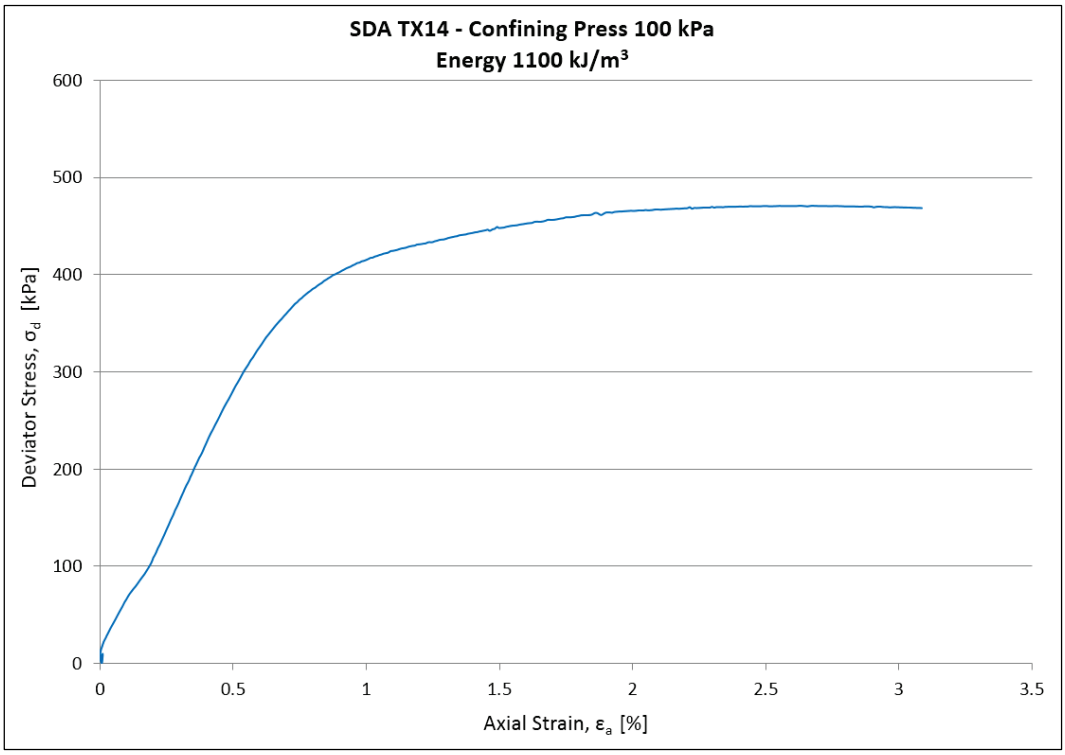
SDA TX14 - Confining Press 100 kPa
Energy 1100 kJ/m³
Deviator Stress, σd [kPa]
Axial Strain, εa [%]
0
100
200
300
400
500
600
0
0.5
1
1.5
2
2.5
3
3.5

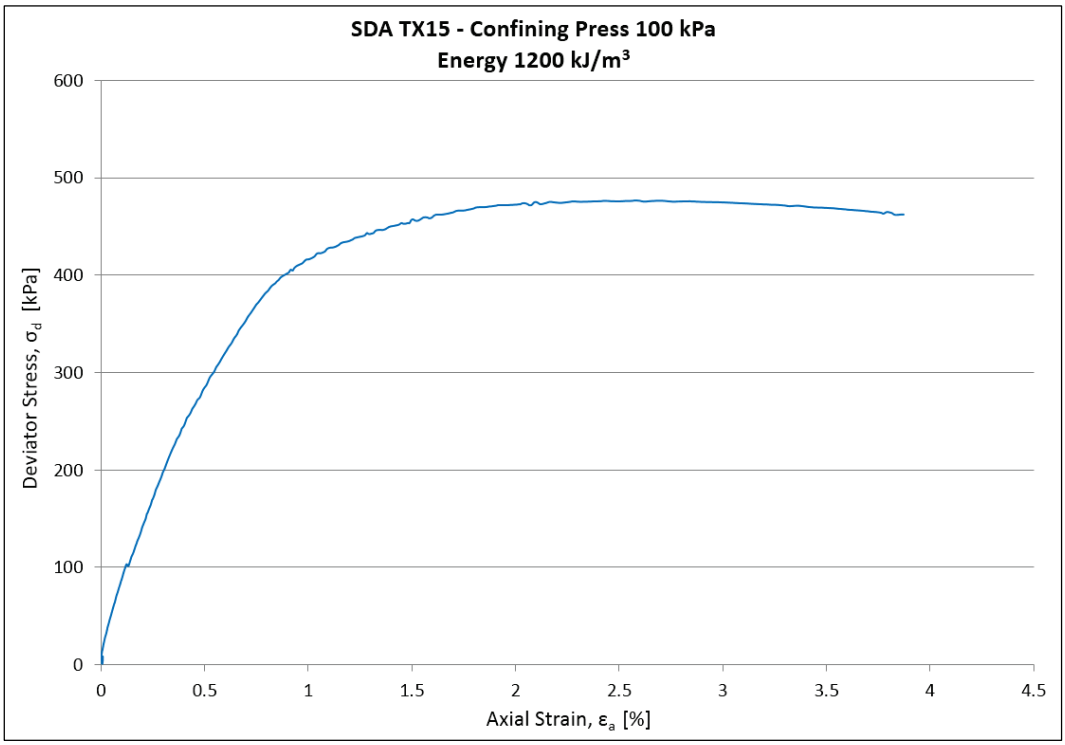
SDA TX15 - Confining Press 100 kPa
Energy 1200 kJ/m³
Deviator Stress, σd [kPa]
Axial Strain, εa [%]
0
100
200
300
400
500
600
0
0.5
1
1.5
2
2.5
3
3.5
4
4.5

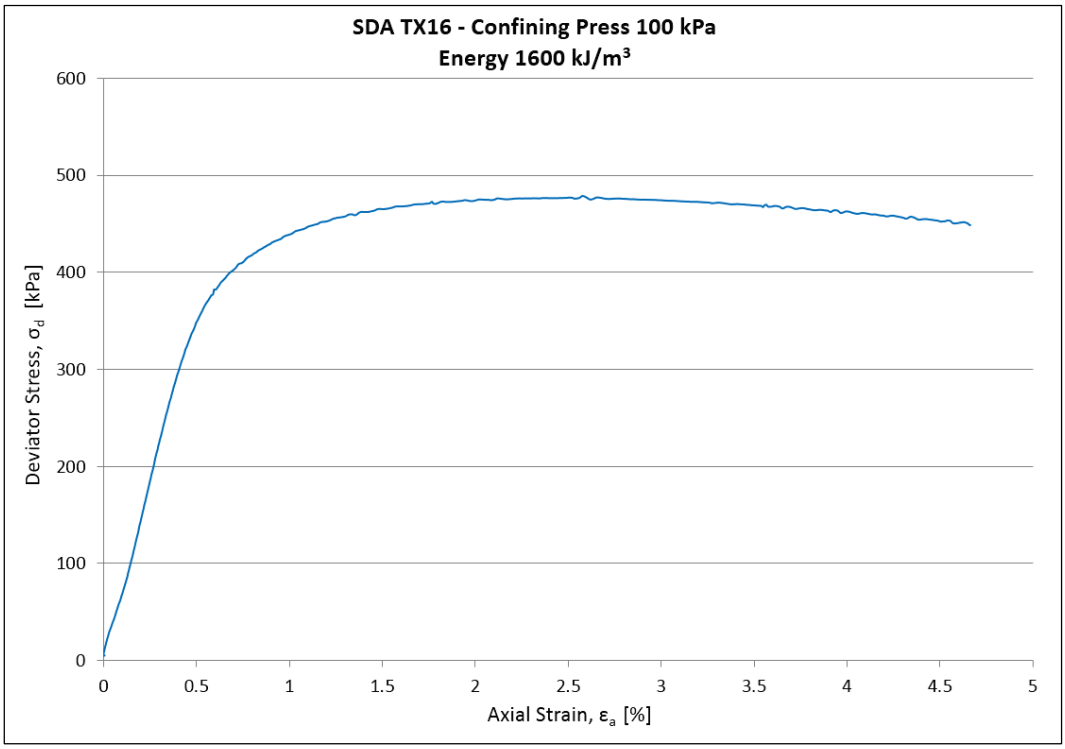
SDA TX16 - Confining Press 100 kPa
Energy 1600 kJ/m3
Deviator Stress, σd [kPa]
600
500
400
300
200
100
0
0
0.5
1
1.5
2
2.5
3
3.5
4
4.5
5
Axial Strain, εa [%]

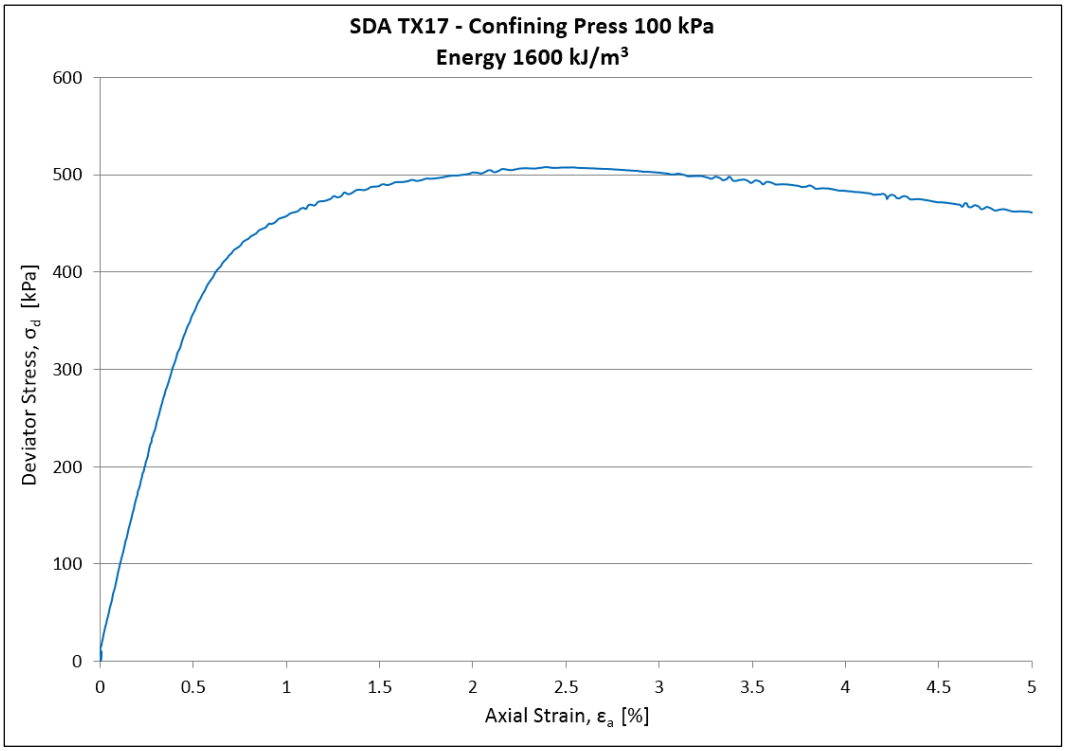
SDA TX17 - Confining Press 100 kPa
Energy 1600 kJ/m3
Deviator Stress, σd [kPa]
600
500
400
300
200
100
0
0
0.5
1
1.5
2
2.5
3
3.5
4
4.5
5
Axial Strain, εa [%]

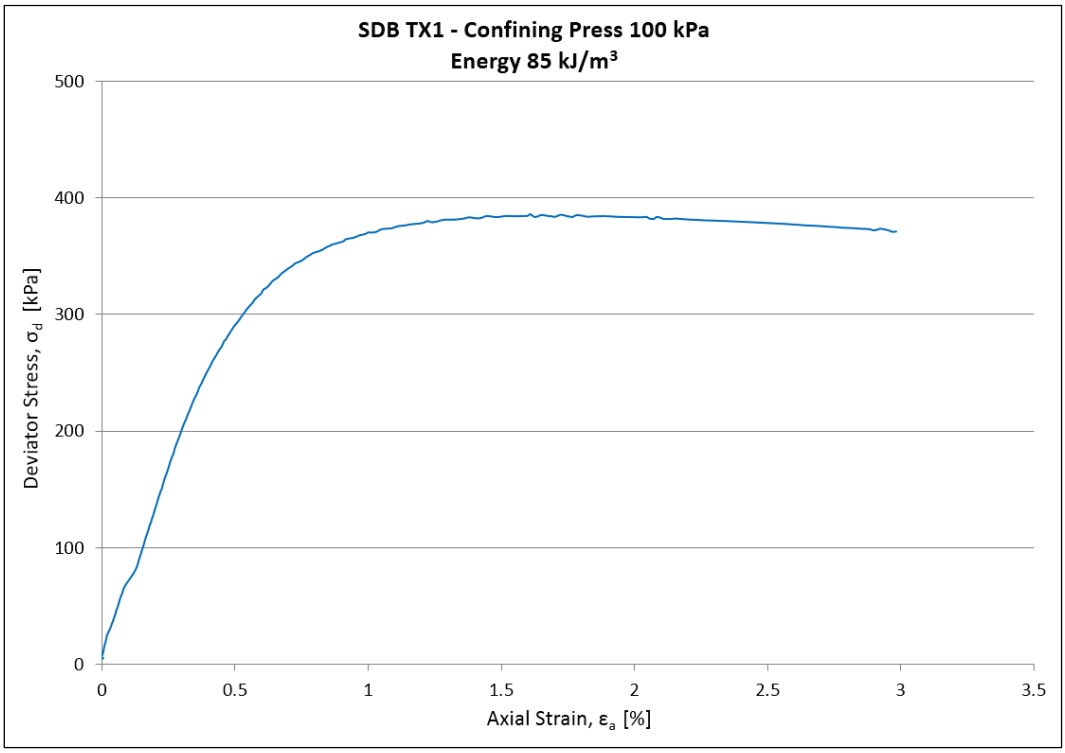
SDB TX1 - Confining Press 100 kPa
Energy 85 kJ/m³
Deviator Stress, σd [kPa]
0
100
200
300
400
500
0
0.5
1
1.5
2
2.5
3
3.5
Axial Strain, εa [%]

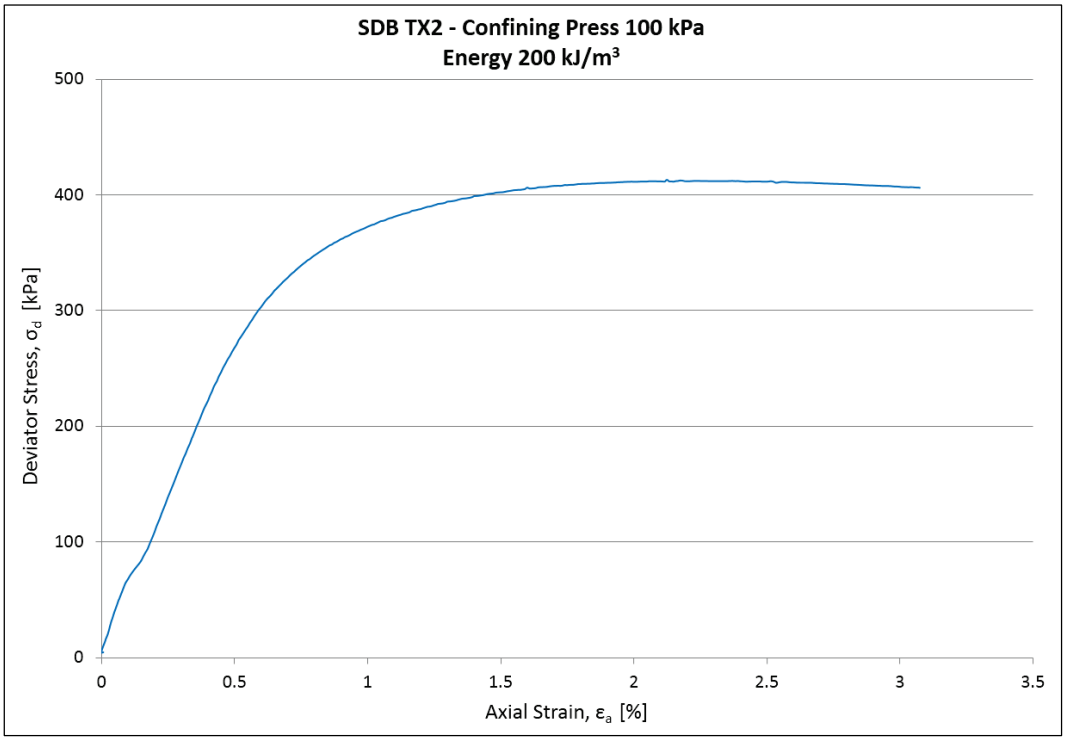
SDB TX2 - Confining Press 100 kPa
Energy 200 kJ/m³
Deviator Stress, σd [kPa]
0
100
200
300
400
500
0
0.5
1
1.5
2
2.5
3
3.5
Axial Strain, εa [%]

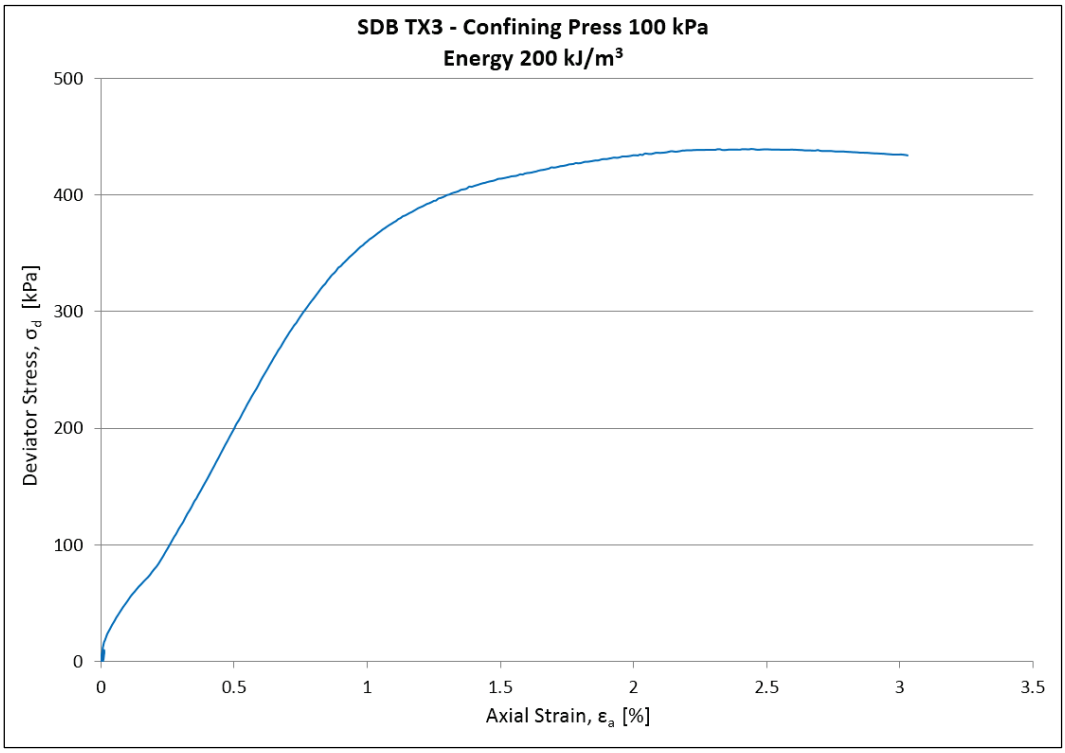
SDB TX3 - Confining Press 100 kPa
Energy 200 kJ/m³
Deviator Stress, σd [kPa]
0
100
200
300
400
500
0
0.5
1
1.5
2
2.5
3
3.5
Axial Strain, εa [%]

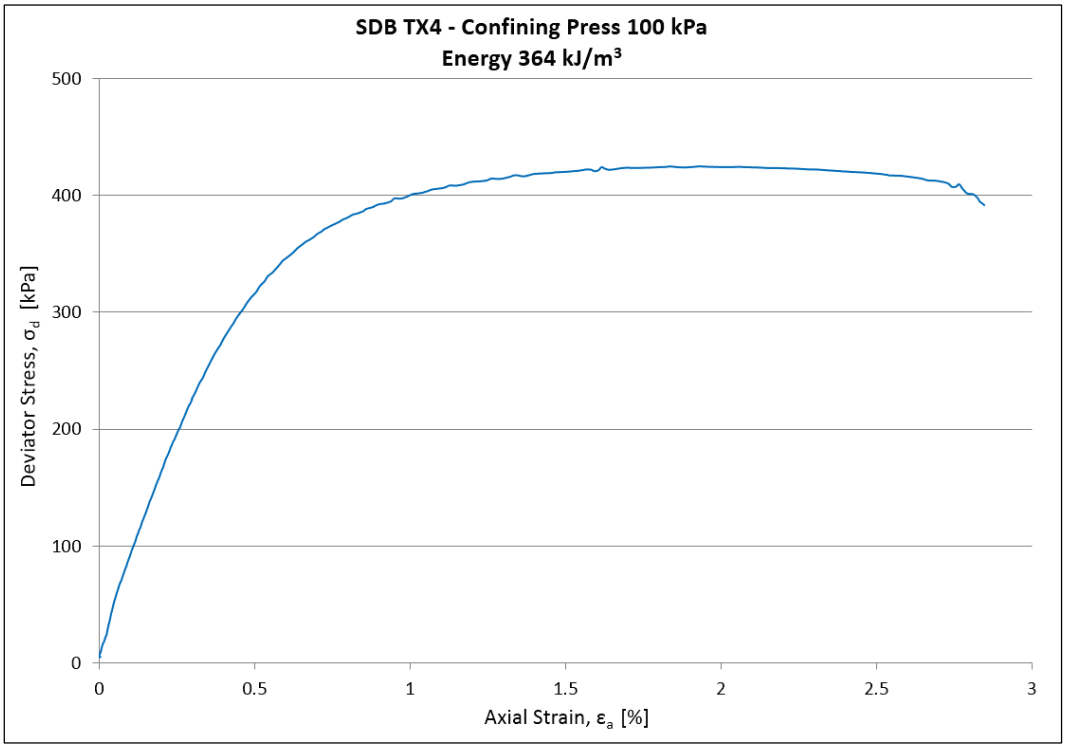
SDB TX4 - Confining Press 100 kPa
Energy 364 kJ/m³
Deviator Stress, σd [kPa]
0
100
200
300
400
500
0
0.5
1
1.5
2
2.5
3
Axial Strain, εa [%]

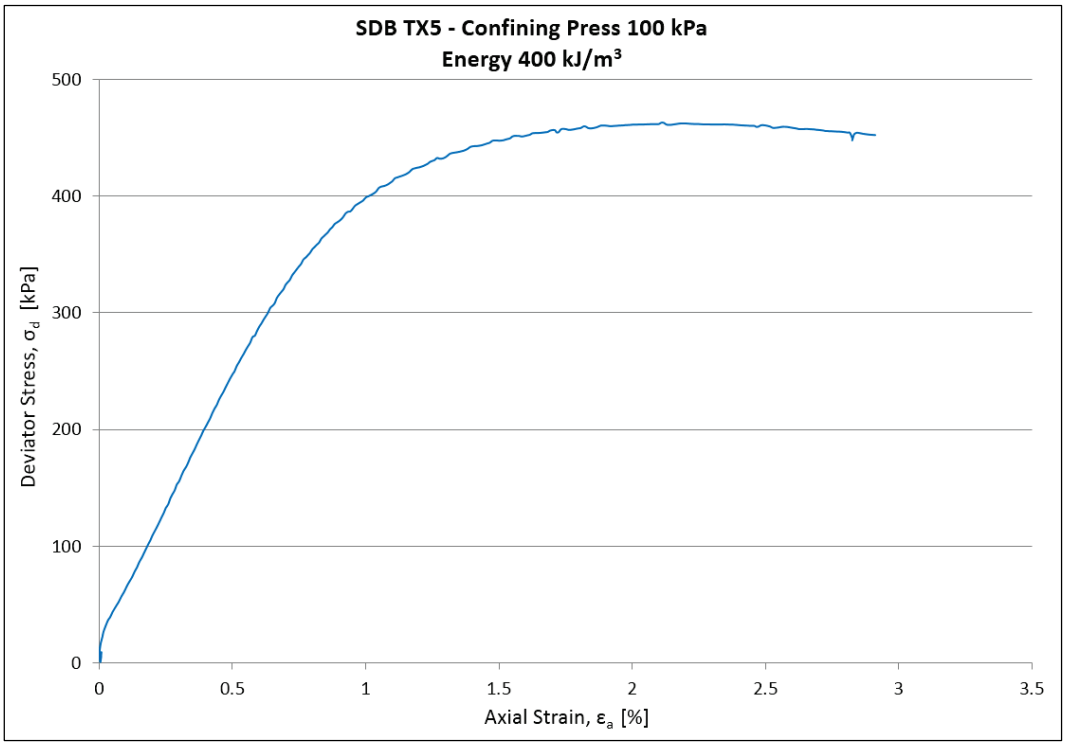
SDB TX5 - Confining Press 100 kPa
Energy 400 kJ/m³
Deviator Stress, σd [kPa]
0
100
200
300
400
500
0
0.5
1
1.5
2
2.5
3
3.5
Axial Strain, εa [%]

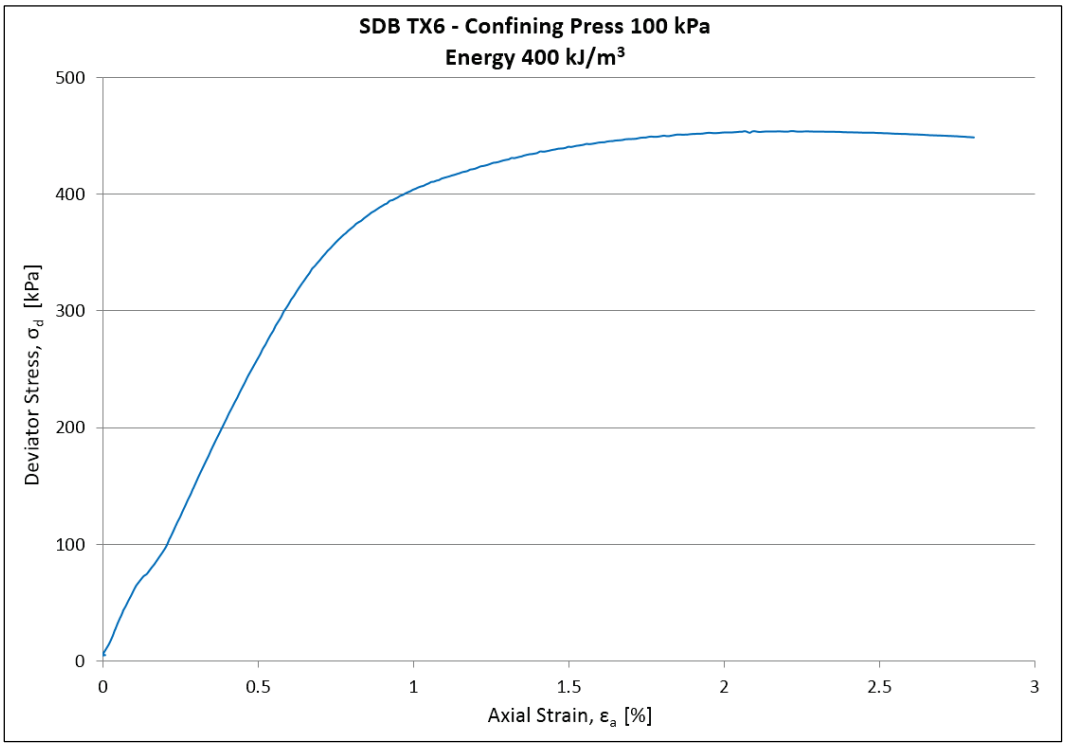
SDB TX6 - Confining Press 100 kPa
Energy 400 kJ/m³
Deviator Stress, σd [kPa]
0
100
200
300
400
500
0
0.5
1
1.5
2
2.5
3
Axial Strain, εa [%]

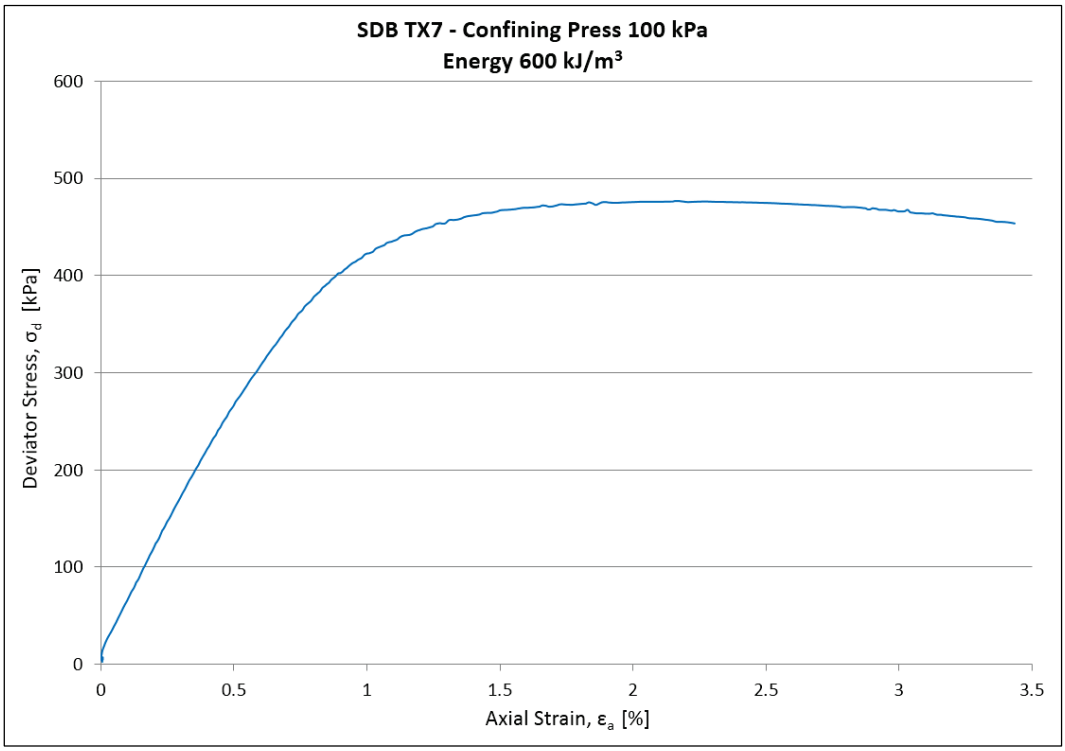
SDB TX7 - Confining Press 100 kPa
Energy 600 kJ/m³
Deviator Stress, σd [kPa]
600
500
400
300
200
100
0
0
0.5
1
1.5
2
2.5
3
3.5
Axial Strain, εa [%]

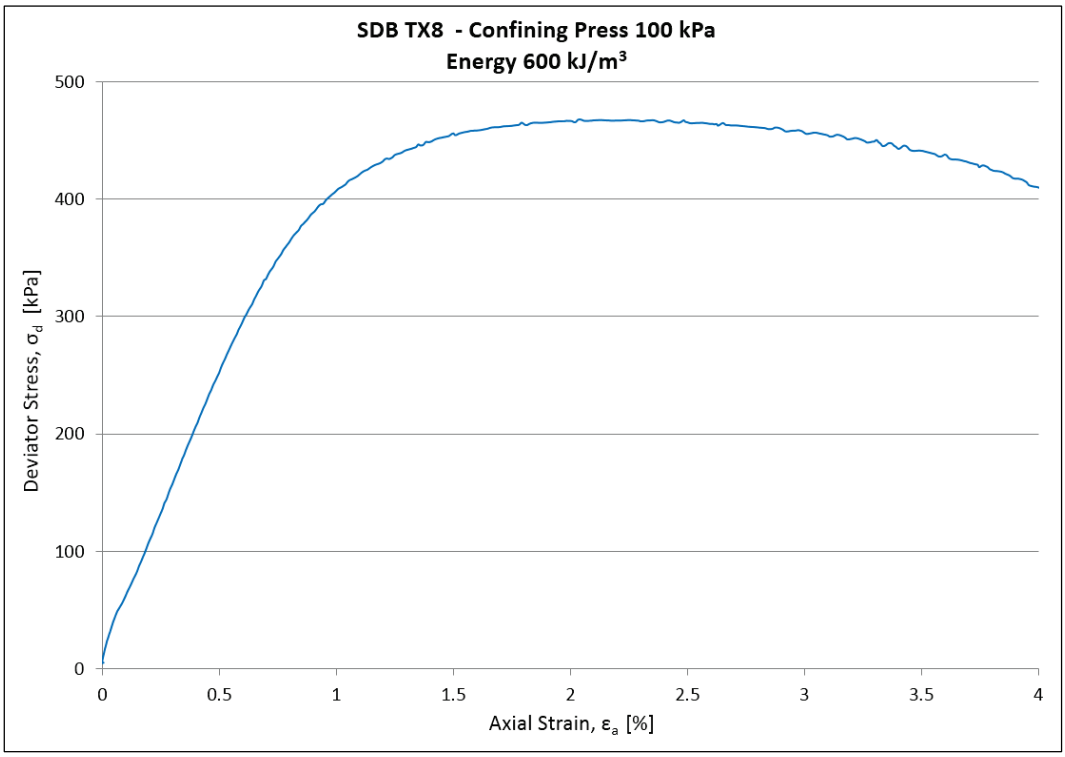
SDB TX8 - Confining Press 100 kPa
Energy 600 kJ/m³
Deviator Stress, σd [kPa]
500
400
300
200
100
0
0
0.5
1
1.5
2
2.5
3
3.5
4
Axial Strain, εa [%]

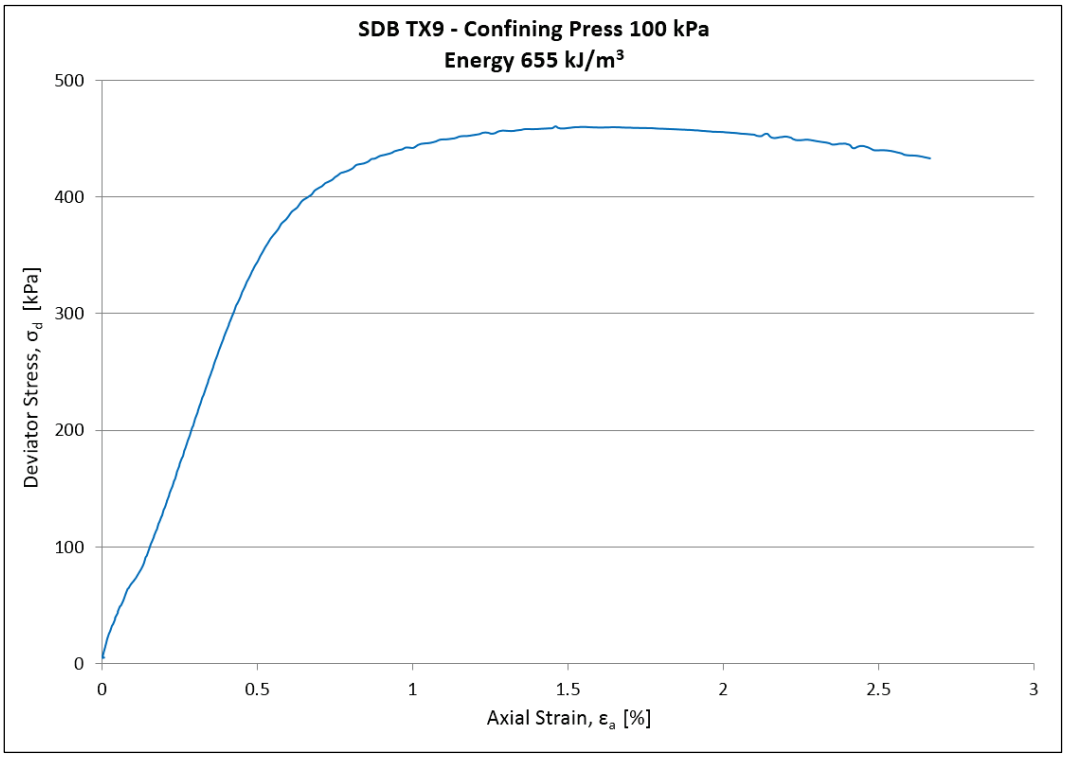
SDB TX9 - Confining Press 100 kPa
Energy 655 kJ/m³
Deviator Stress, σd [kPa]
0
100
200
300
400
500
0
0.5
1
1.5
2
2.5
3
Axial Strain, εa [%]

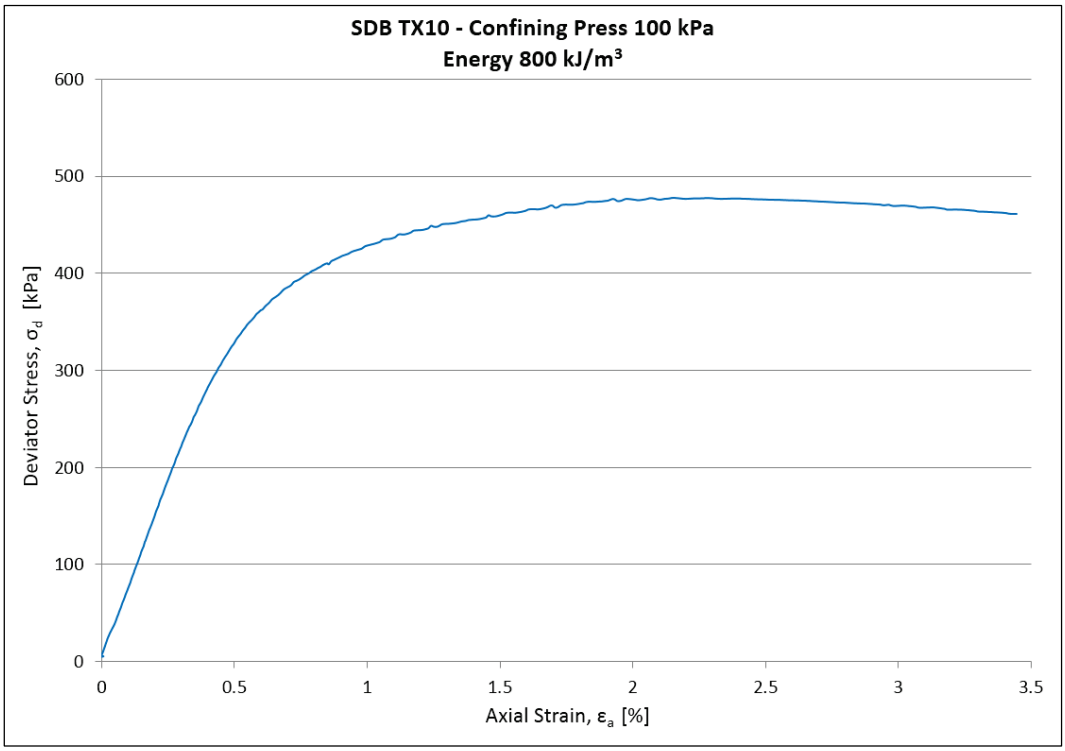
SDB TX10 - Confining Press 100 kPa
Energy 800 kJ/m³
Deviator Stress, σd [kPa]
0
100
200
300
400
500
600
0
0.5
1
1.5
2
2.5
3
3.5
Axial Strain, εa [%]

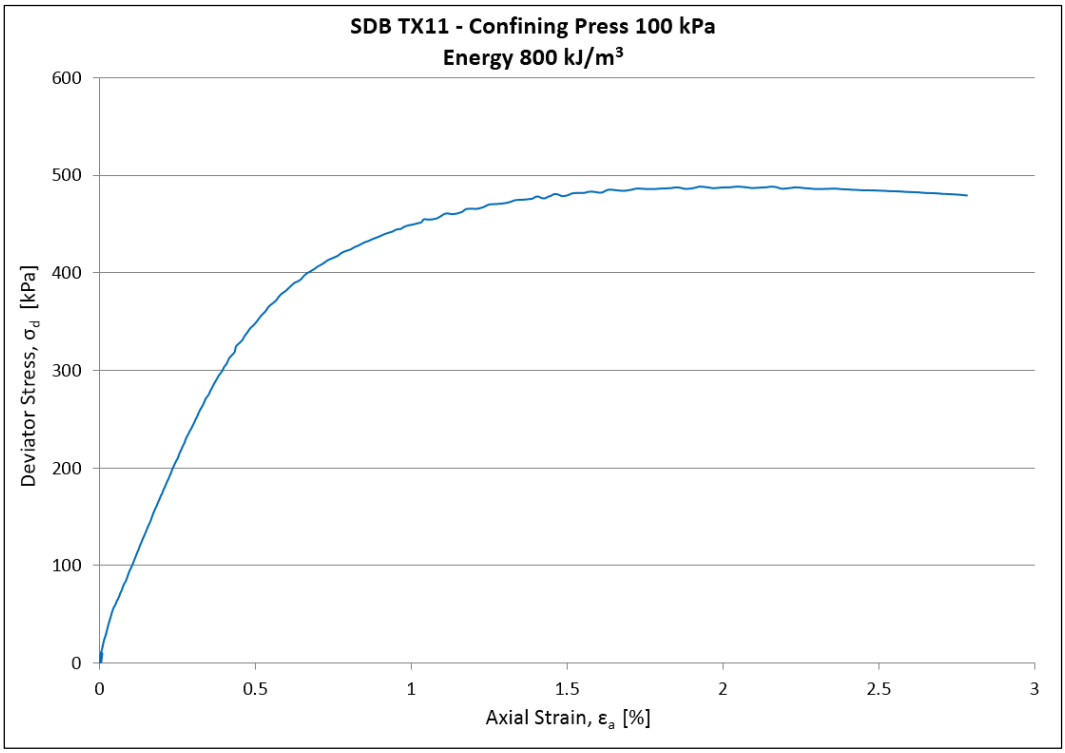
SDB TX11 - Confining Press 100 kPa
Energy 800 kJ/m³
Deviator Stress, σd [kPa]
600
500
400
300
200
100
0
0
0.5
1
1.5
2
2.5
3
Axial Strain, εa [%]

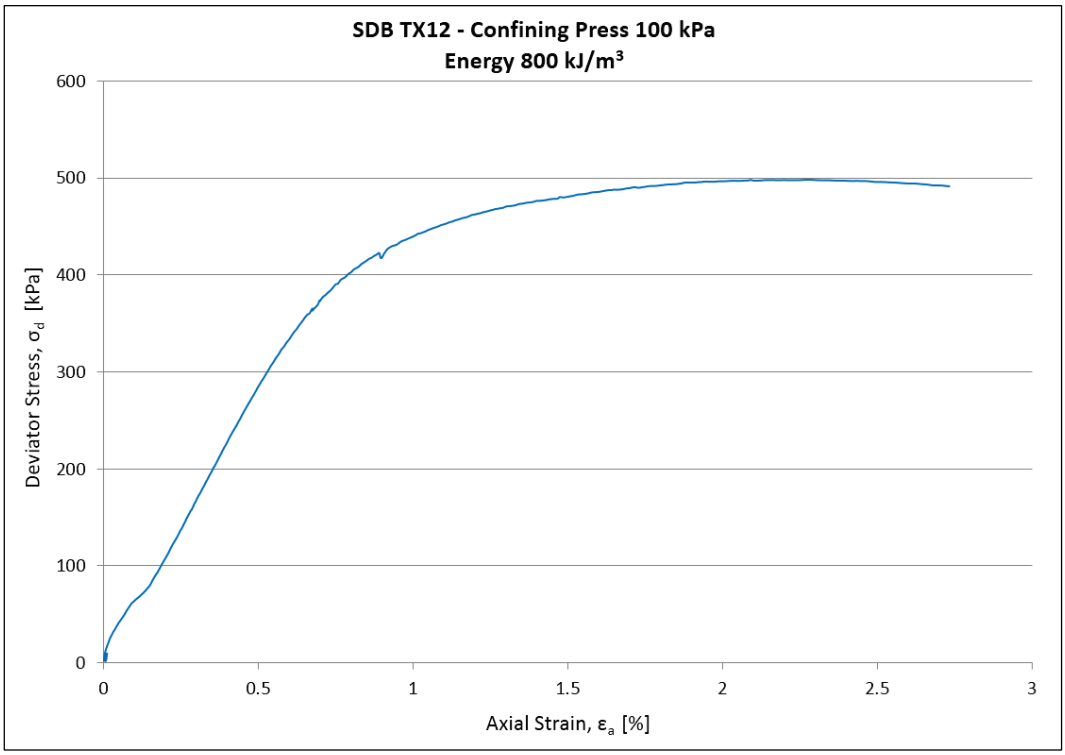
SDB TX12 - Confining Press 100 kPa
Energy 800 kJ/m³
Deviator Stress, σd [kPa]
600
500
400
300
200
100
0
0
0.5
1
1.5
2
2.5
3
Axial Strain, εa [%]

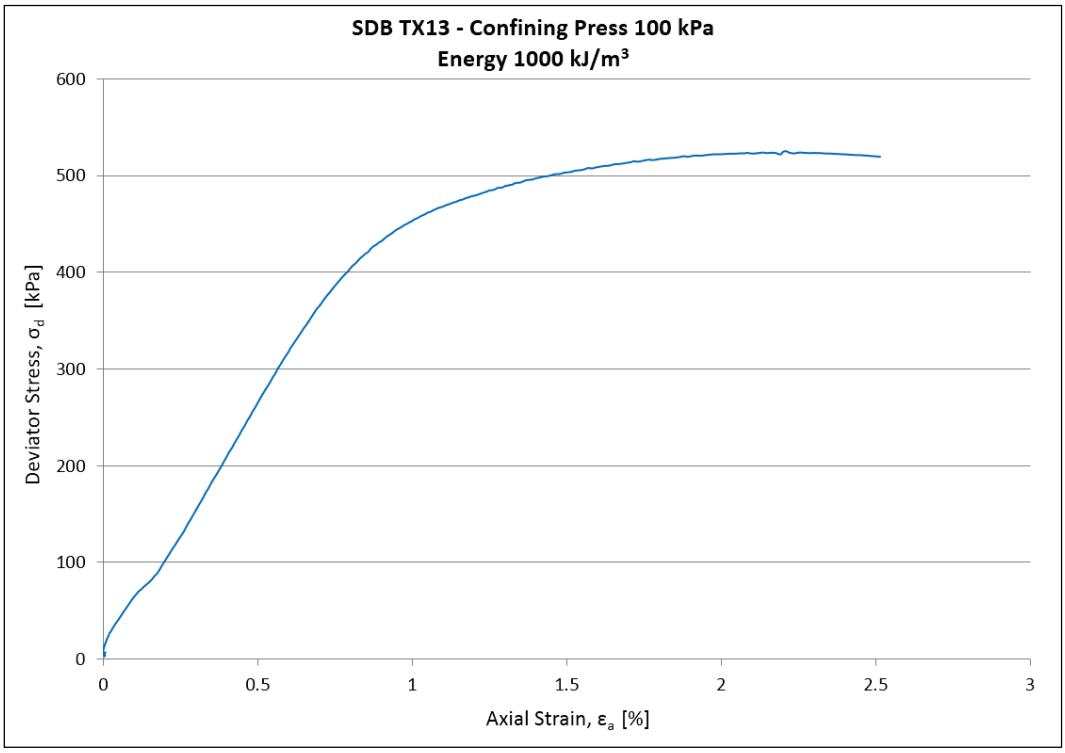
SDB TX13 - Confining Press 100 kPa
Energy 1000 kJ/m³
Deviator Stress, σd [kPa]
600
500
400
300
200
100
0
0
0.5
1
1.5
2
2.5
3
Axial Strain, εa [%]

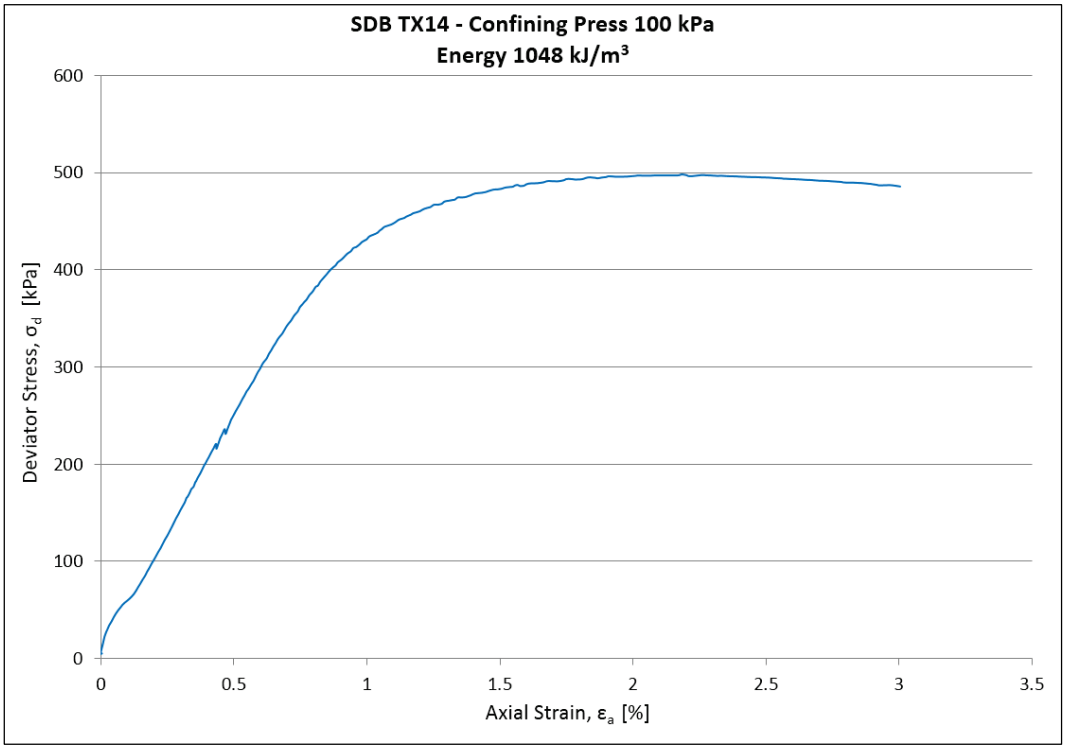
SDB TX14 - Confining Press 100 kPa
Energy 1048 kJ/m³
Deviator Stress, σd [kPa]
600
500
400
300
200
100
0
0
0.5
1
1.5
2
2.5
3
3.5
Axial Strain, εa [%]

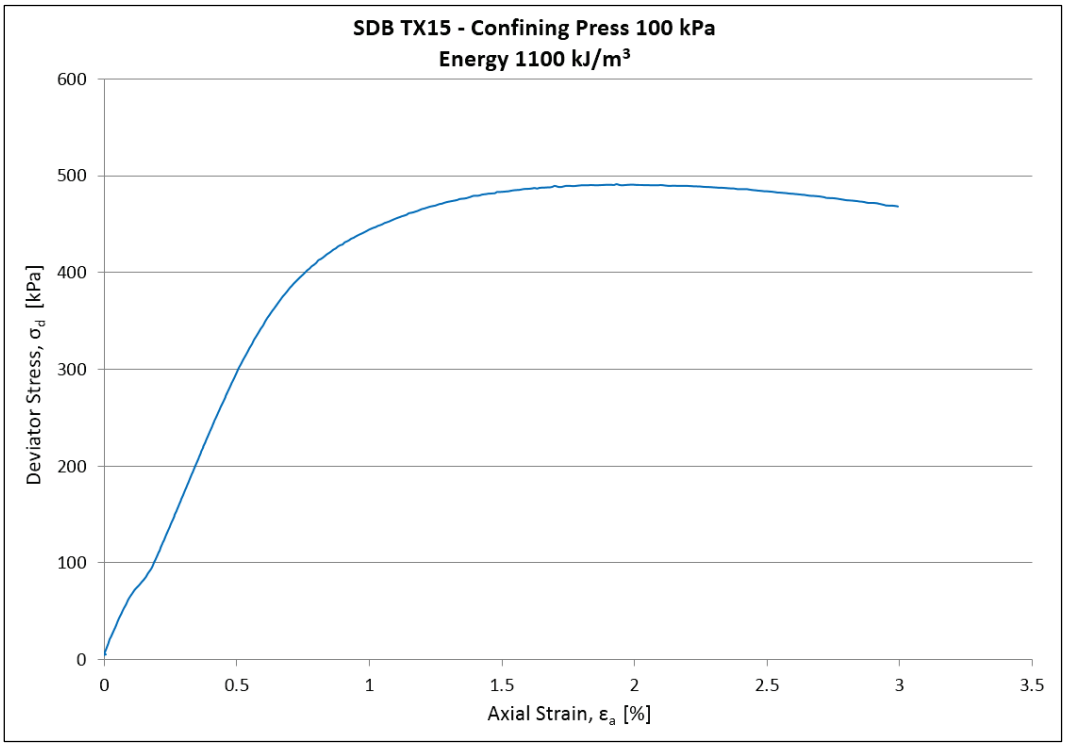
SDB TX15 - Confining Press 100 kPa
Energy 1100 kJ/m³
Deviator Stress, σd [kPa]
600
500
400
300
200
100
0
0
0.5
1
1.5
2
2.5
3
3.5
Axial Strain, εa [%]

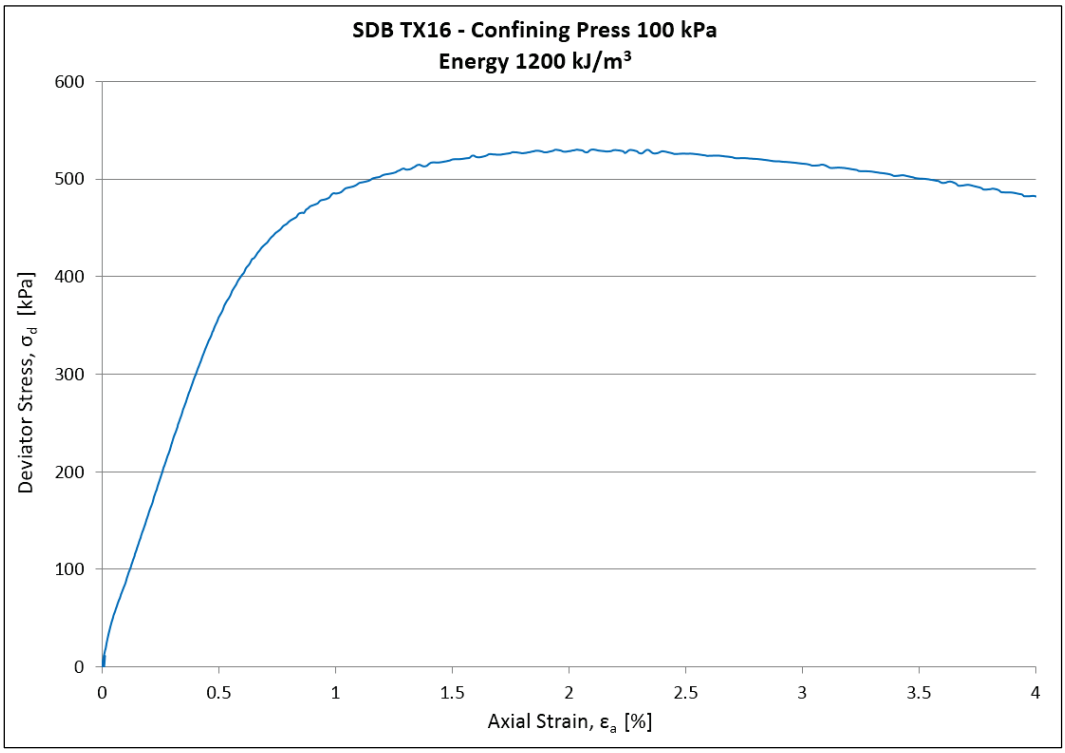
SDB TX16 - Confining Press 100 kPa
Energy 1200 kJ/m³
Deviator Stress, σd [kPa]
600
500
400
300
200
100
0
0
0.5
1
1.5
2
2.5
3
3.5
4
Axial Strain, εa [%]

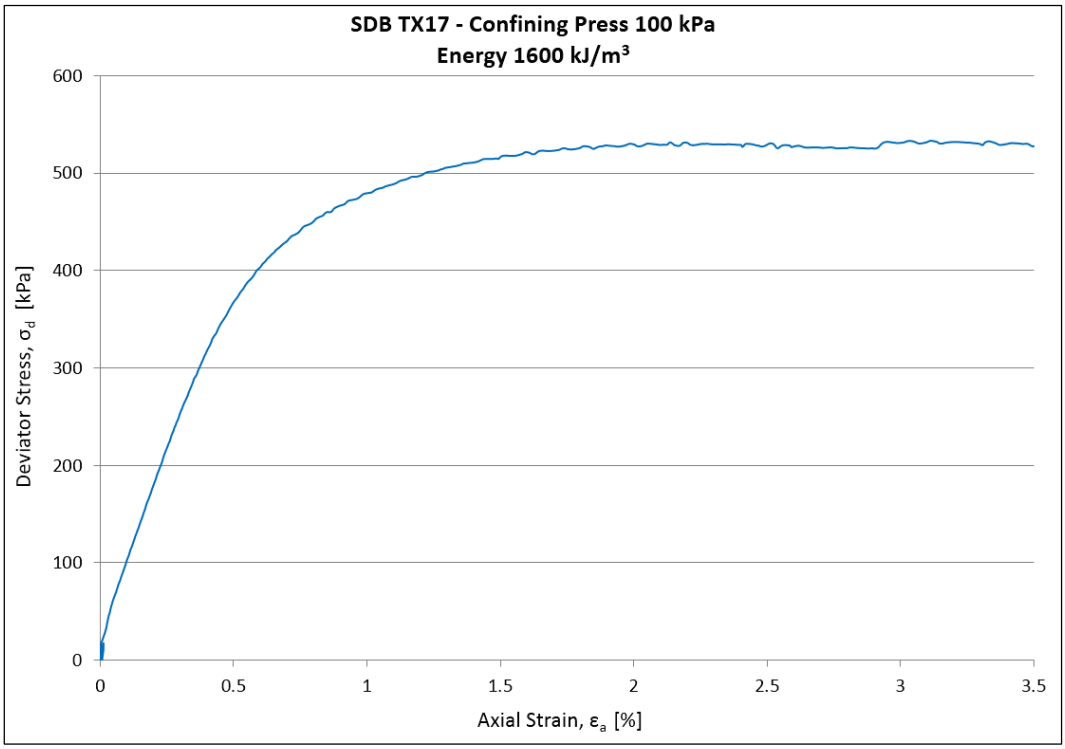

Test No.	ENERGY	HEIGHT		DRY DENSITY			AT FAILURE					
				Target	Actual	% Error	σ_d	CP	U_w	ε_a	ε_r	ε_v
	kJ/m3	Final	% of Target	ρ_d, g/cc	ρ_d, g/cc	%	kPa	kPa	kPa	%	%	%
SDA TX18	125	299.65	99.9%	1.637	1.634	0.2%	211	50	0	2.770	-0.001	-0.155
SDA TX19	200	296.30	98.8%	1.650	1.669	-1.2%	218	50	0	2.420	0.000	-0.241
SDA TX20	600	294.86	98.3%	1.680	1.704	-1.4%	257	50	0	2.818	0.001	-0.186
SDA TX21	1000	296.25	98.8%	1.693	1.712	-1.1%	271	50	0	2.006	-0.003	-0.342
SDA TX22	1150	295.80	98.6%	1.697	1.719	-1.3%	263	50	0	2.293	-0.002	-0.289
SDB TX18	200	296.13	98.7%	1.744	1.762	-1.0%	227	50	0	2.005	-0.002	-0.117
SDB TX19	400	297.07	99.0%	1.764	1.777	-0.7%	254	50	0	1.636	-0.004	-0.159
SDB TX20	800	296.45	98.8%	1.784	1.804	-1.1%	280	50	0	1.684	0.001	-0.163
SDB TX21	800	297.09	99.0%	1.784	1.796	-0.7%	276	50	0	1.976	0.006	-0.143
SDB TX22	1000	296.71	98.9%	1.790	1.807	-0.9%	280	50	0	1.984	-0.004	-0.141
SDB TX23	1150	296.71	98.9%	1.794	1.812	-1.0%	296	50	0	1.707	0.002	-0.187

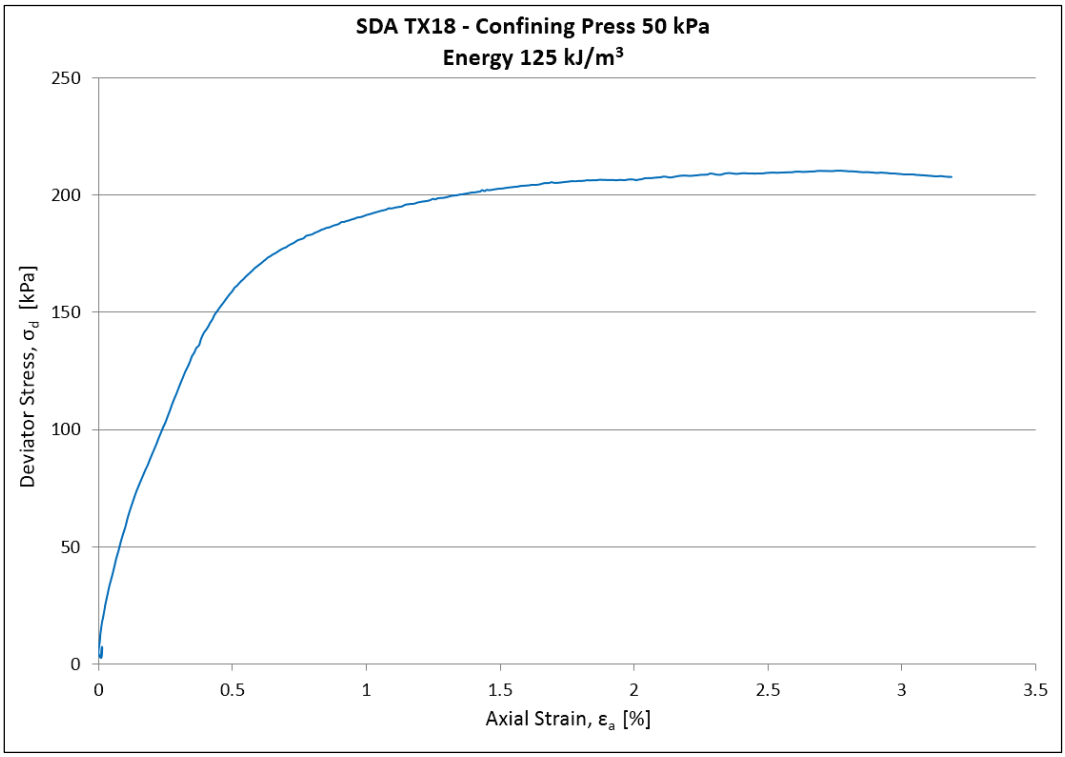
SDA TX18 - Confining Press 50 kPa
Energy 125 kJ/m³
Deviator Stress, σd [kPa]
250
200
150
100
50
0
0
0.5
1
1.5
2
2.5
3
3.5
Axial Strain, εa [%]

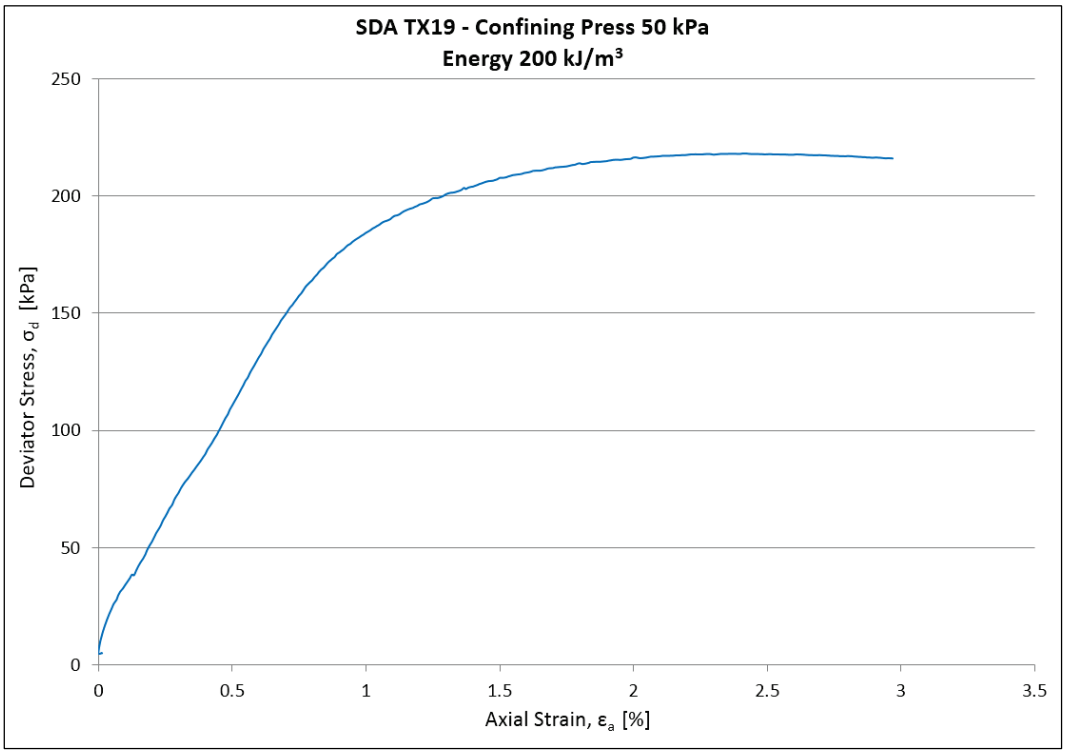
SDA TX19 - Confining Press 50 kPa
Energy 200 kJ/m³
Deviator Stress, σd [kPa]
250
200
150
100
50
0
0
0.5
1
1.5
2
2.5
3
3.5
Axial Strain, εa [%]

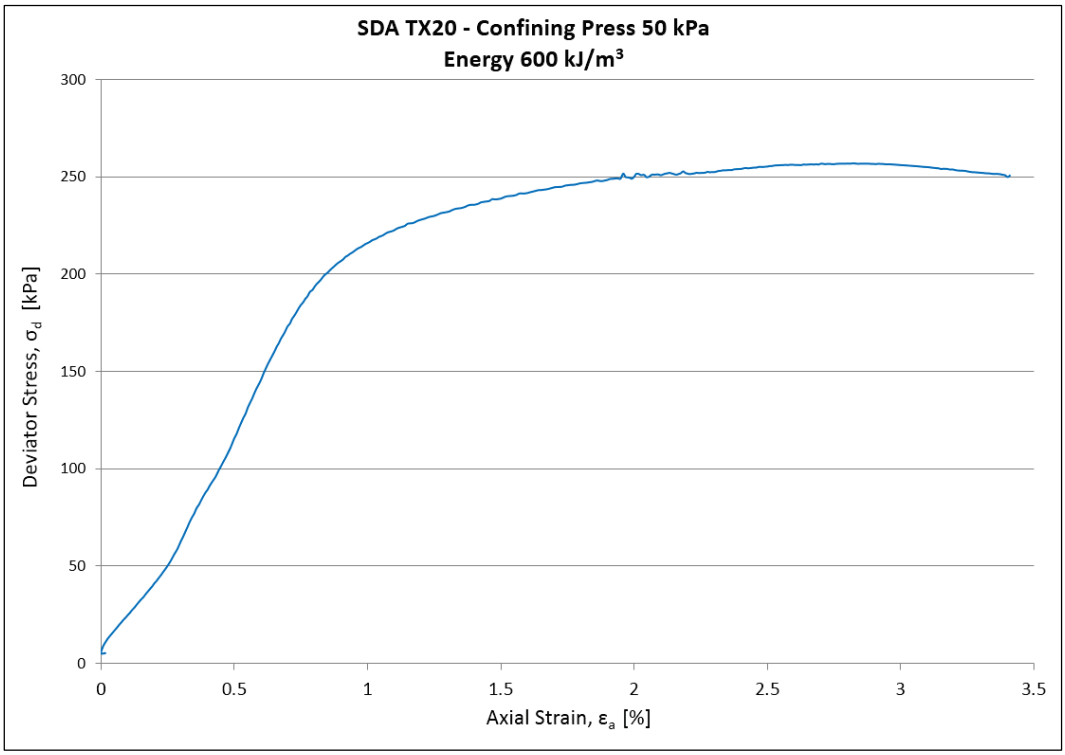
SDA TX20 - Confining Press 50 kPa
Energy 600 kJ/m³
Deviator Stress, σd [kPa]
Axial Strain, εa [%]
0
50
100
150
200
250
300
0
0.5
1
1.5
2
2.5
3
3.5

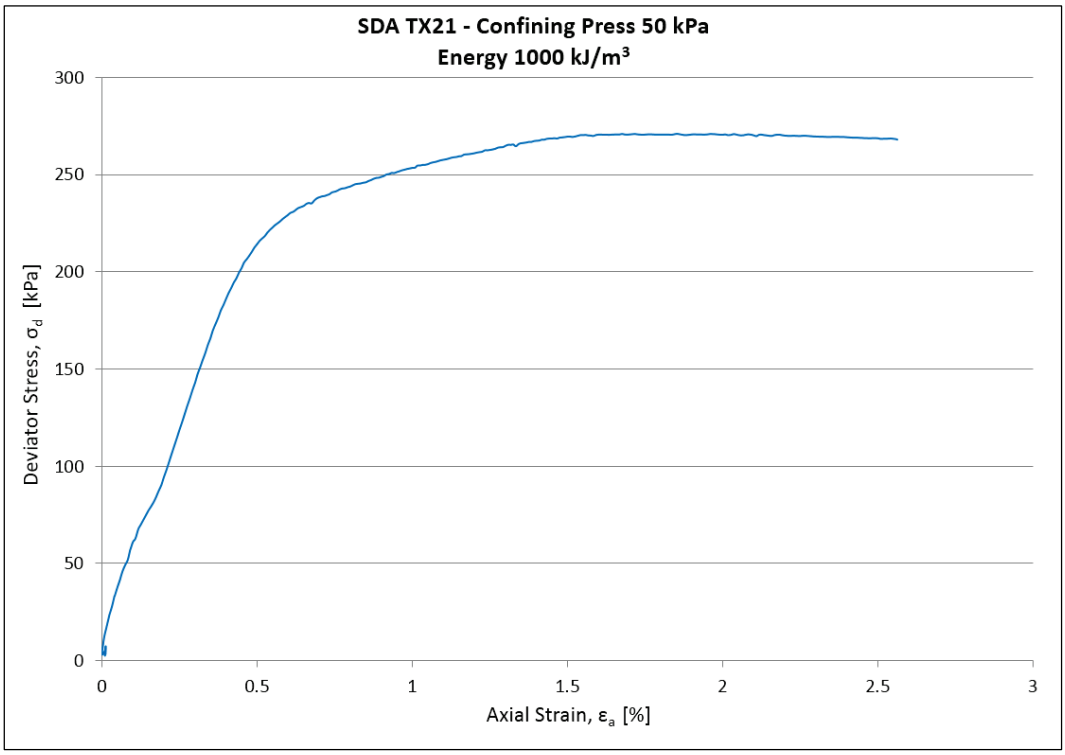
SDA TX21 - Confining Press 50 kPa
Energy 1000 kJ/m³
Deviator Stress, σd [kPa]
Axial Strain, εa [%]
0
50
100
150
200
250
300
0
0.5
1
1.5
2
2.5
3

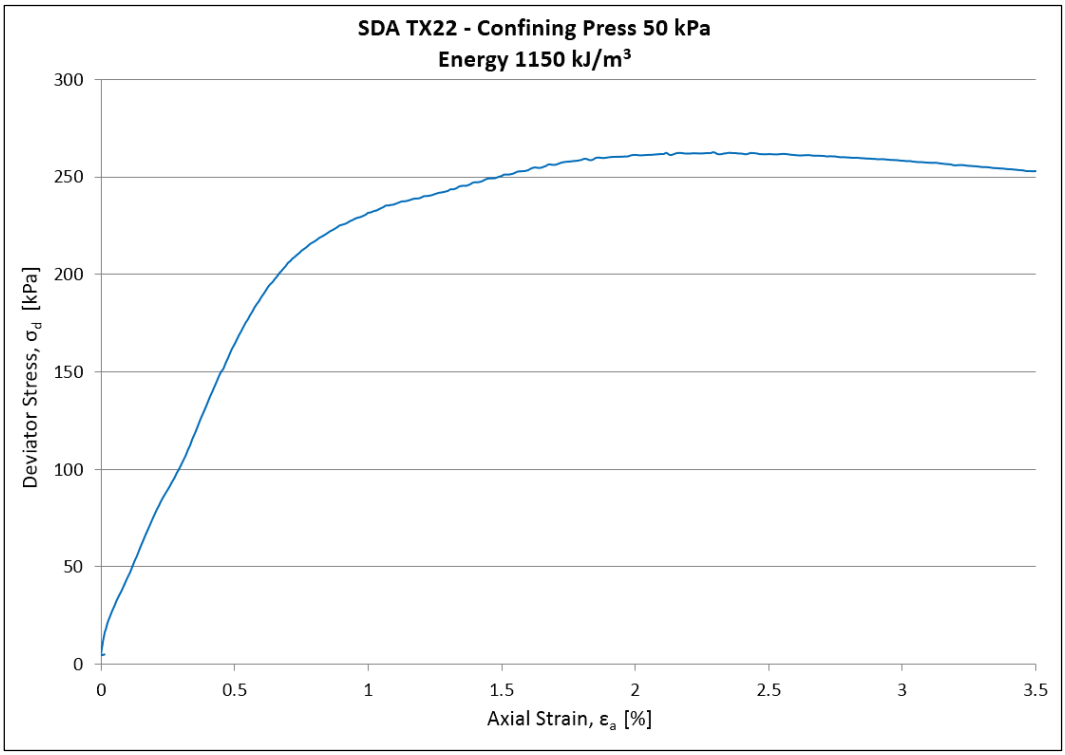
SDA TX22 - Confining Press 50 kPa
Energy 1150 kJ/m³
Deviator Stress, σd [kPa]
Axial Strain, εa [%]
0
50
100
150
200
250
300
0
0.5
1
1.5
2
2.5
3
3.5

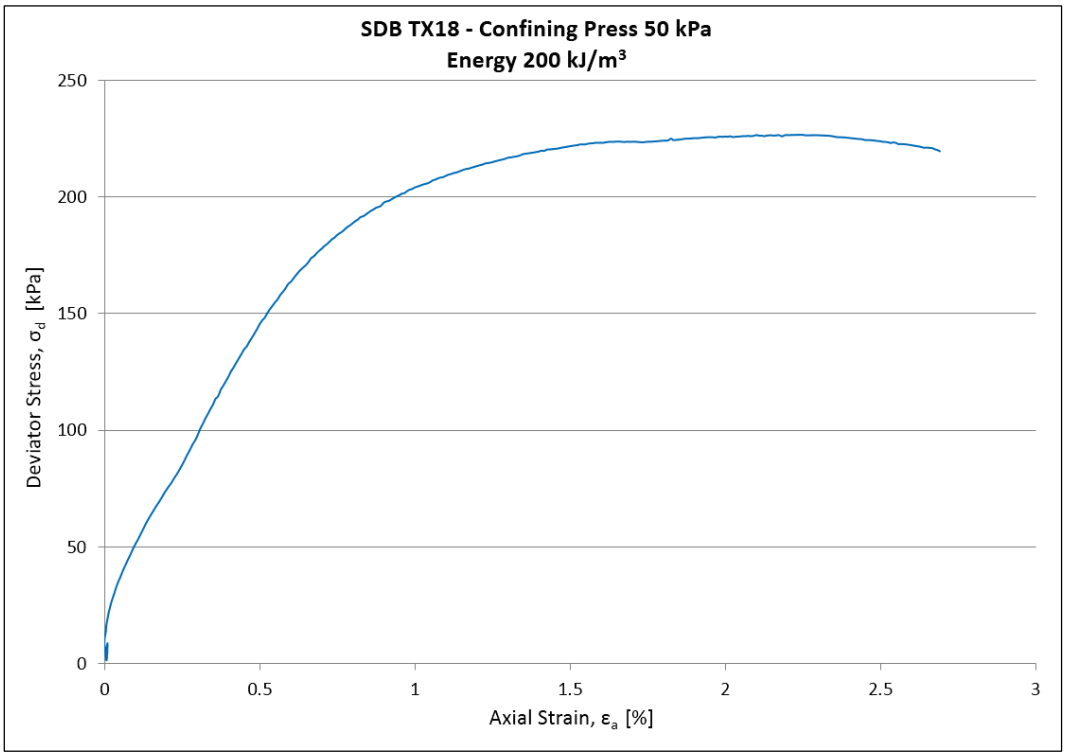
SDB TX18 - Confining Press 50 kPa
Energy 200 kJ/m³
Deviator Stress, σd [kPa]
Axial Strain, εa [%]
0
50
100
150
200
250
0
0.5
1
1.5
2
2.5
3

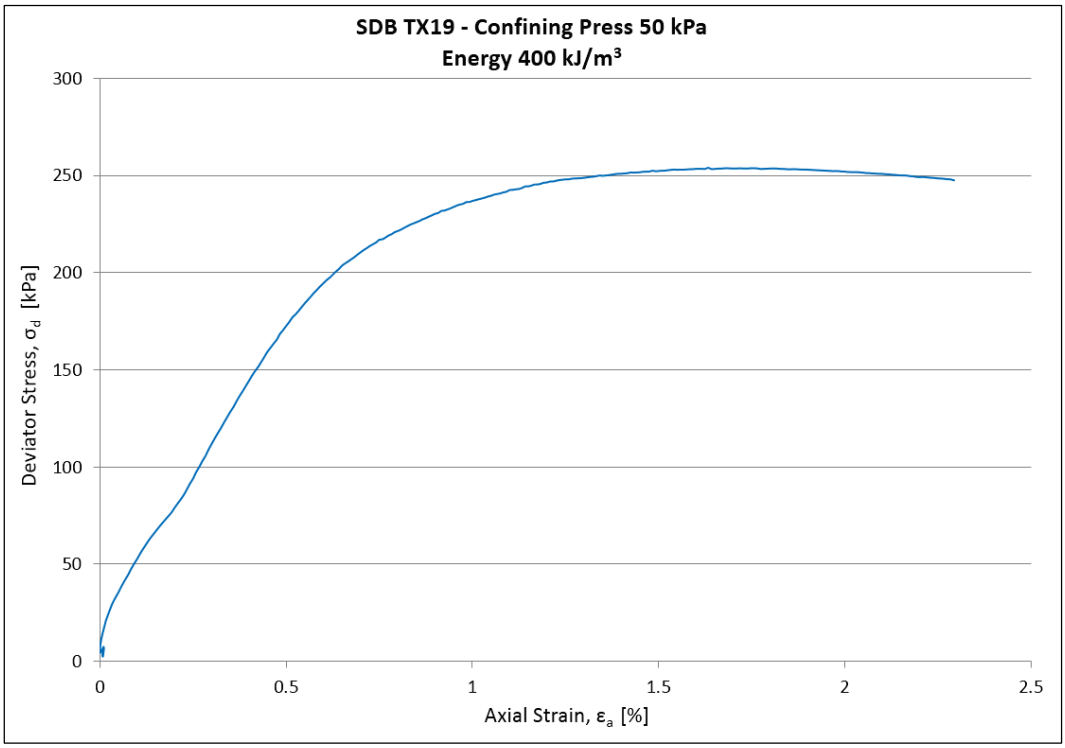
SDB TX19 - Confining Press 50 kPa
Energy 400 kJ/m³
Deviator Stress, σd [kPa]
300
250
200
150
100
50
0
0
0.5
1
1.5
2
2.5
Axial Strain, εa [%]

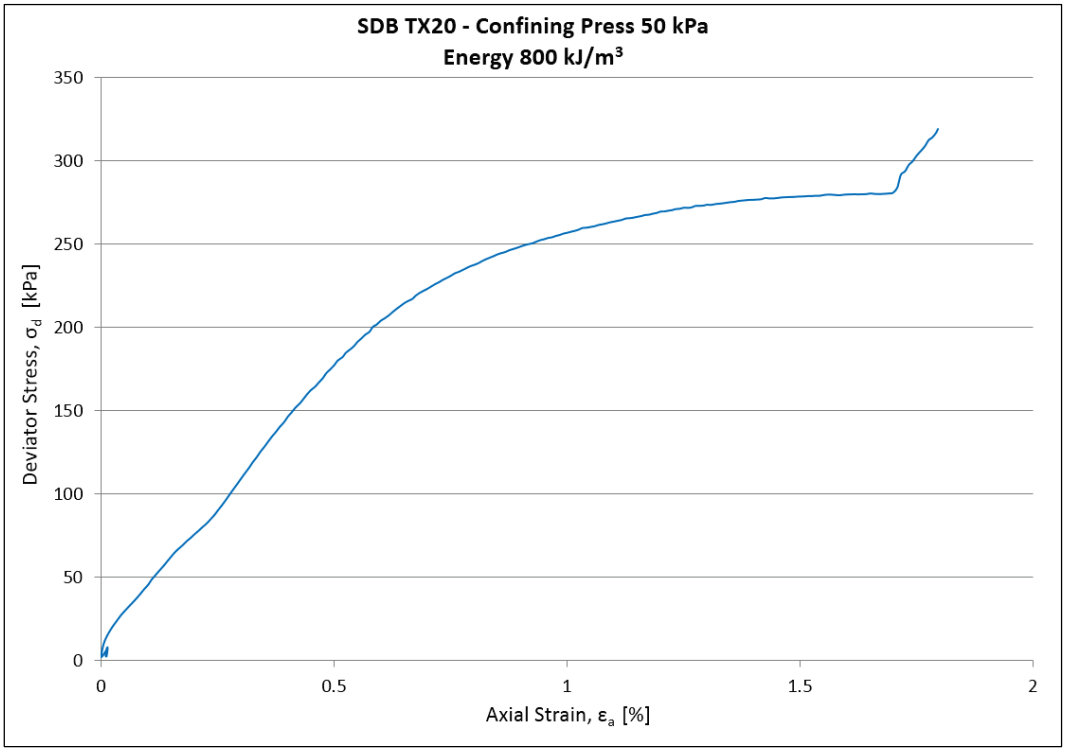
SDB TX20 - Confining Press 50 kPa
Energy 800 kJ/m³
Deviator Stress, σd [kPa]
350
300
250
200
150
100
50
0
0
0.5
1
1.5
2
Axial Strain, εa [%]

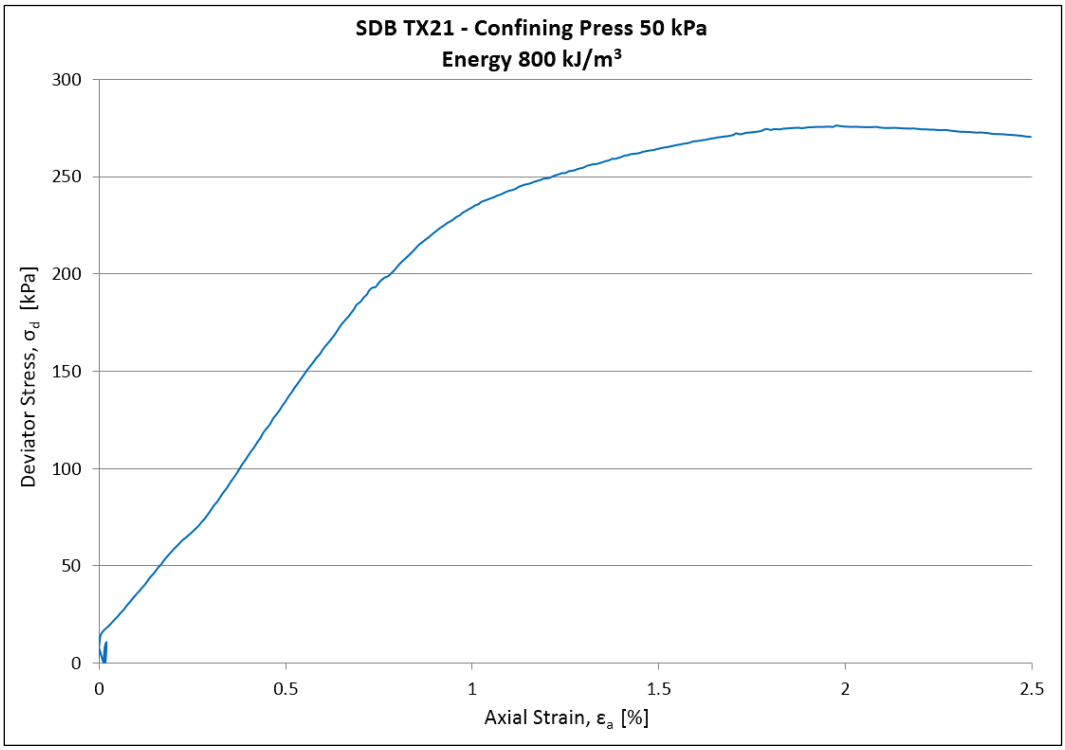
SDB TX21 - Confining Press 50 kPa
Energy 800 kJ/m³
Deviator Stress, σd [kPa]
300
250
200
150
100
50
0
0
0.5
1
1.5
2
2.5
Axial Strain, εa [%]

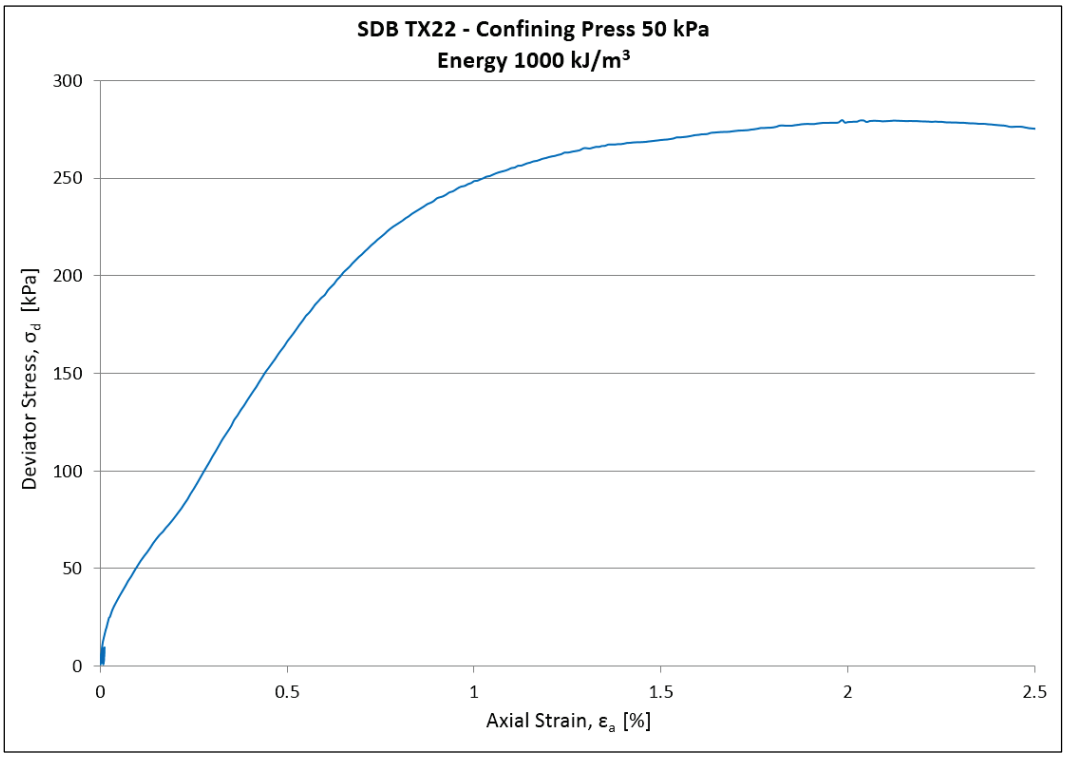
SDB TX22 - Confining Press 50 kPa
Energy 1000 kJ/m³
Deviator Stress, σd [kPa]
300
250
200
150
100
50
0
0
0.5
1
1.5
2
2.5
Axial Strain, εa [%]

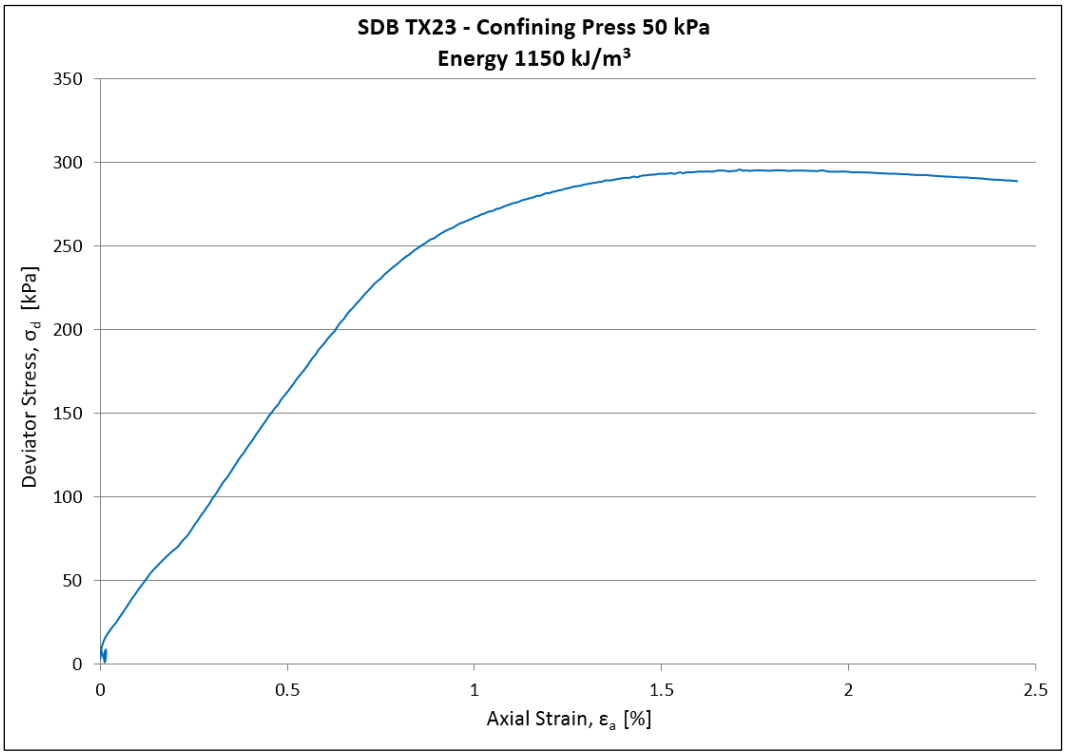
SDB TX23 - Confining Press 50 kPa
Energy 1150 kJ/m³
Deviator Stress, σd [kPa]
350
300
250
200
150
100
50
0
0
0.5
1
1.5
2
2.5
Axial Strain, εa [%]

Appendix C: Ring Shear Test Data

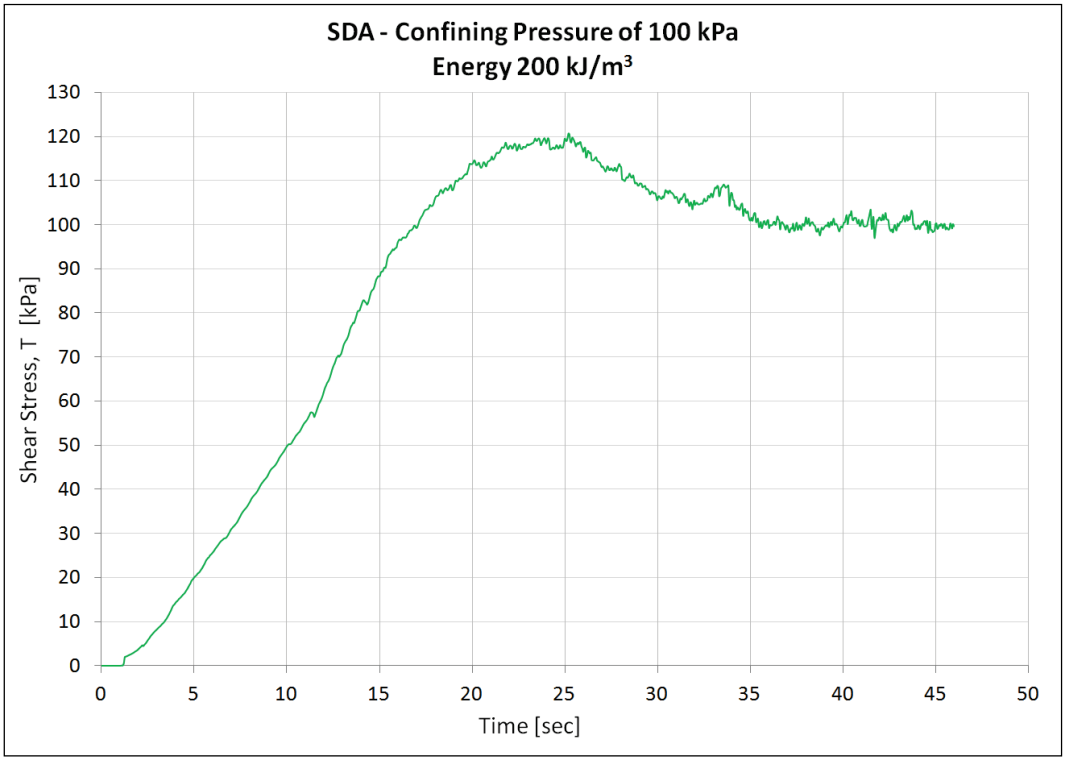

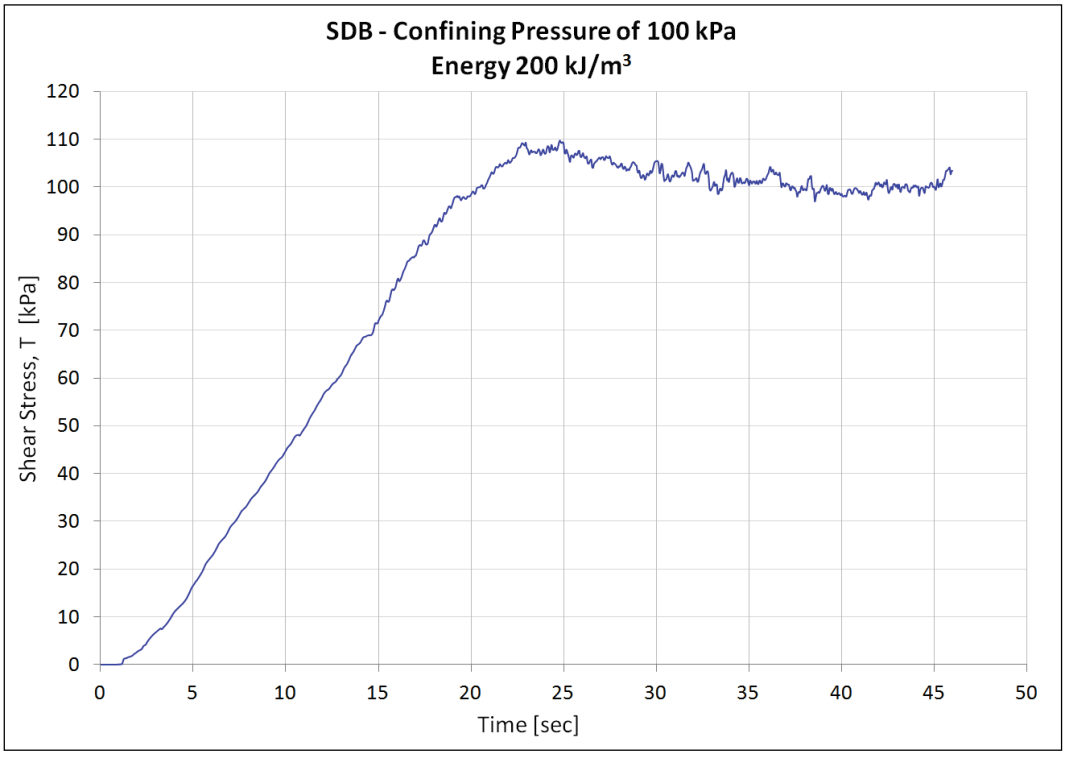

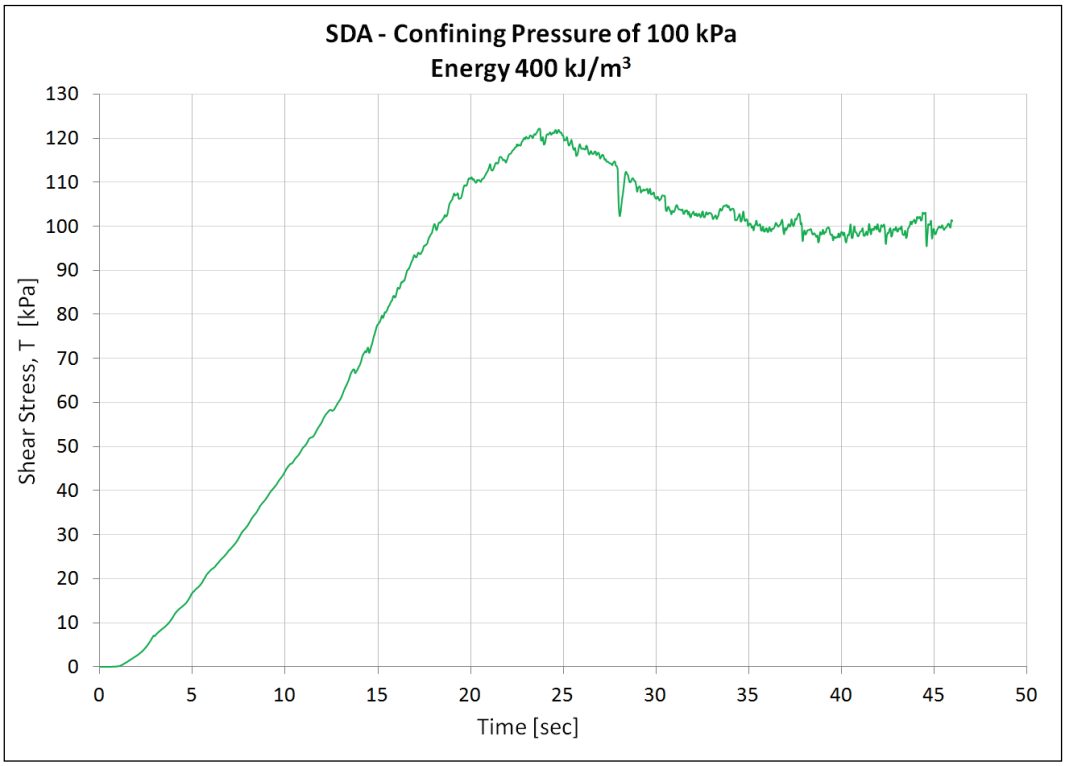
SDA - Confining Pressure of 100 kPa
Energy 400 kJ/m3
Shear Stress, T [kPa]
Time [sec]
0
10
20
30
40
50
60
70
80
90
100
110
120
130
0
5
10
15
20
25
30
35
40
45
50

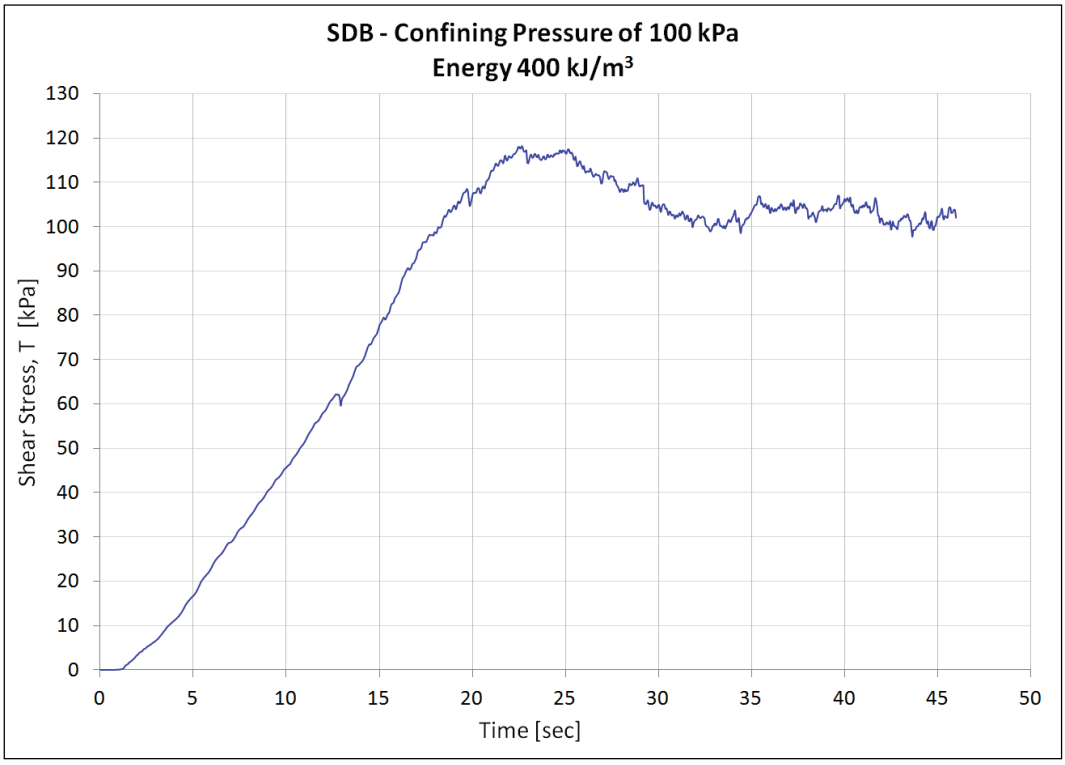
SDB - Confining Pressure of 100 kPa
Energy 400 kJ/m3
Shear Stress, T [kPa]
Time [sec]
0
10
20
30
40
50
60
70
80
90
100
110
120
130
0
5
10
15
20
25
30
35
40
45
50

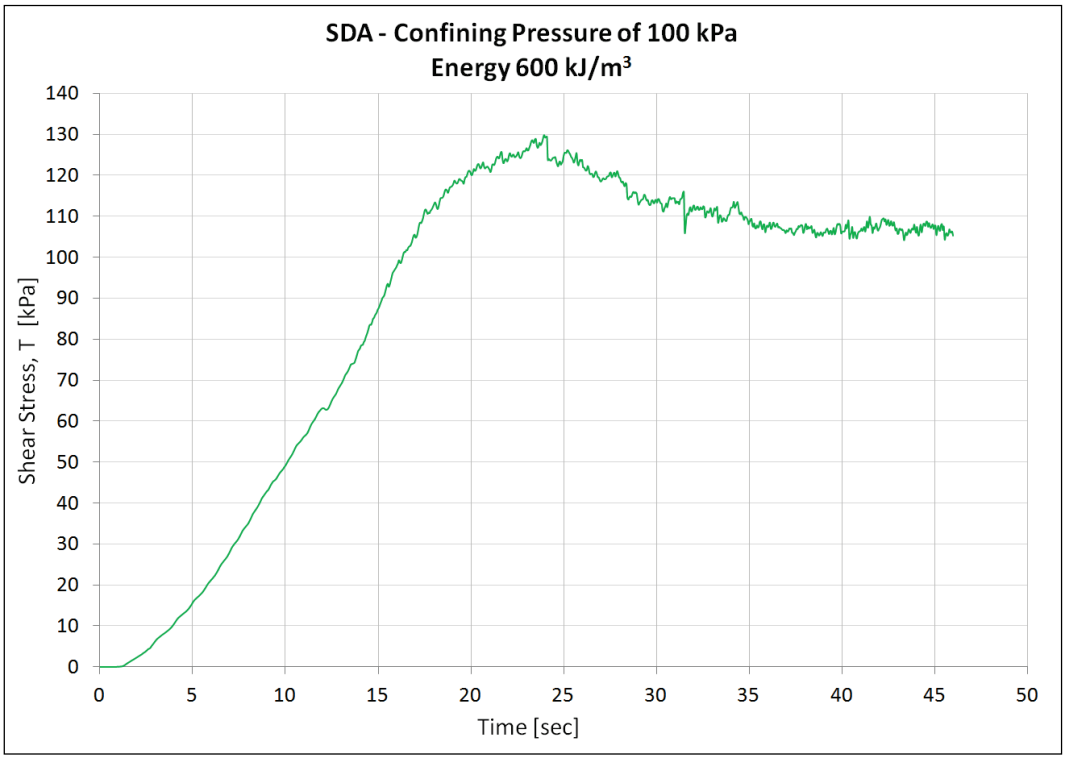
SDA - Confining Pressure of 100 kPa
Energy 600 kJ/m³
Shear Stress, T [kPa]
Time [sec]
0
10
20
30
40
50
60
70
80
90
100
110
120
130
140
0
5
10
15
20
25
30
35
40
45
50

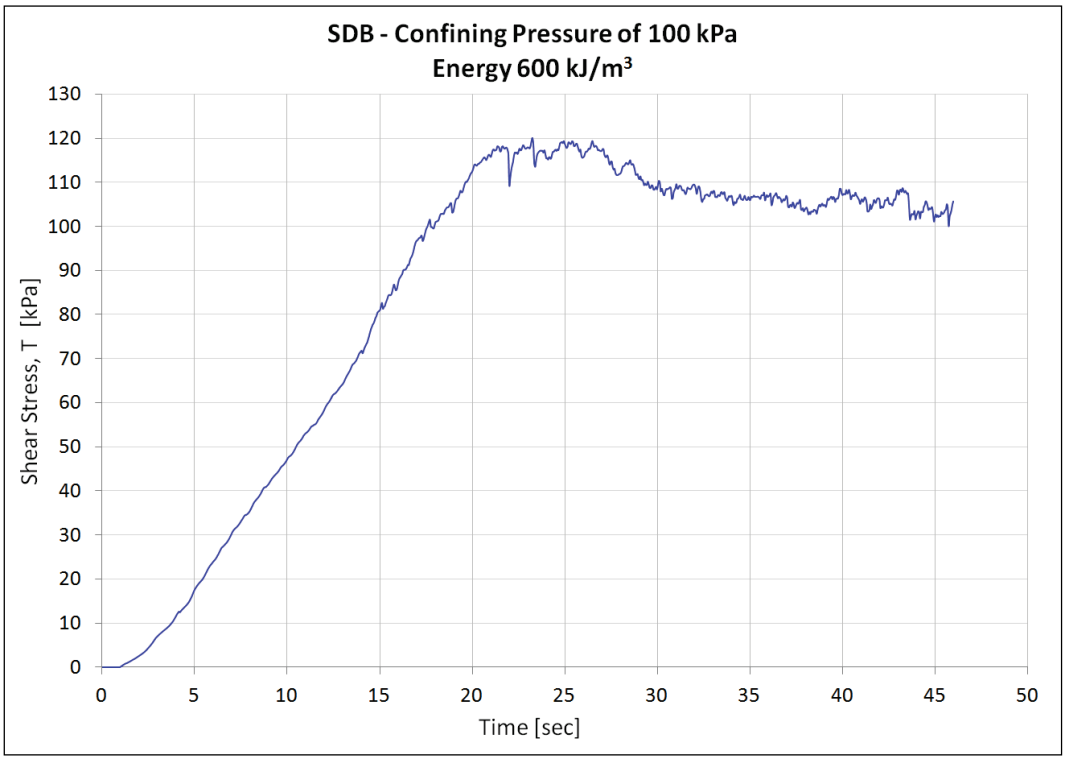
SDB - Confining Pressure of 100 kPa
Energy 600 kJ/m³
Shear Stress, T [kPa]
Time [sec]
0
10
20
30
40
50
60
70
80
90
100
110
120
130
0
5
10
15
20
25
30
35
40
45
50

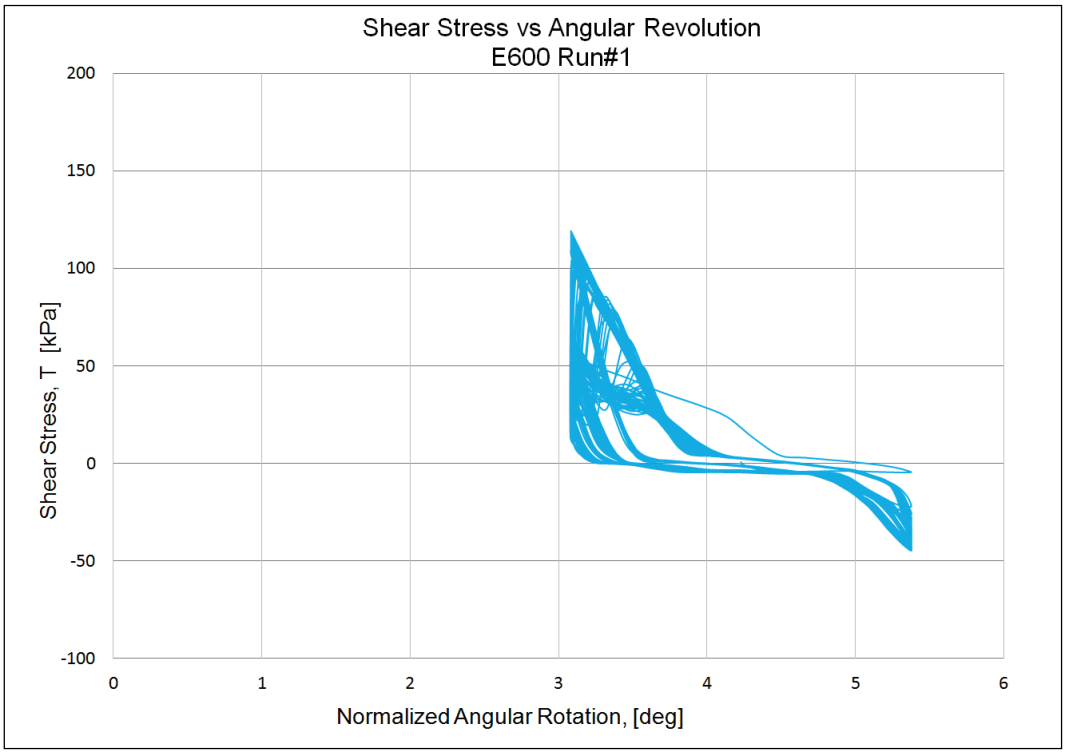
Shear Stress vs Angular Revolution
E600 Run#1
Shear Stress, T [kPa]
200
150
100
50
0
-50
-100
0
1
2
3
4
5
6
Normalized Angular Rotation, [deg]

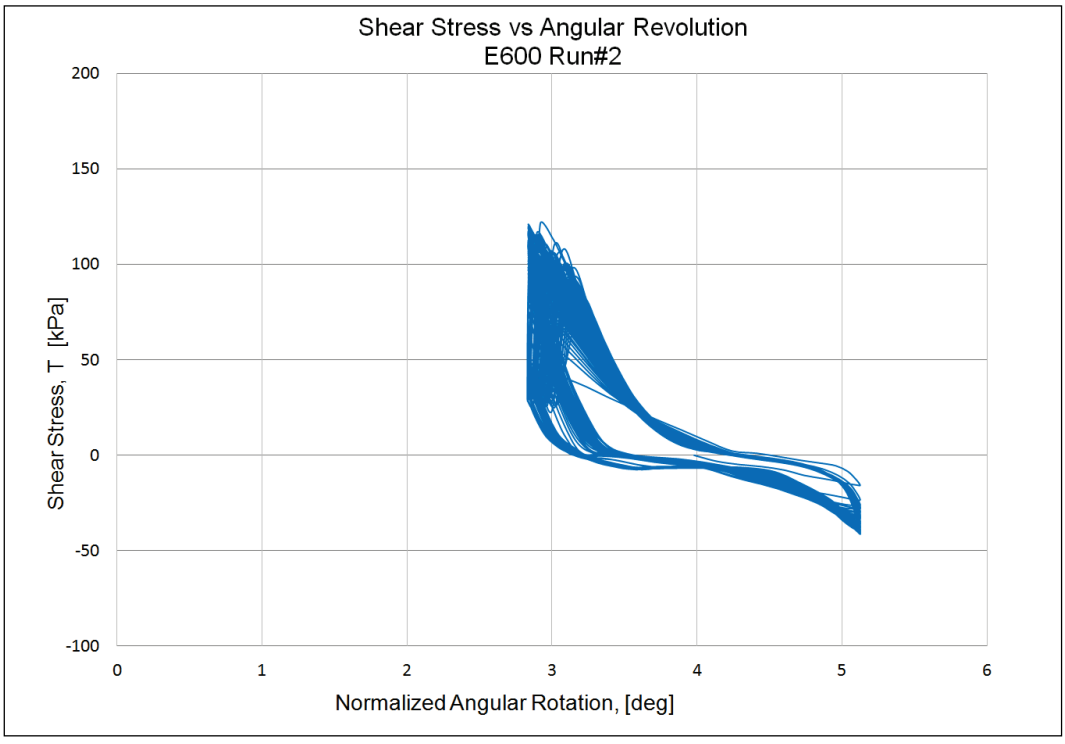
Shear Stress vs Angular Revolution
E600 Run#2
Shear Stress, T [kPa]
200
150
100
50
0
-50
-100
0
1
2
3
4
5
6
Normalized Angular Rotation, [deg]

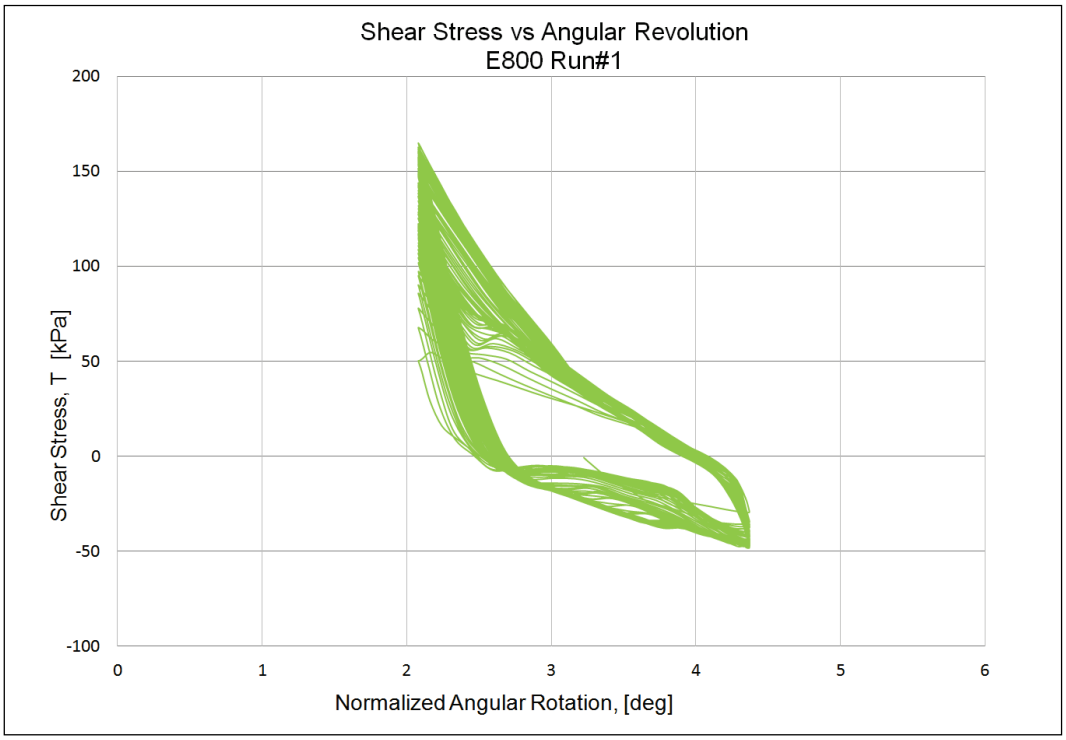
Shear Stress vs Angular Revolution
E800 Run#1
Shear Stress, T [kPa]
200
150
100
50
0
-50
-100
0
1
2
3
4
5
6
Normalized Angular Rotation, [deg]

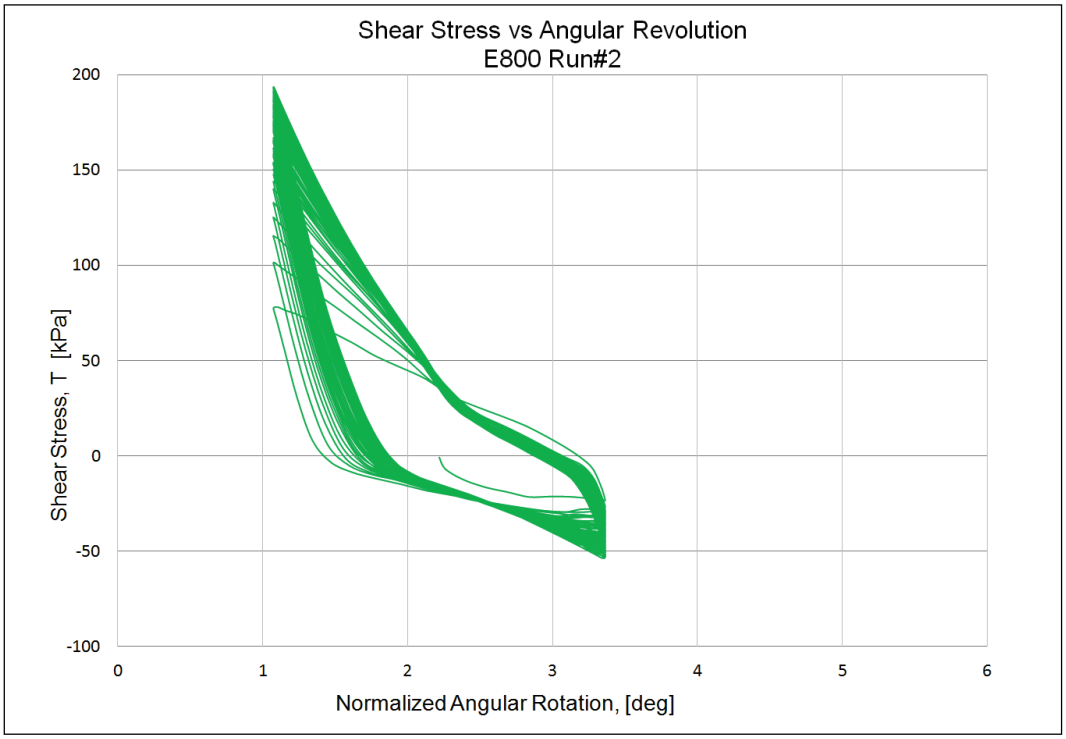
Shear Stress vs Angular Revolution
E800 Run#2
Shear Stress, T [kPa]
200
150
100
50
0
-50
-100
0
1
2
3
4
5
6
Normalized Angular Rotation, [deg]

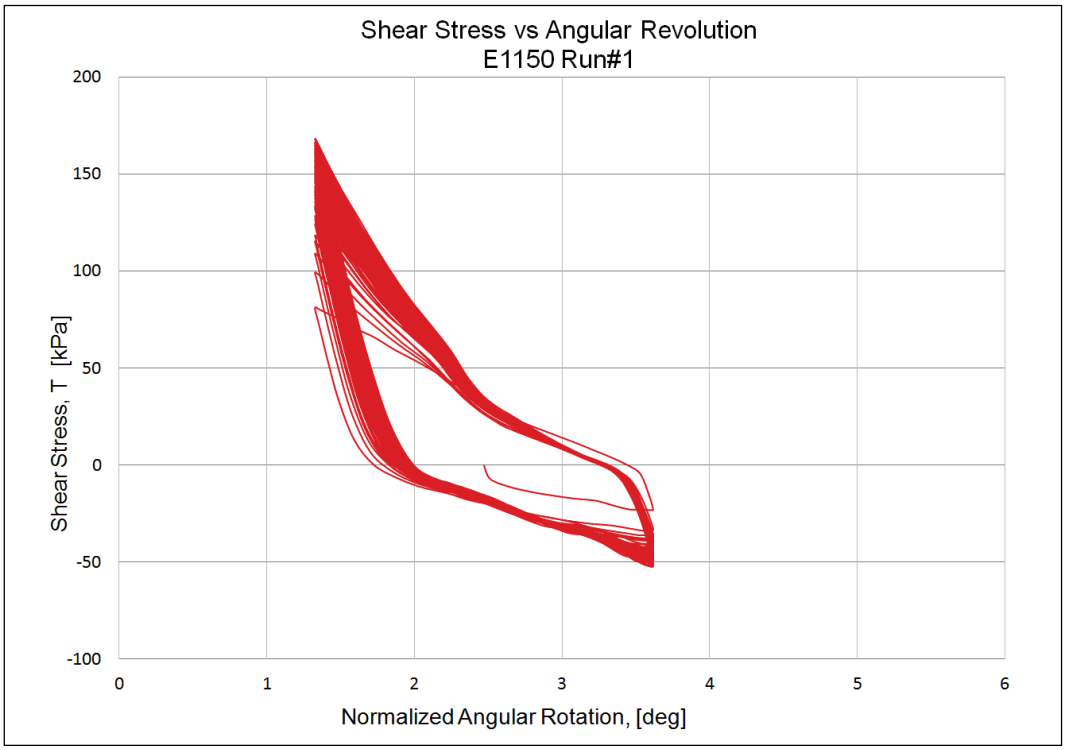
Shear Stress vs Angular Revolution
E1150 Run#1
Shear Stress, T [kPa]
200
150
100
50
0
-50
-100
0
1
2
3
4
5
6
Normalized Angular Rotation, [deg]

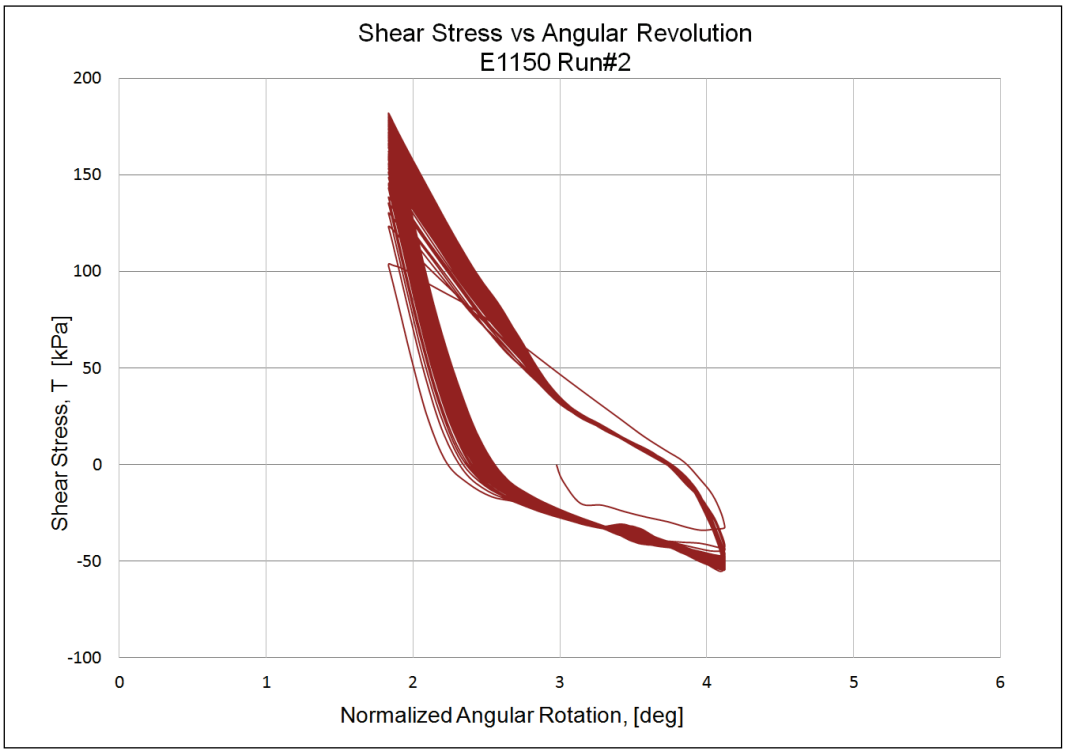
Shear Stress vs Angular Revolution
E1150 Run#2
Shear Stress, T [kPa]
200
150
100
50
0
-50
-100
0
1
2
3
4
5
6
Normalized Angular Rotation, [deg]

Appendix D: Hollow Core Test Data

Test No.	CONFINING PRESSURE	ENERGY	WATER CONTENT			HEIGHT		AT FAILURE	
								T	E_s
	kPa	kJ/m3	Target	Actual	% Error	Final	% of Target	kPa	%
SDA HC1	100	**200**	5.59%	5.48%	-2.0%	300.1	100.0%	**72.5**	2.5
SDA HC2	100	**200**	5.59%	5.67%	1.4%	300.8	100.3%	**73.5**	2.5
SDA HC3	100	**200**	5.59%	5.54%	-0.9%	302.2	100.7%	**70.0**	2.5
SDA HC4	100	**400**	5.42%	5.36%	-1.1%	299.7	99.9%	**71.0**	2.5
SDA HC5	100	**400**	5.42%	5.42%	0.0%	300.7	100.2%	**74.7**	2.5
SDA HC6	100	**400**	5.42%	5.38%	-0.7%	301.1	100.4%	**76.1**	2.5
SDA HC7	100	**600**	5.32%	5.24%	-1.5%	300.4	100.1%	**74.0**	2.5
SDA HC8	100	**600**	5.32%	5.30%	-0.4%	299.6	99.9%	**77.0**	2.5
SDA HC9	100	**600**	5.32%	5.38%	1.1%	300.8	100.3%	**78.0**	2.5
SDA HC10	100	**800**	5.25%	5.17%	-1.5%	303.5	101.2%	**76.8**	2.5
SDA HC11	100	**800**	5.25%	5.37%	2.3%	304.0	101.3%	**78.0**	2.5
SDA HC12	100	**800**	5.25%	5.28%	0.6%	301.3	100.4%	**76.0**	2.5
SDA HC13	100	**1000**	5.20%	5.23%	0.6%	303.1	101.0%	**78.0**	2.5
SDA HC14	100	**1000**	5.20%	5.13%	-1.3%	301.7	100.6%	**77.0**	2.5
SDA HC15	100	**1000**	5.20%	5.24%	0.8%	301.9	100.6%	**75.1**	2.5
SDB HC1	100	**200**	4.93%	4.84%	-1.8%	298.1	99.4%	**75.0**	2.5
SDB HC2	100	**200**	4.93%	4.81%	-2.4%	296.5	98.8%	**73.0**	2.5
SDB HC3	100	**200**	4.93%	4.98%	1.0%	294.9	98.3%	**72.0**	2.5
SDB HC4	100	**400**	4.77%	4.70%	-1.5%	296.9	99.0%	**73.5**	2.5
SDB HC5	100	**400**	4.77%	4.65%	-2.5%	296.5	98.8%	**74.0**	2.5
SDB HC6	100	**400**	4.77%	4.88%	2.3%	296.4	98.8%	**72.0**	2.5
SDB HC7	100	**600**	4.68%	4.66%	-0.4%	296.2	98.7%	**79.0**	2.5
SDB HC8	100	**600**	4.68%	4.61%	-1.5%	297.0	99.0%	**72.0**	2.5
SDB HC9	100	**600**	4.68%	4.79%	2.4%	298.6	99.5%	**76.0**	2.5
SDB HC10	100	**800**	4.61%	4.63%	0.4%	297.6	99.2%	**75.0**	2.5
SDB HC11	100	**800**	4.61%	4.65%	0.9%	297.9	99.3%	**75.5**	2.5
SDB HC12	100	**800**	4.61%	4.69%	1.7%	299.3	99.8%	**72.0**	2.5
SDB HC13	100	**1000**	4.56%	4.70%	3.0%	298.4	99.5%	**74.5**	2.5
SDB HC14	100	**1000**	4.56%	4.62%	1.3%	297.1	99.0%	**72.0**	2.5
SDB HC15	100	**1000**	4.56%	4.53%	-0.7%	297.5	99.2%	**75.6**	2.5

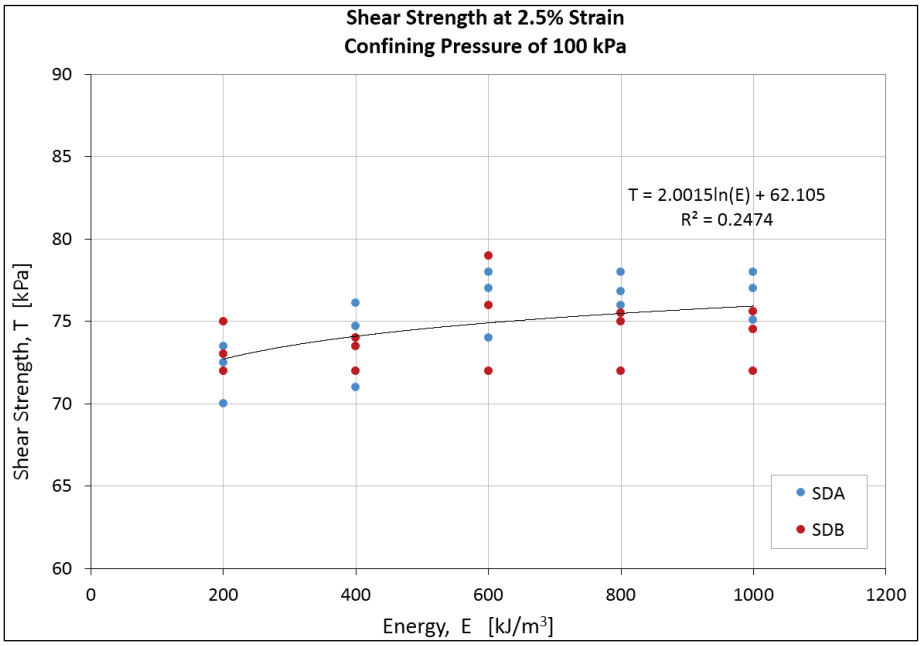
Shear Strength at 2.5% Strain
Confining Pressure of 100 kPa
T = 2.0015ln(E) + 62.105
R² = 0.2474
SDA
SDB
Shear Strength, T [kPa]
Energy, E [kJ/m³]
90
85
80
75
70
65
60
0
200
400
600
800
1000
1200

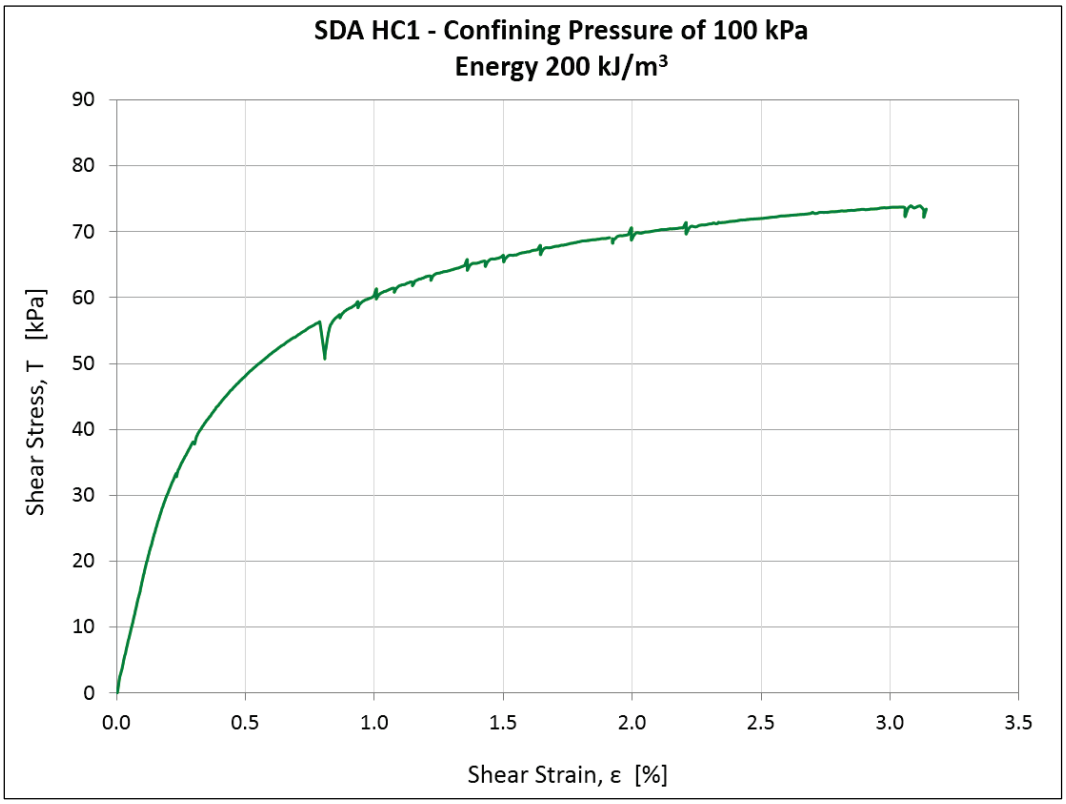
SDA HC1 - Confining Pressure of 100 kPa
Energy 200 kJ/m³
Shear Stress, T [kPa]
Shear Strain, ε [%]
90
80
70
60
50
40
30
20
10
0
0.0
0.5
1.0
1.5
2.0
2.5
3.0
3.5

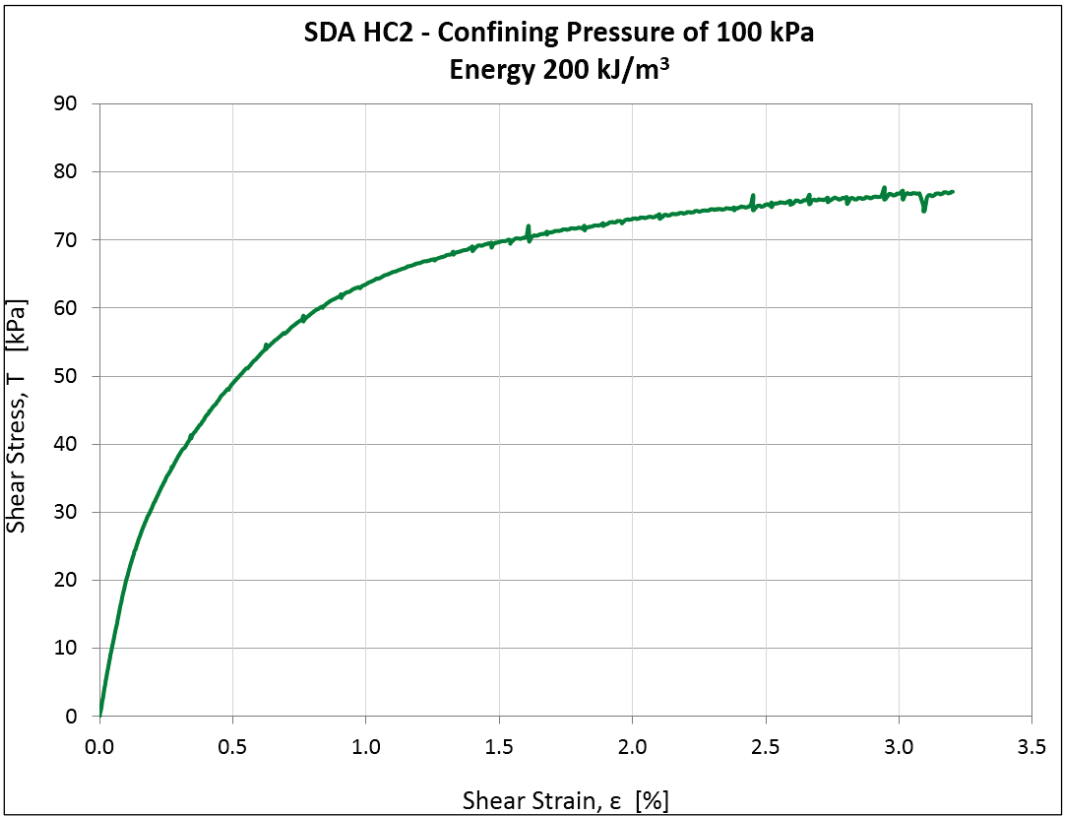
SDA HC2 - Confining Pressure of 100 kPa
Energy 200 kJ/m³
Shear Stress, T [kPa]
Shear Strain, ε [%]
0
10
20
30
40
50
60
70
80
90
0.0
0.5
1.0
1.5
2.0
2.5
3.0
3.5

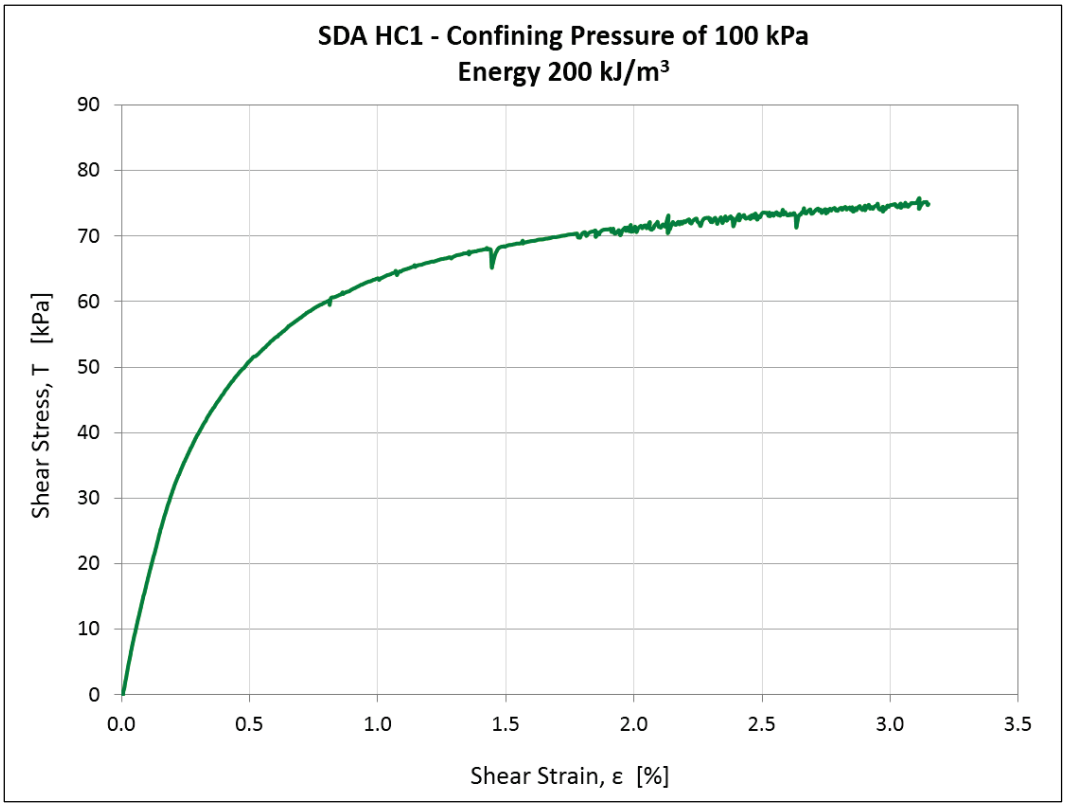
SDA HC1 - Confining Pressure of 100 kPa
Energy 200 kJ/m³
Shear Stress, T [kPa]
Shear Strain, ε [%]
0
10
20
30
40
50
60
70
80
90
0.0
0.5
1.0
1.5
2.0
2.5
3.0
3.5

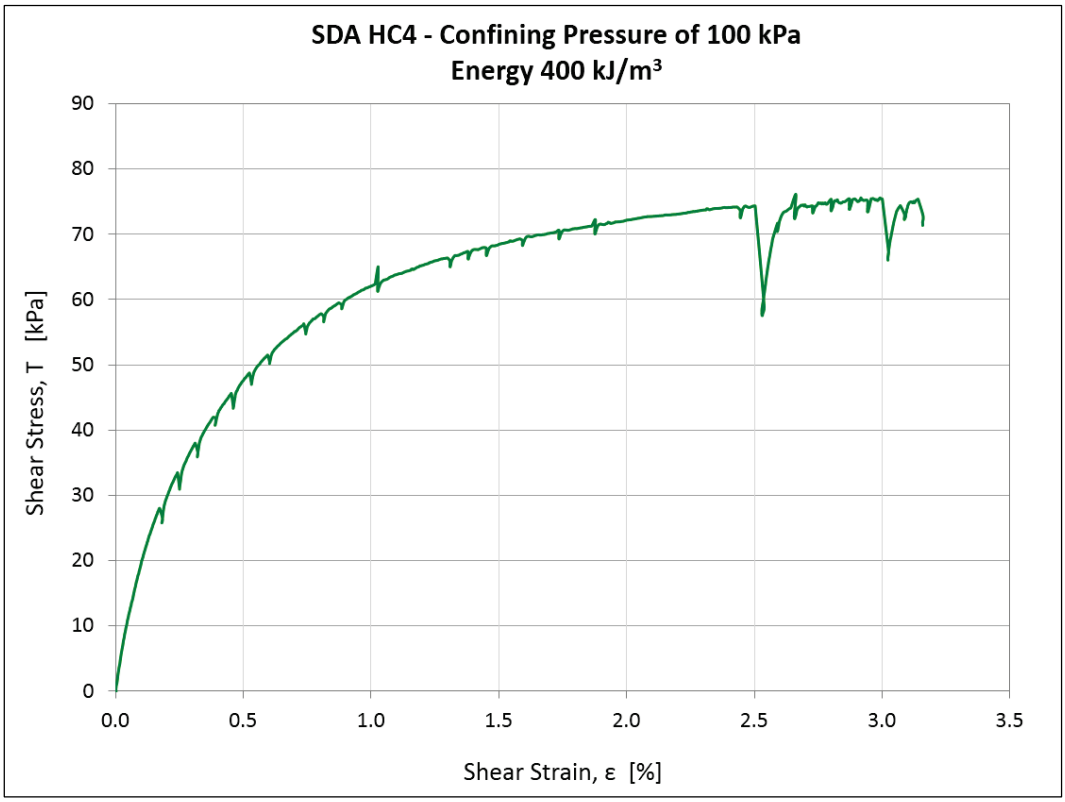
SDA HC4 - Confining Pressure of 100 kPa
Energy 400 kJ/m³
Shear Stress, T [kPa]
Shear Strain, ε [%]
0
10
20
30
40
50
60
70
80
90
0.0
0.5
1.0
1.5
2.0
2.5
3.0
3.5

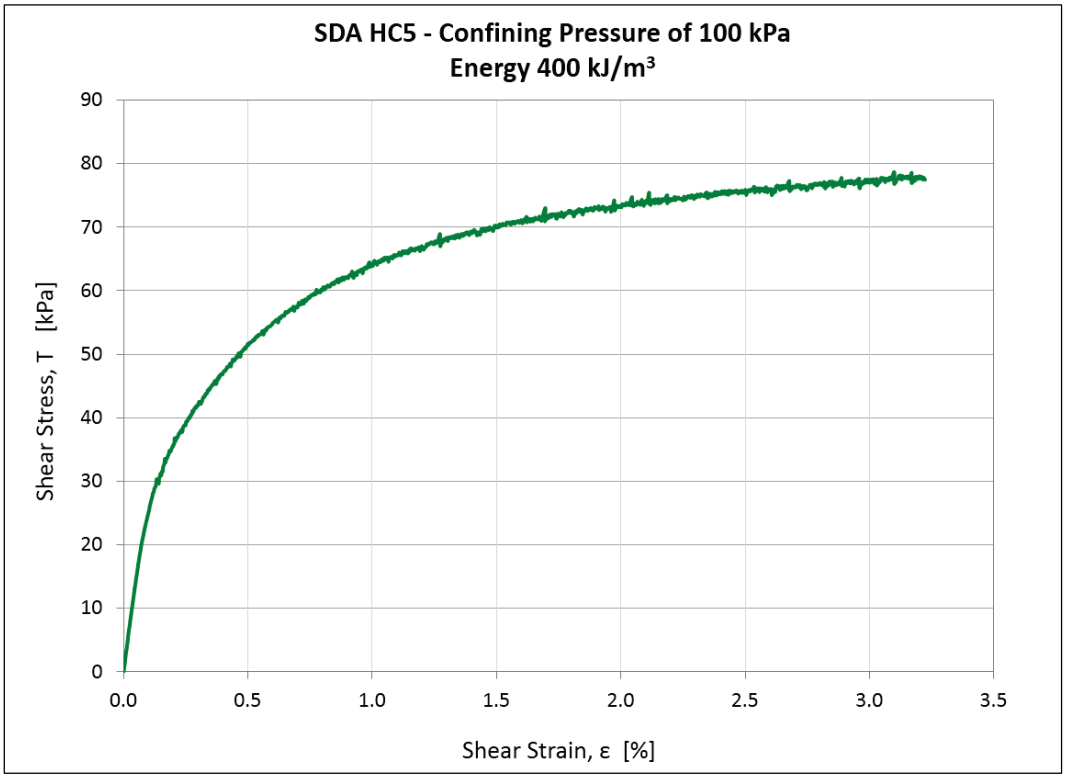
SDA HC5 - Confining Pressure of 100 kPa
Energy 400 kJ/m³
Shear Stress, T [kPa]
Shear Strain, ε [%]
0
10
20
30
40
50
60
70
80
90
0.0
0.5
1.0
1.5
2.0
2.5
3.0
3.5

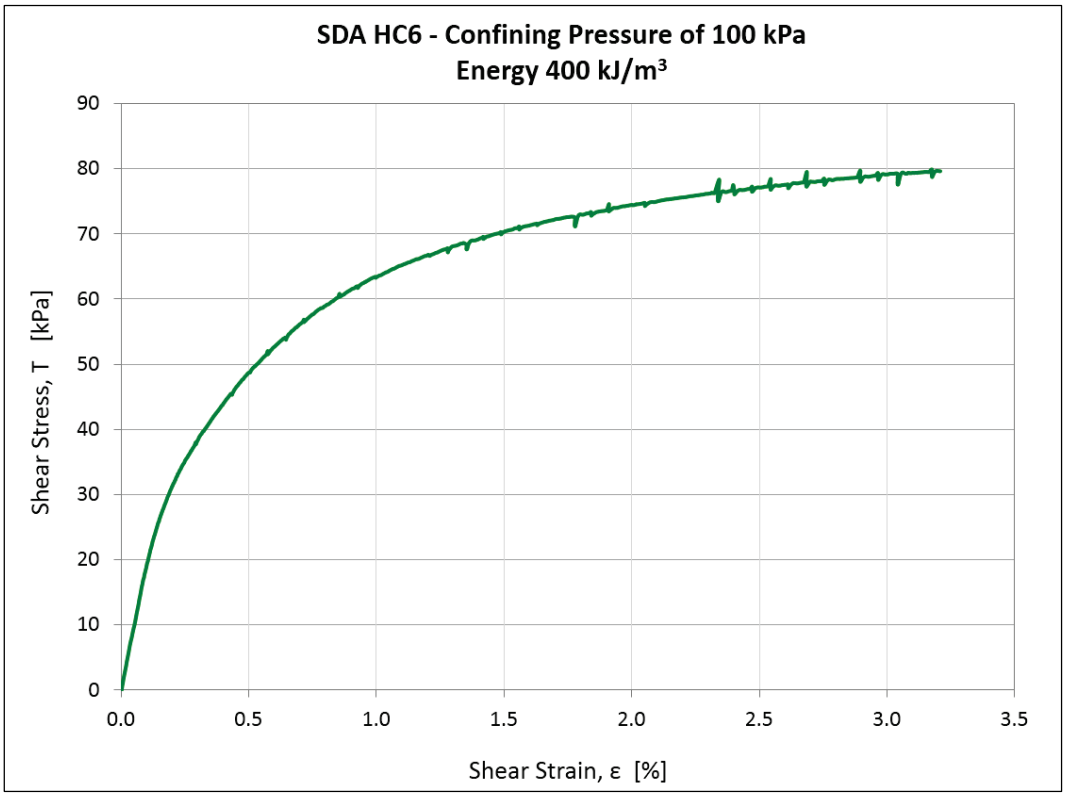
SDA HC6 - Confining Pressure of 100 kPa
Energy 400 kJ/m³
Shear Stress, T [kPa]
Shear Strain, ε [%]
0
10
20
30
40
50
60
70
80
90
0.0
0.5
1.0
1.5
2.0
2.5
3.0
3.5

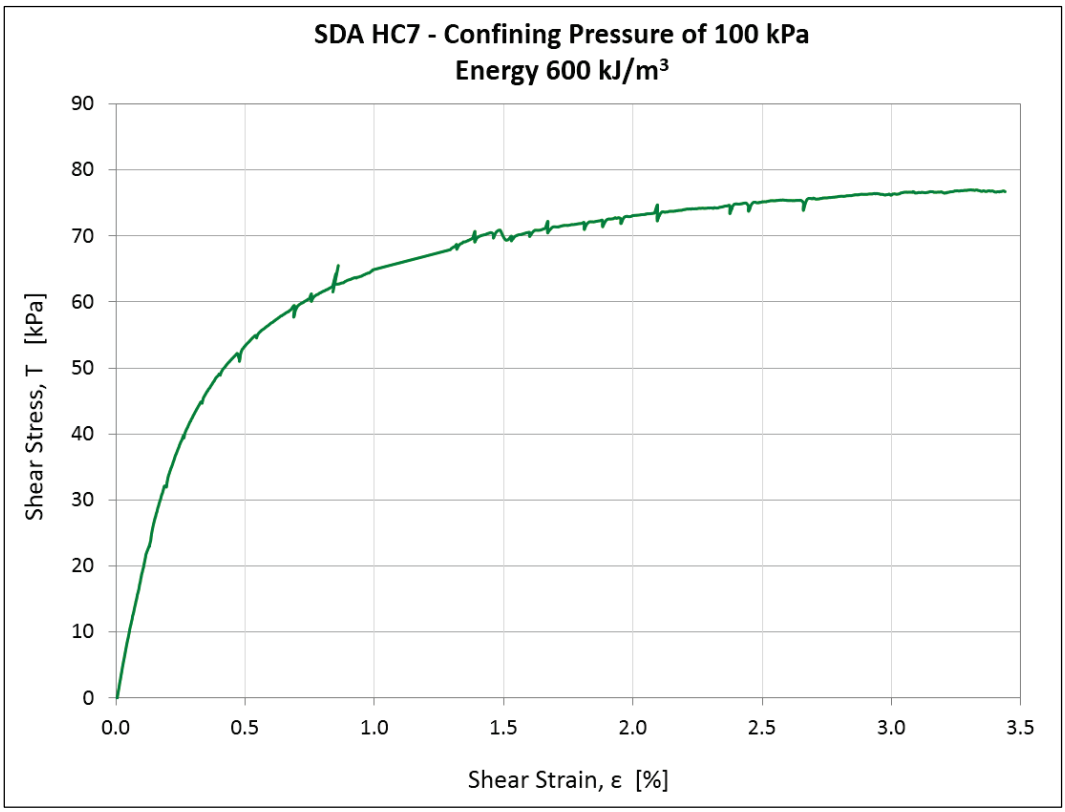
SDA HC7 - Confining Pressure of 100 kPa
Energy 600 kJ/m³
Shear Stress, T [kPa]
Shear Strain, ε [%]
0
10
20
30
40
50
60
70
80
90
0.0
0.5
1.0
1.5
2.0
2.5
3.0
3.5

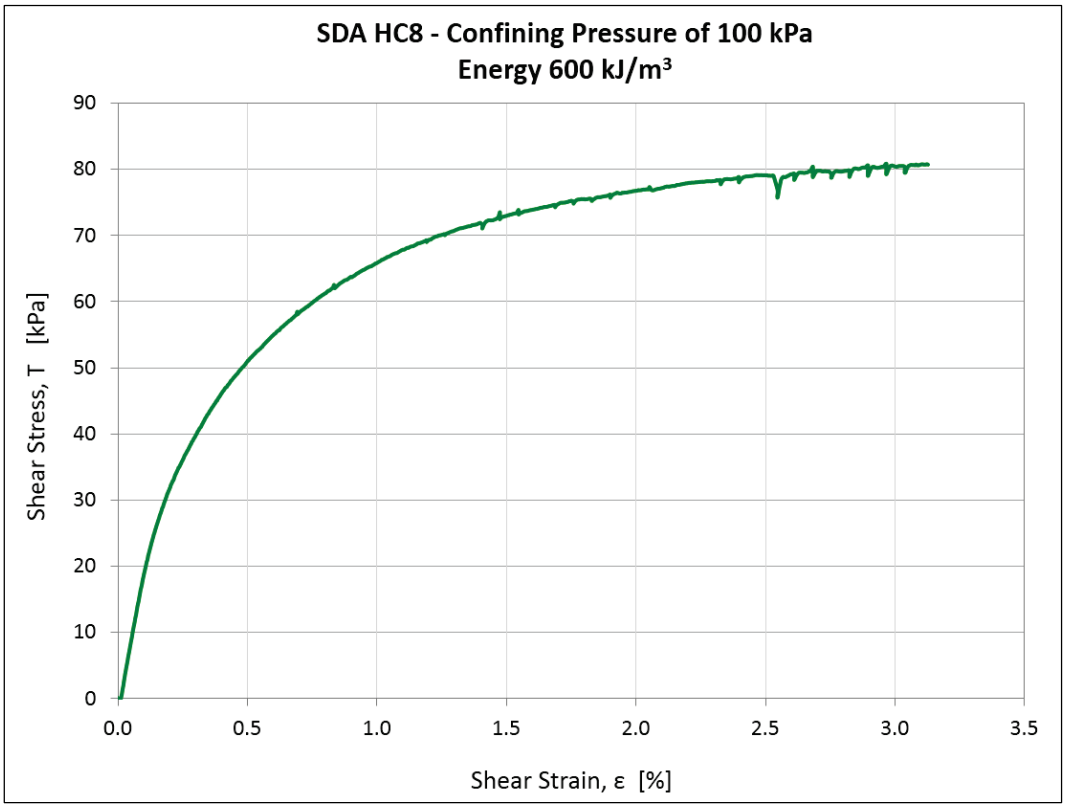
SDA HC8 - Confining Pressure of 100 kPa
Energy 600 kJ/m³
Shear Stress, T [kPa]
0
10
20
30
40
50
60
70
80
90
0.0
0.5
1.0
1.5
2.0
2.5
3.0
3.5
Shear Strain, ε [%]

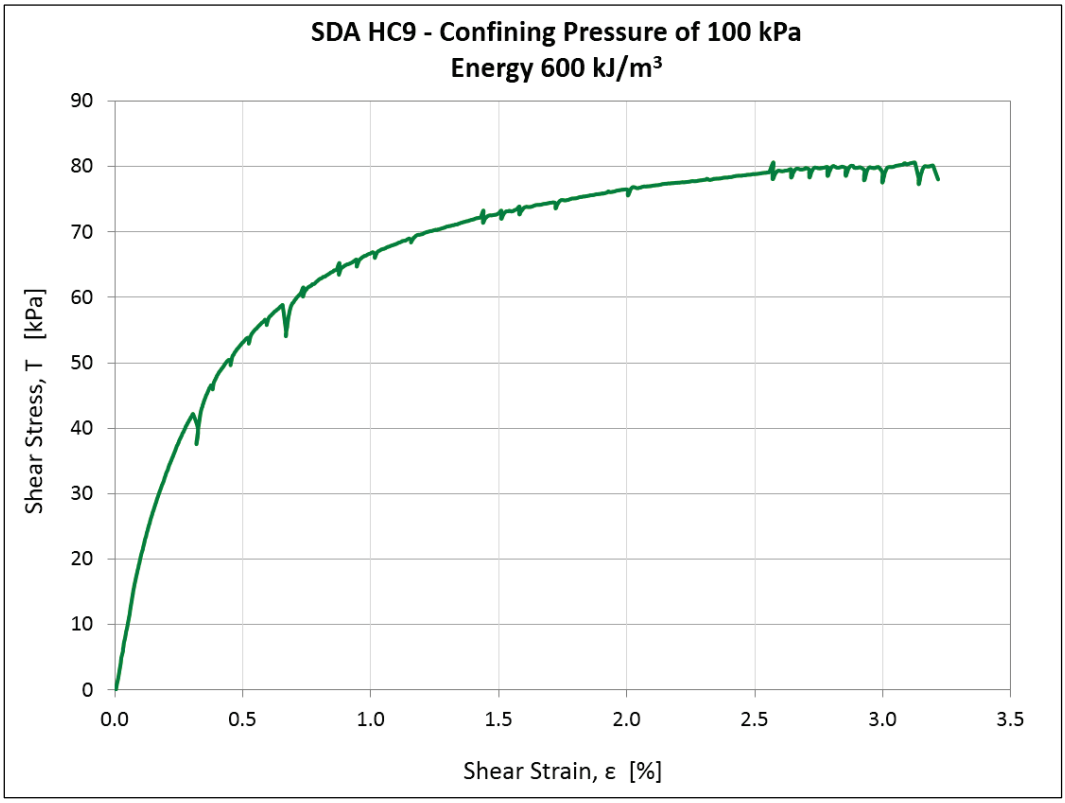
SDA HC9 - Confining Pressure of 100 kPa
Energy 600 kJ/m³
Shear Stress, T [kPa]
0
10
20
30
40
50
60
70
80
90
0.0
0.5
1.0
1.5
2.0
2.5
3.0
3.5
Shear Strain, ε [%]

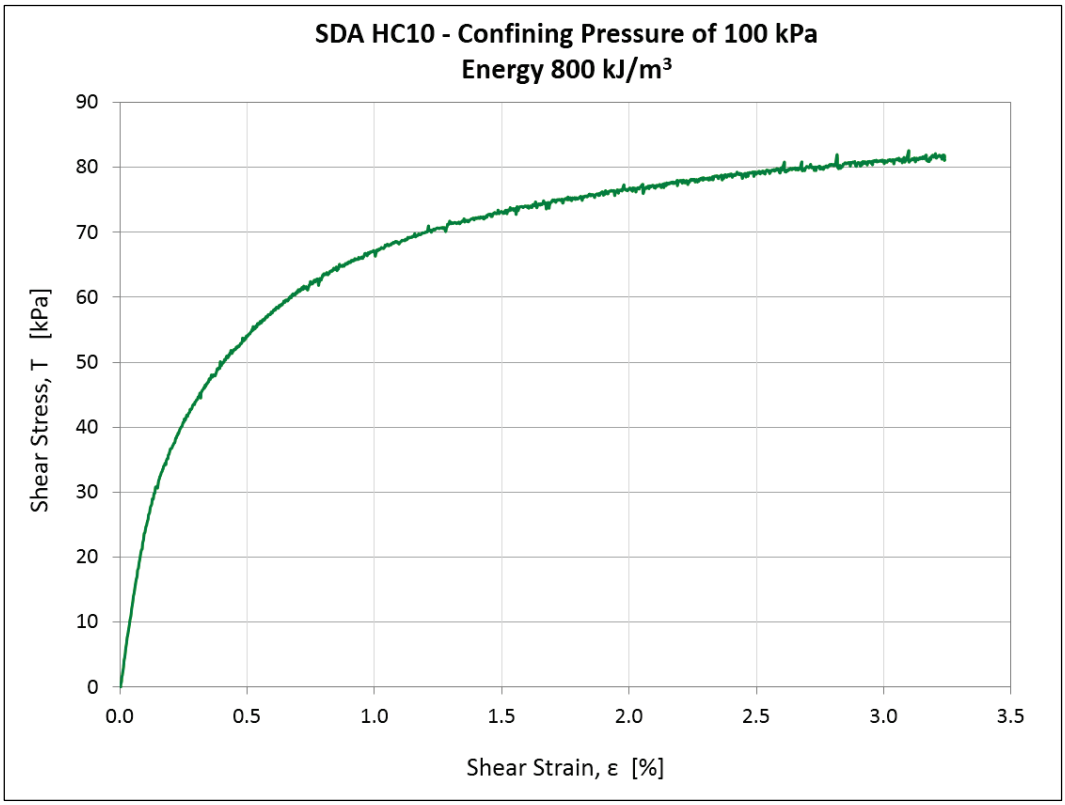
SDA HC10 - Confining Pressure of 100 kPa
Energy 800 kJ/m³
Shear Stress, T [kPa]
Shear Strain, ε [%]
0
10
20
30
40
50
60
70
80
90
0.0
0.5
1.0
1.5
2.0
2.5
3.0
3.5

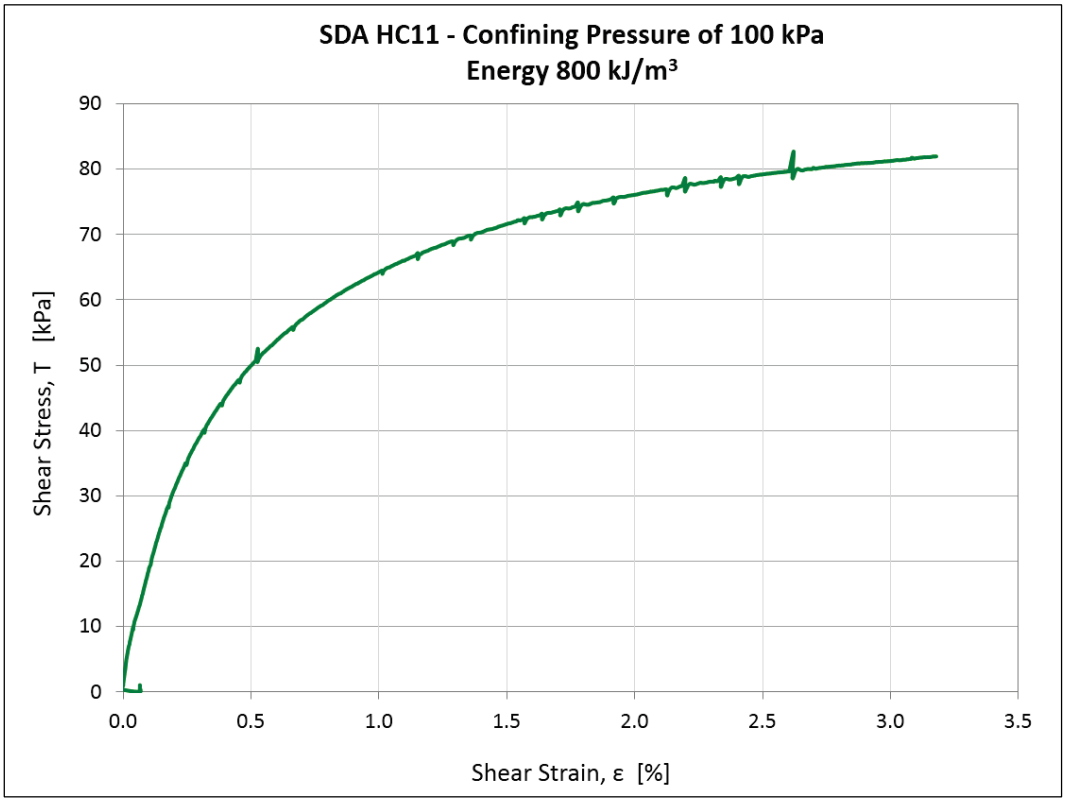
SDA HC11 - Confining Pressure of 100 kPa
Energy 800 kJ/m³
Shear Stress, T [kPa]
Shear Strain, ε [%]
0
10
20
30
40
50
60
70
80
90
0.0
0.5
1.0
1.5
2.0
2.5
3.0
3.5

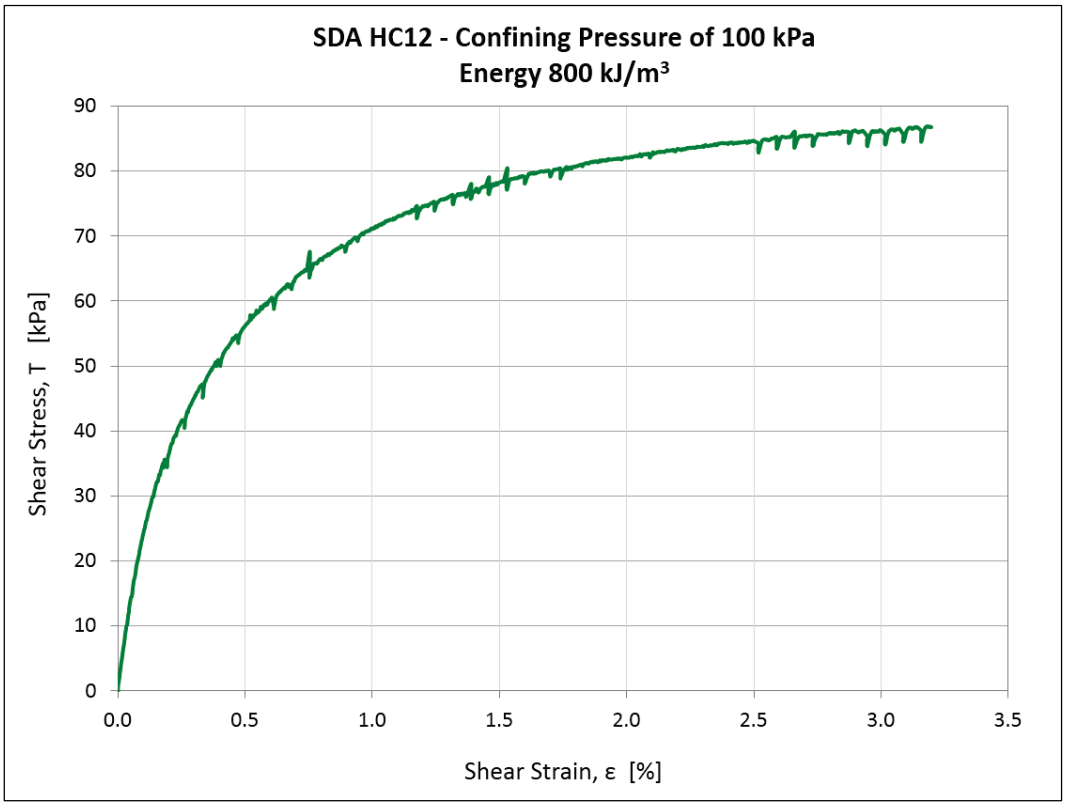
SDA HC12 - Confining Pressure of 100 kPa
Energy 800 kJ/m³
Shear Stress, T [kPa]
Shear Strain, ε [%]
0
10
20
30
40
50
60
70
80
90
0.0
0.5
1.0
1.5
2.0
2.5
3.0
3.5

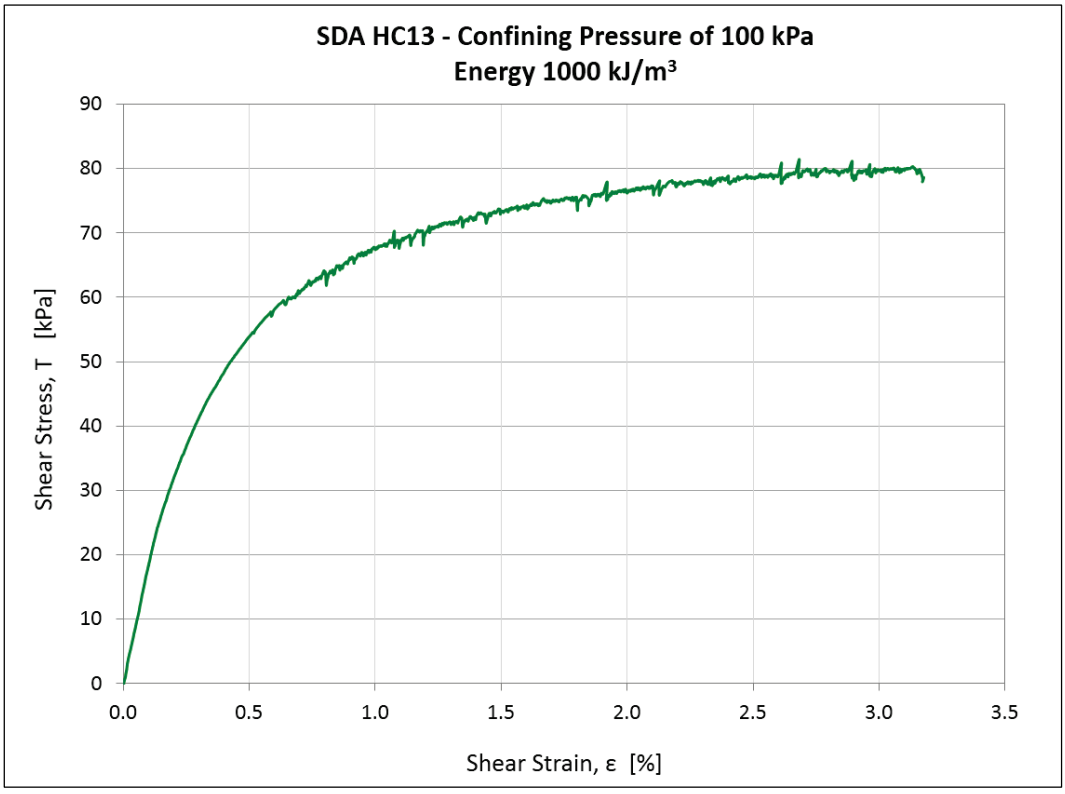
SDA HC13 - Confining Pressure of 100 kPa
Energy 1000 kJ/m³
Shear Stress, T [kPa]
Shear Strain, ε [%]
0
10
20
30
40
50
60
70
80
90
0.0
0.5
1.0
1.5
2.0
2.5
3.0
3.5

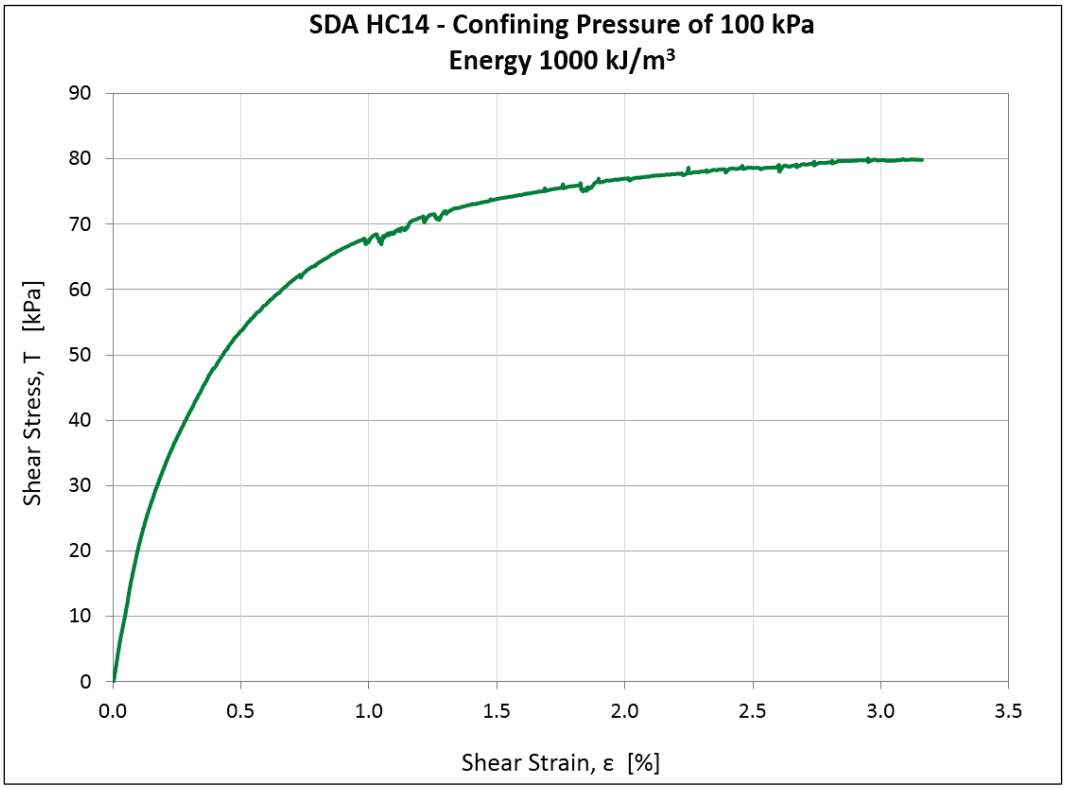
SDA HC14 - Confining Pressure of 100 kPa
Energy 1000 kJ/m³
Shear Stress, T [kPa]
Shear Strain, ε [%]
0
10
20
30
40
50
60
70
80
90
0.0
0.5
1.0
1.5
2.0
2.5
3.0
3.5

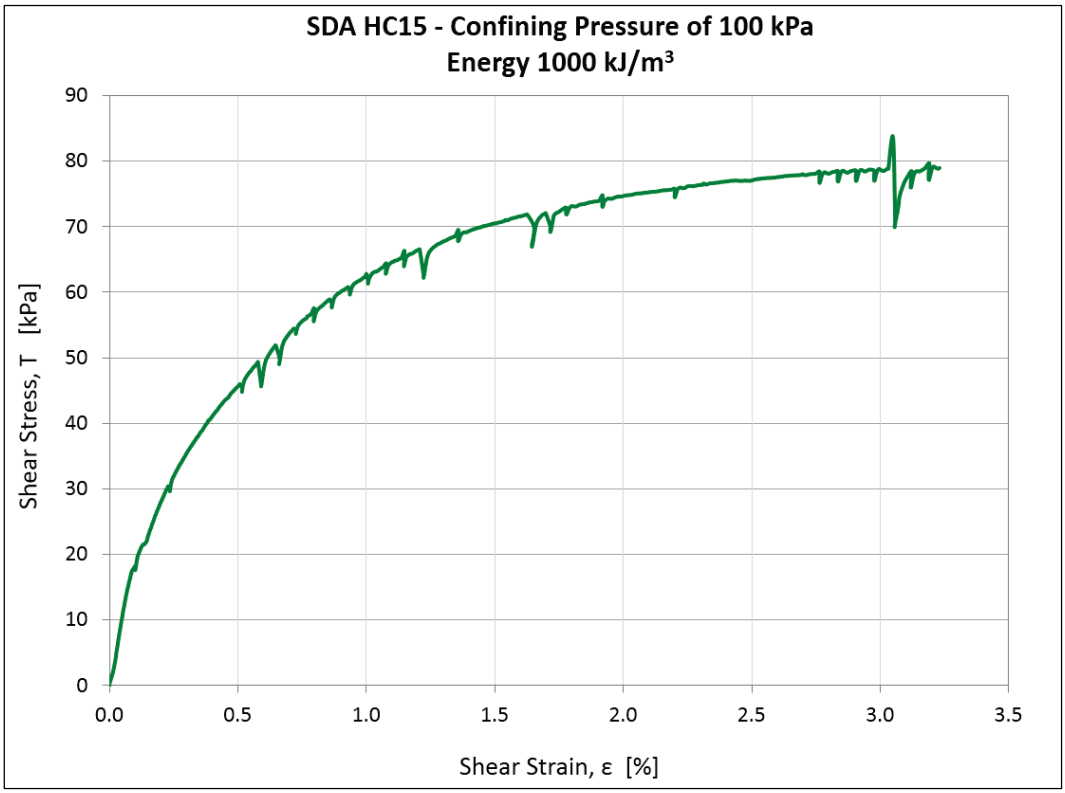
SDA HC15 - Confining Pressure of 100 kPa
Energy 1000 kJ/m³
Shear Stress, T [kPa]
Shear Strain, ε [%]
0
10
20
30
40
50
60
70
80
90
0.0
0.5
1.0
1.5
2.0
2.5
3.0
3.5

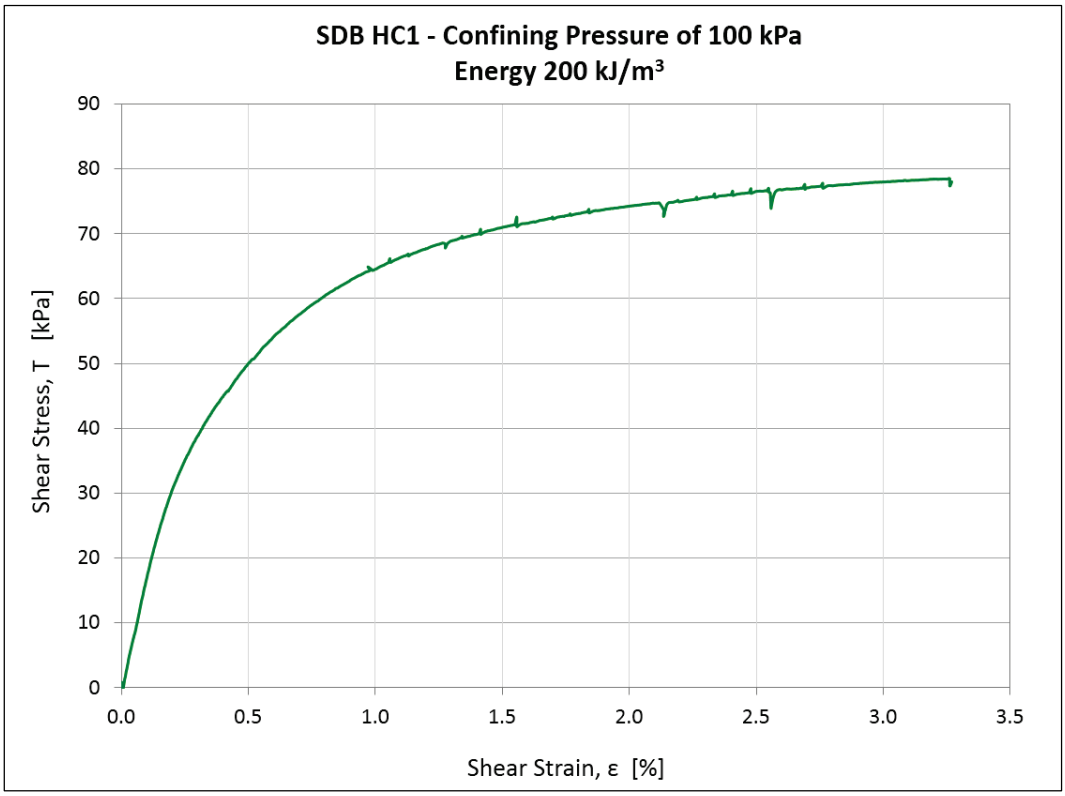
SDB HC1 - Confining Pressure of 100 kPa
Energy 200 kJ/m³
Shear Stress, T [kPa]
Shear Strain, ε [%]
0
10
20
30
40
50
60
70
80
90
0.0
0.5
1.0
1.5
2.0
2.5
3.0
3.5

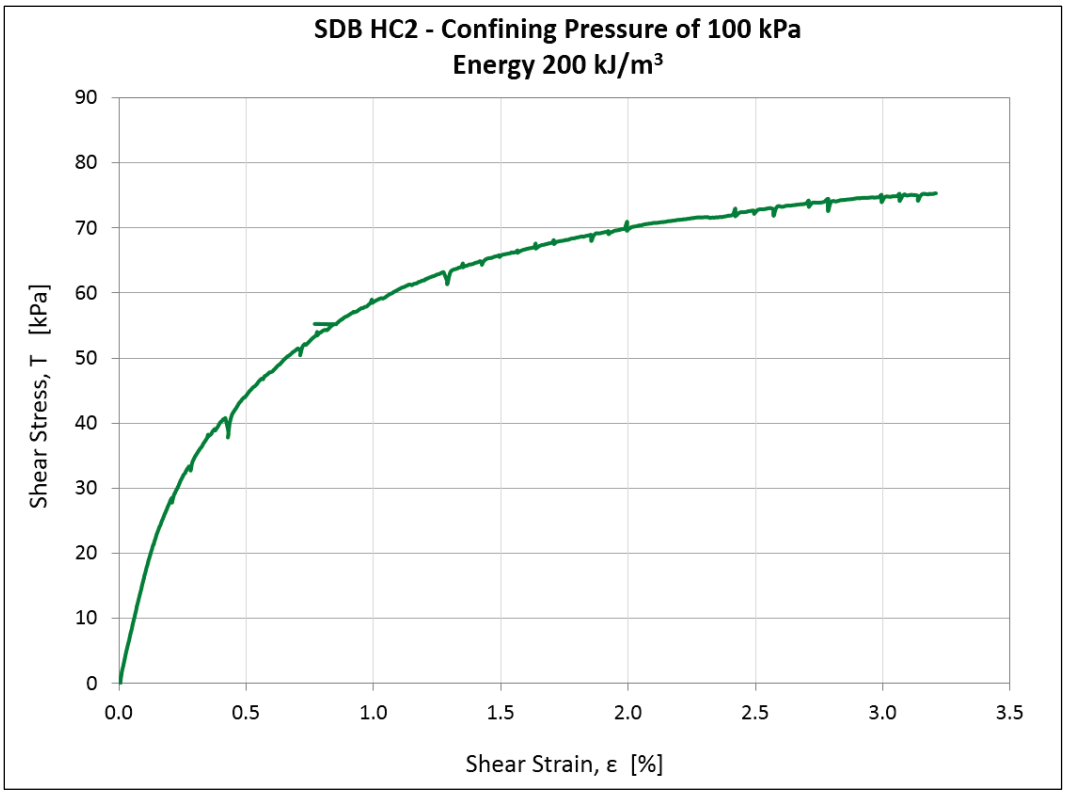
SDB HC2 - Confining Pressure of 100 kPa
Energy 200 kJ/m³
Shear Stress, T [kPa]
Shear Strain, ε [%]
0
10
20
30
40
50
60
70
80
90
0.0
0.5
1.0
1.5
2.0
2.5
3.0
3.5

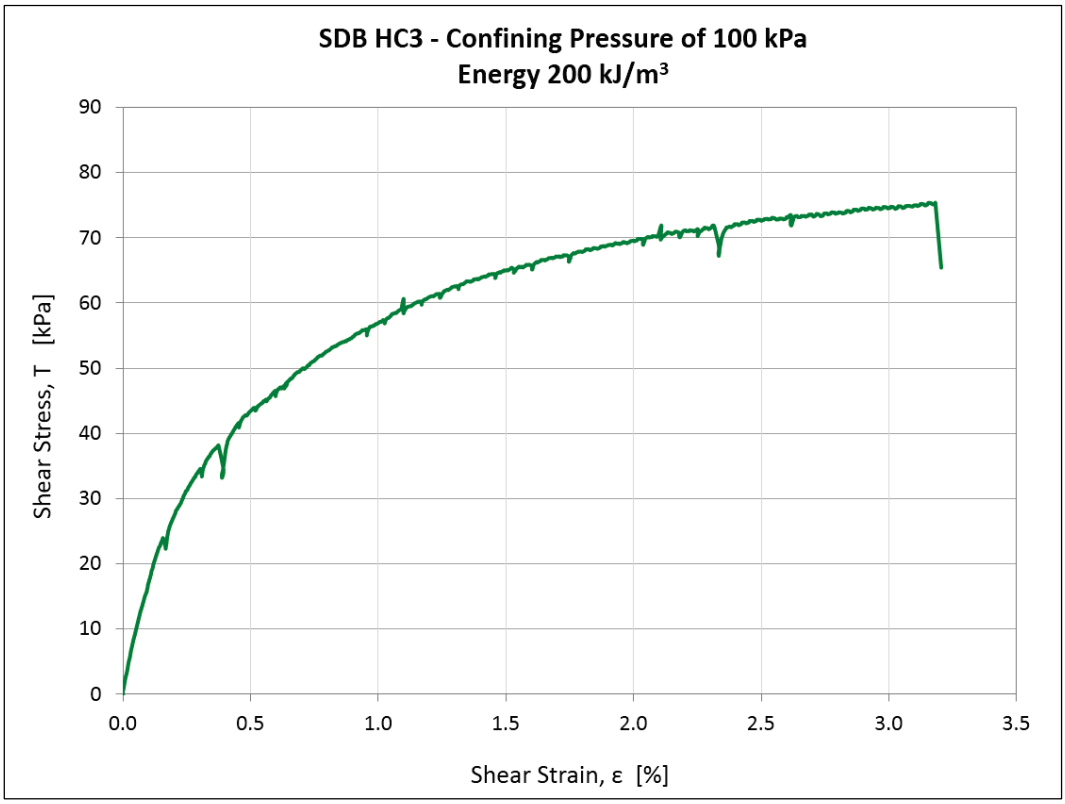
SDB HC3 - Confining Pressure of 100 kPa
Energy 200 kJ/m³
Shear Stress, T [kPa]
Shear Strain, ε [%]
0
10
20
30
40
50
60
70
80
90
0.0
0.5
1.0
1.5
2.0
2.5
3.0
3.5

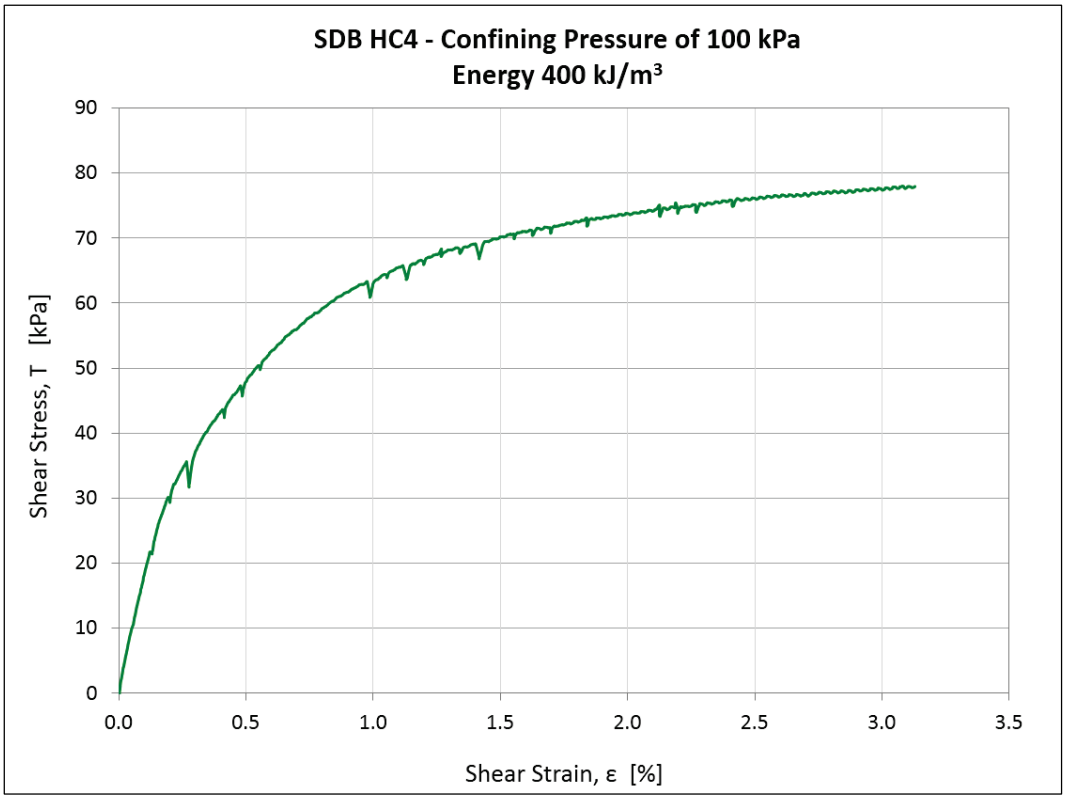
SDB HC4 - Confining Pressure of 100 kPa
Energy 400 kJ/m³
Shear Stress, T [kPa]
Shear Strain, ε [%]
0
10
20
30
40
50
60
70
80
90
0.0
0.5
1.0
1.5
2.0
2.5
3.0
3.5

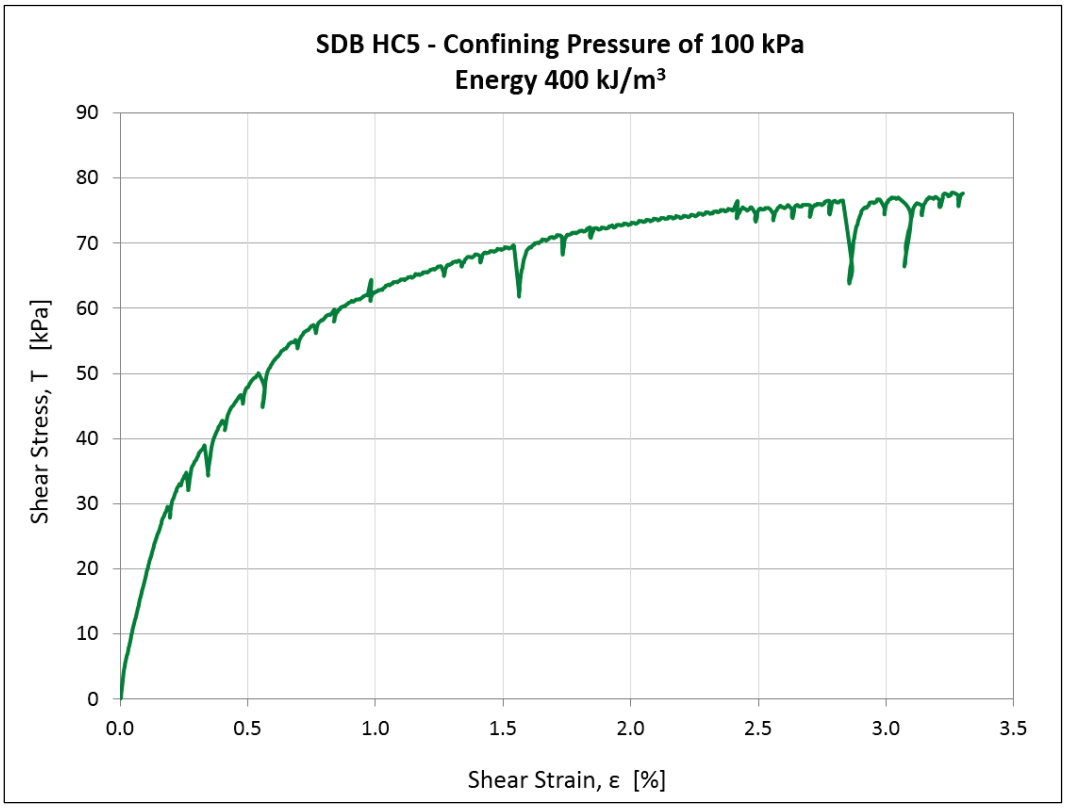
SDB HC5 - Confining Pressure of 100 kPa
Energy 400 kJ/m³
Shear Stress, T [kPa]
Shear Strain, ε [%]
0
10
20
30
40
50
60
70
80
90
0.0
0.5
1.0
1.5
2.0
2.5
3.0
3.5

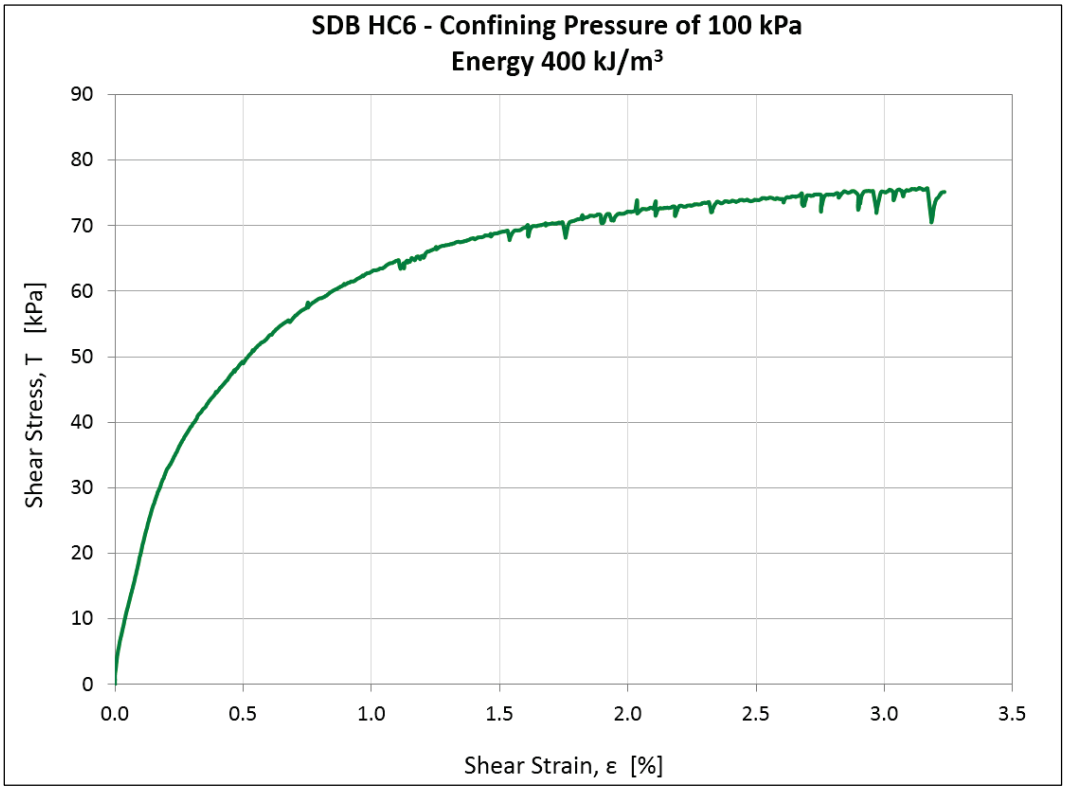
SDB HC6 - Confining Pressure of 100 kPa
Energy 400 kJ/m³
Shear Stress, T [kPa]
Shear Strain, ε [%]
0
10
20
30
40
50
60
70
80
90
0.0
0.5
1.0
1.5
2.0
2.5
3.0
3.5

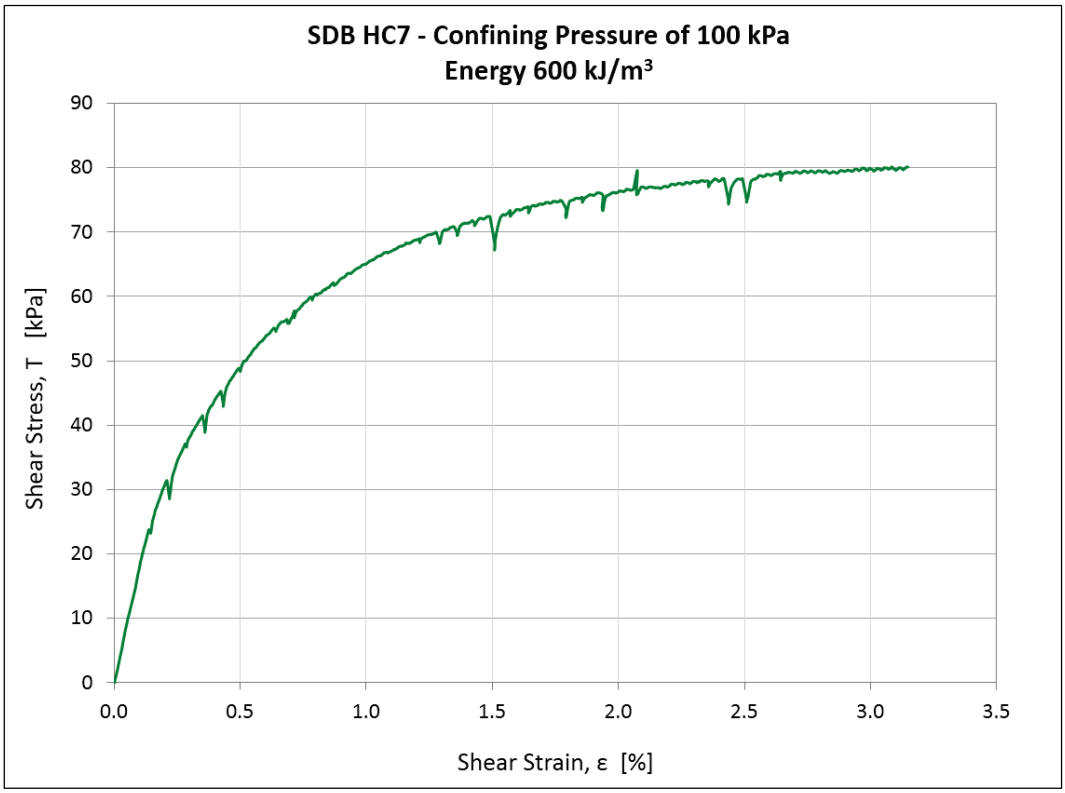
SDB HC7 - Confining Pressure of 100 kPa
Energy 600 kJ/m³
Shear Stress, T [kPa]
Shear Strain, ε [%]
0
10
20
30
40
50
60
70
80
90
0.0
0.5
1.0
1.5
2.0
2.5
3.0
3.5

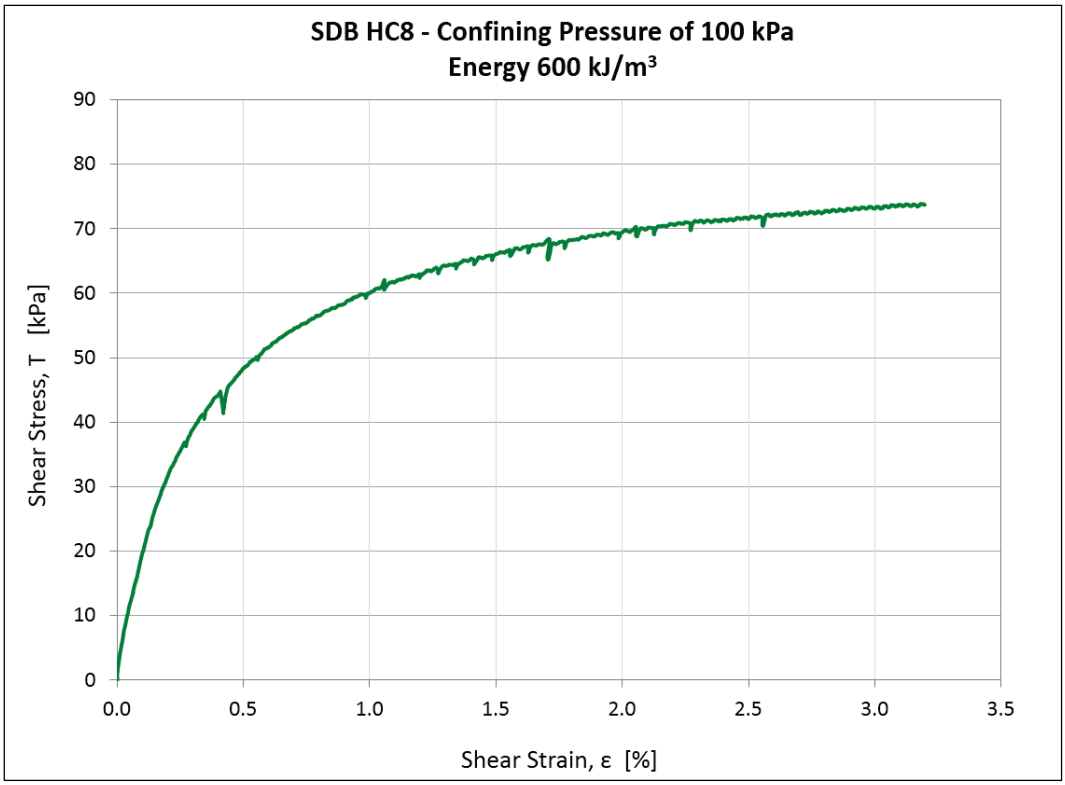
SDB HC8 - Confining Pressure of 100 kPa
Energy 600 kJ/m³
Shear Stress, T [kPa]
Shear Strain, ε [%]
0
10
20
30
40
50
60
70
80
90
0.0
0.5
1.0
1.5
2.0
2.5
3.0
3.5

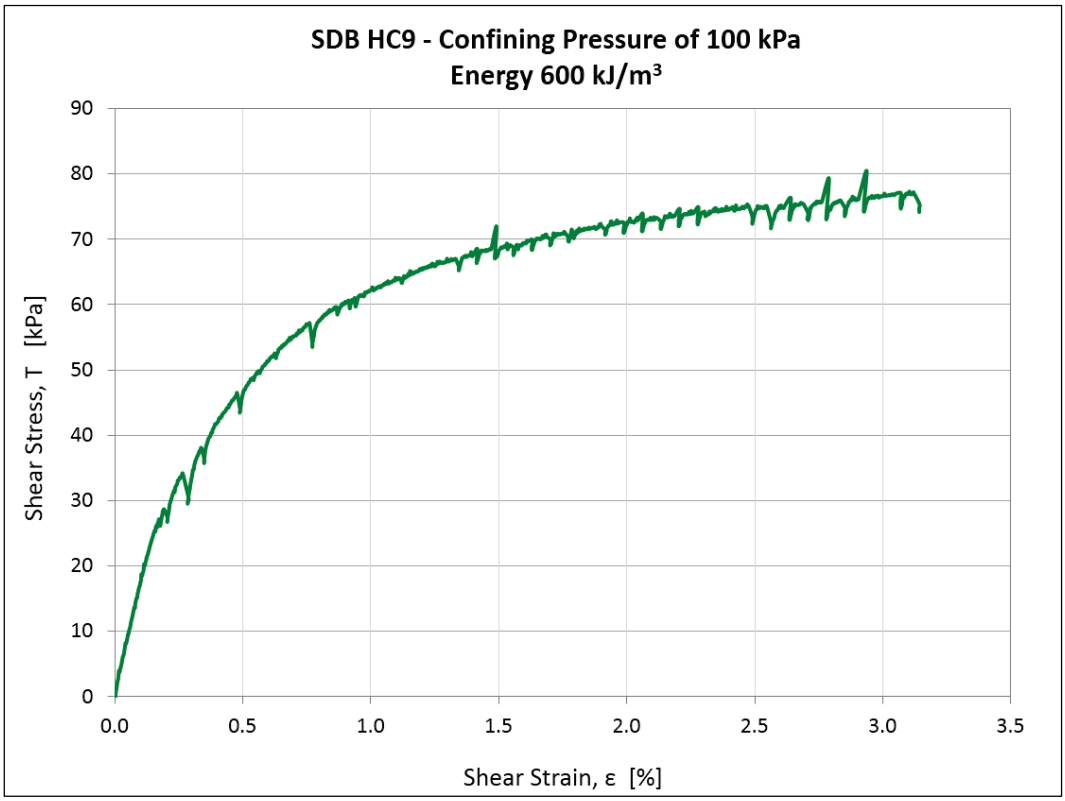
SDB HC9 - Confining Pressure of 100 kPa
Energy 600 kJ/m³
Shear Stress, T [kPa]
Shear Strain, ε [%]
0
10
20
30
40
50
60
70
80
90
0.0
0.5
1.0
1.5
2.0
2.5
3.0
3.5

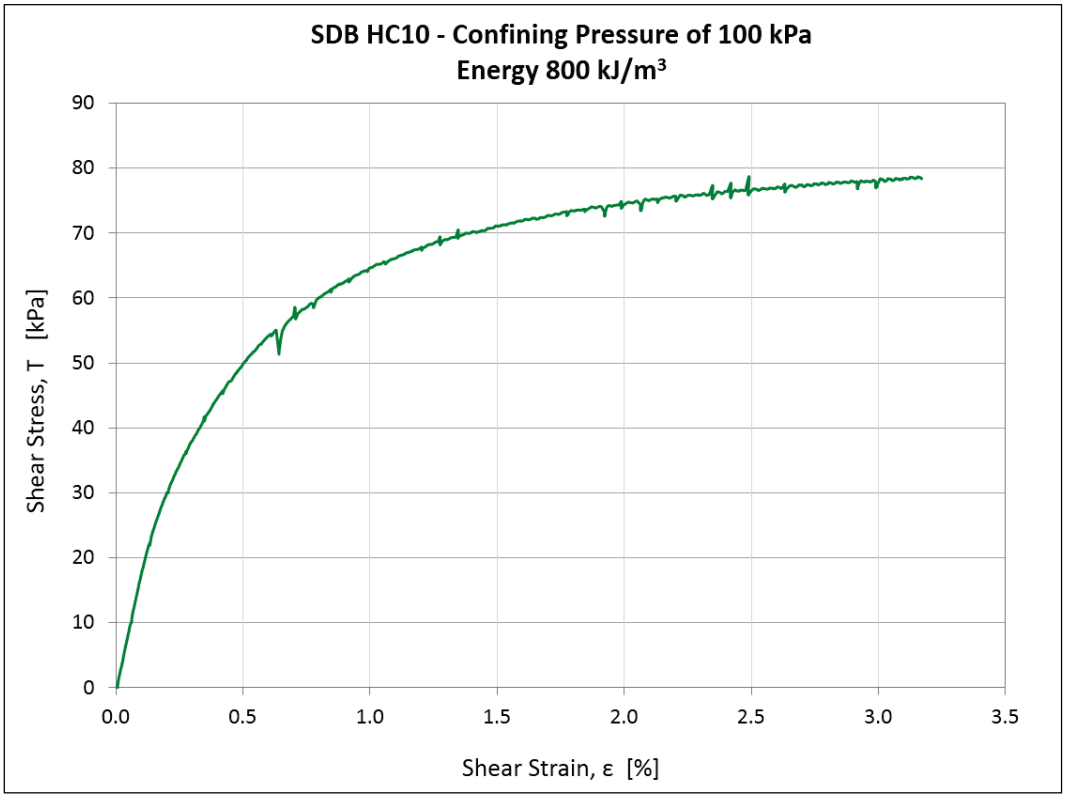
SDB HC10 - Confining Pressure of 100 kPa
Energy 800 kJ/m³
Shear Stress, T [kPa]
Shear Strain, ε [%]
0
10
20
30
40
50
60
70
80
90
0.0
0.5
1.0
1.5
2.0
2.5
3.0
3.5

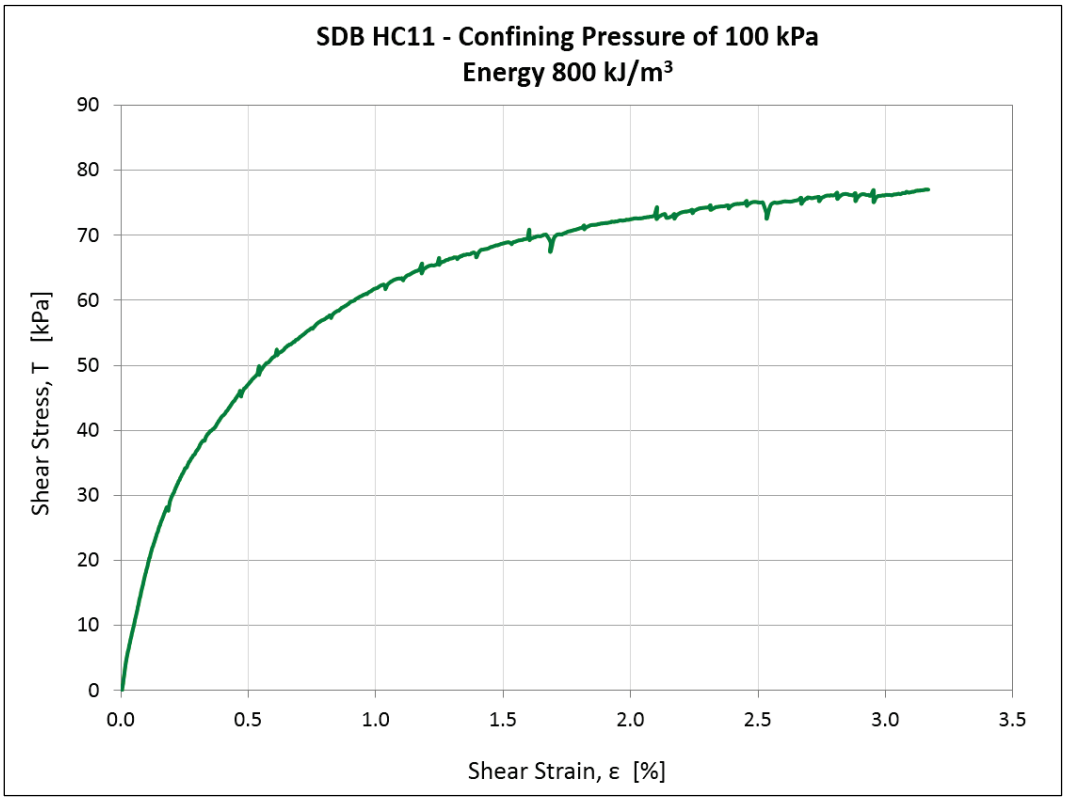
SDB HC11 - Confining Pressure of 100 kPa
Energy 800 kJ/m³
Shear Stress, T [kPa]
Shear Strain, ε [%]
0
10
20
30
40
50
60
70
80
90
0.0
0.5
1.0
1.5
2.0
2.5
3.0
3.5

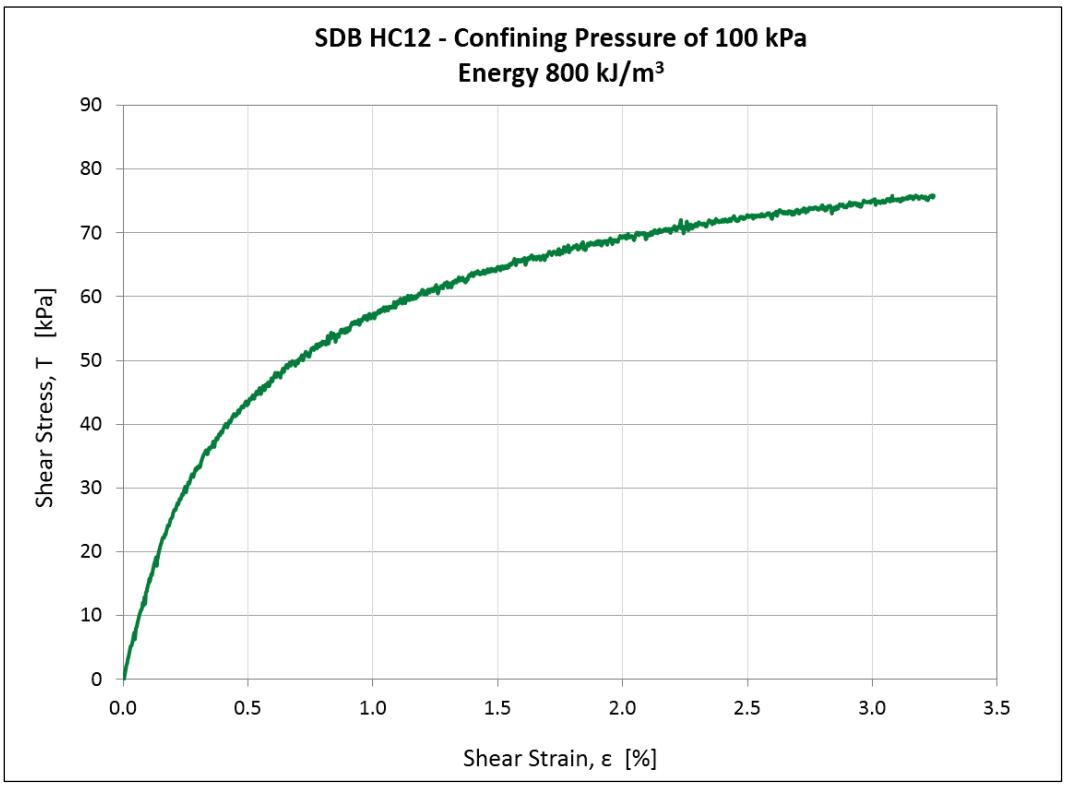
SDB HC12 - Confining Pressure of 100 kPa
Energy 800 kJ/m³
Shear Stress, T [kPa]
Shear Strain, ε [%]
0
10
20
30
40
50
60
70
80
90
0.0
0.5
1.0
1.5
2.0
2.5
3.0
3.5

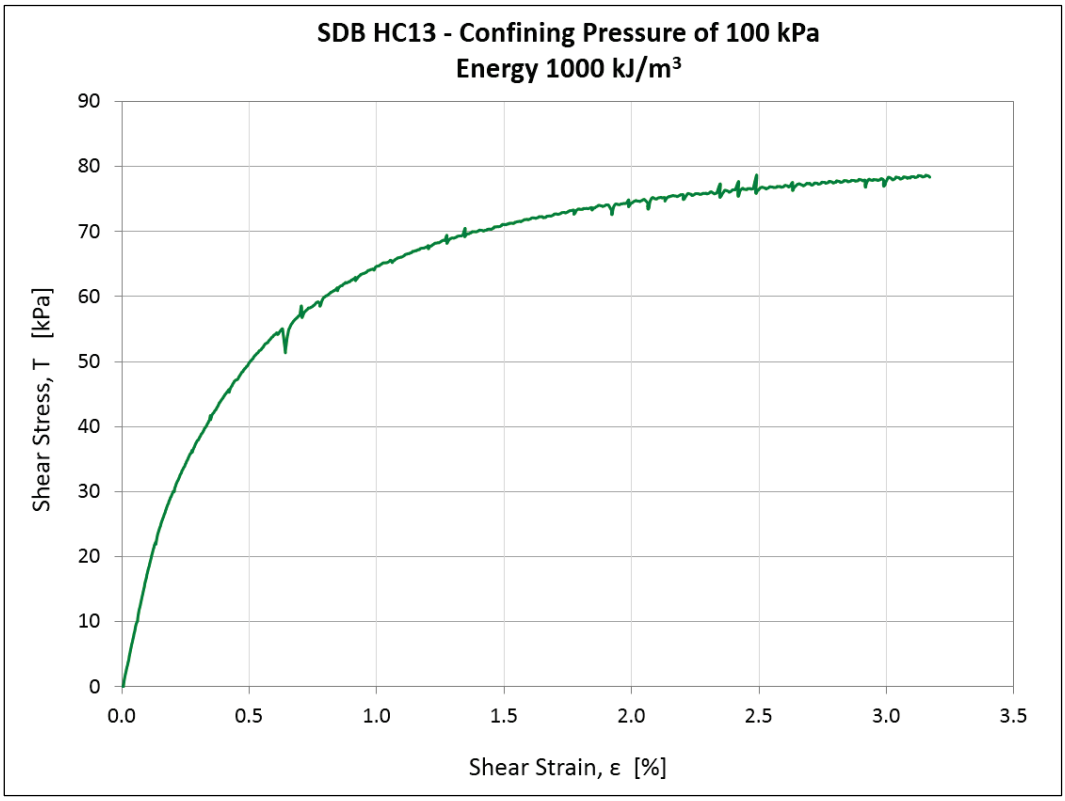
SDB HC13 - Confining Pressure of 100 kPa
Energy 1000 kJ/m³
Shear Stress, T [kPa]
Shear Strain, ε [%]
0
10
20
30
40
50
60
70
80
90
0.0
0.5
1.0
1.5
2.0
2.5
3.0
3.5

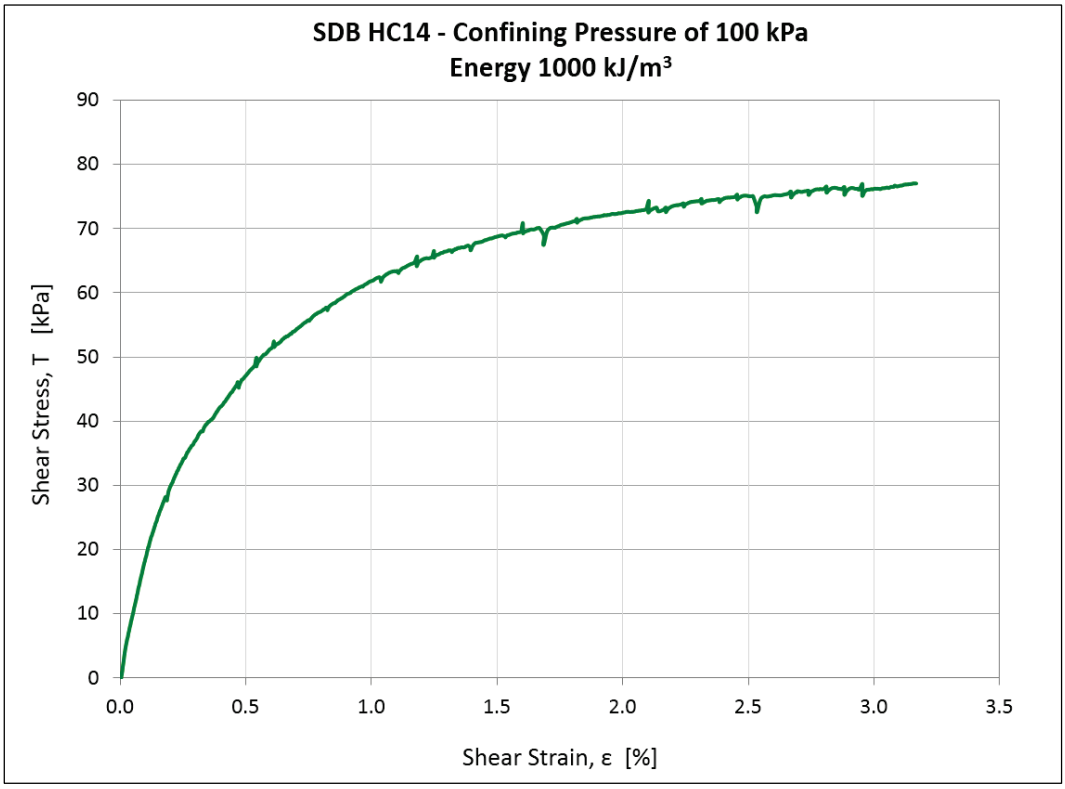
SDB HC14 - Confining Pressure of 100 kPa
Energy 1000 kJ/m³
Shear Stress, T [kPa]
Shear Strain, ε [%]
0
10
20
30
40
50
60
70
80
90
0.0
0.5
1.0
1.5
2.0
2.5
3.0
3.5

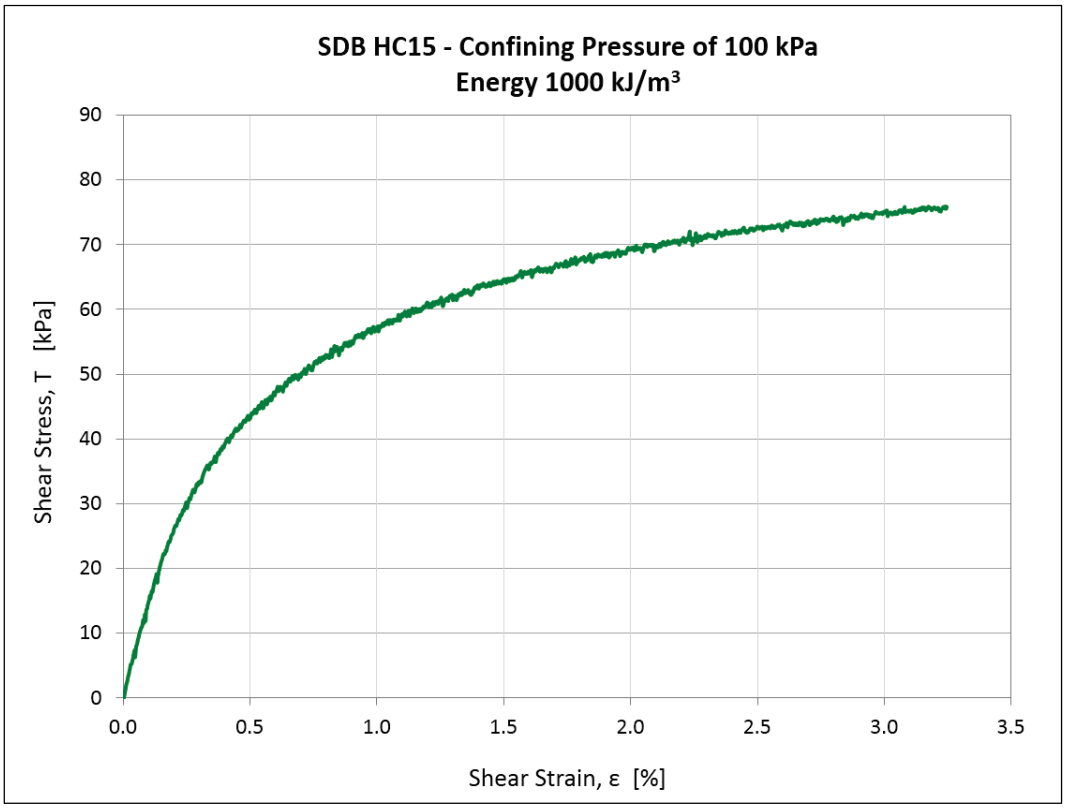
SDB HC15 - Confining Pressure of 100 kPa
Energy 1000 kJ/m3
Shear Stress, T [kPa]
Shear Strain, ε [%]
0
10
20
30
40
50
60
70
80
90
0.0
0.5
1.0
1.5
2.0
2.5
3.0
3.5

Appendix E: Simple Shear Test Data

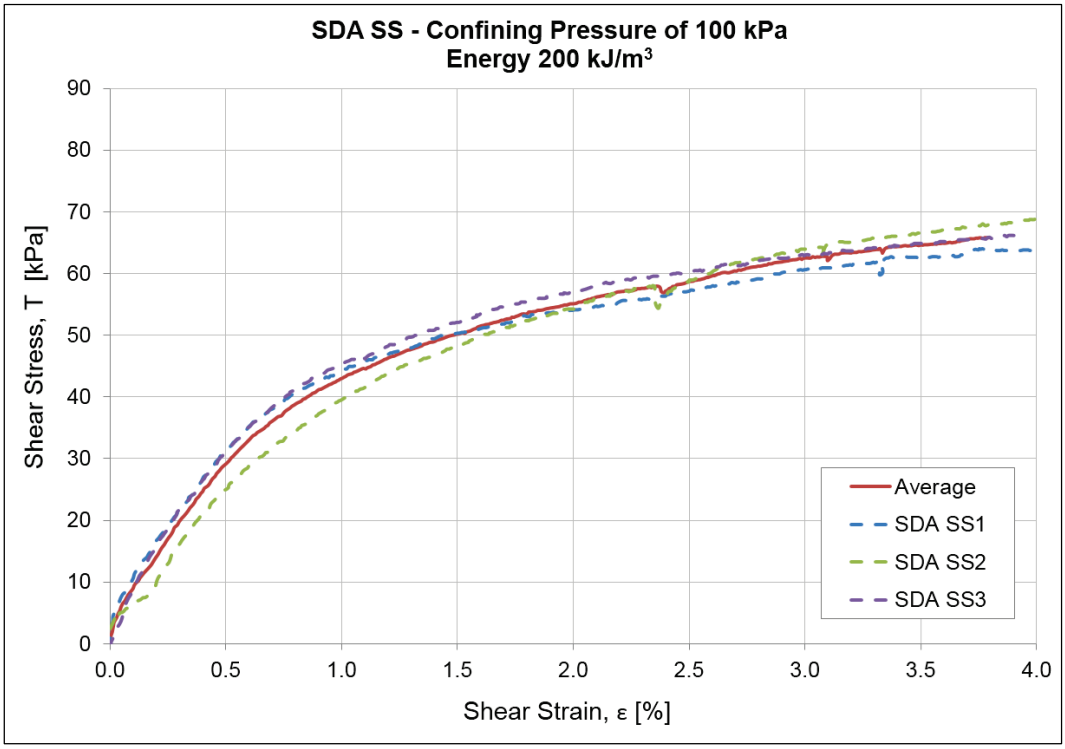

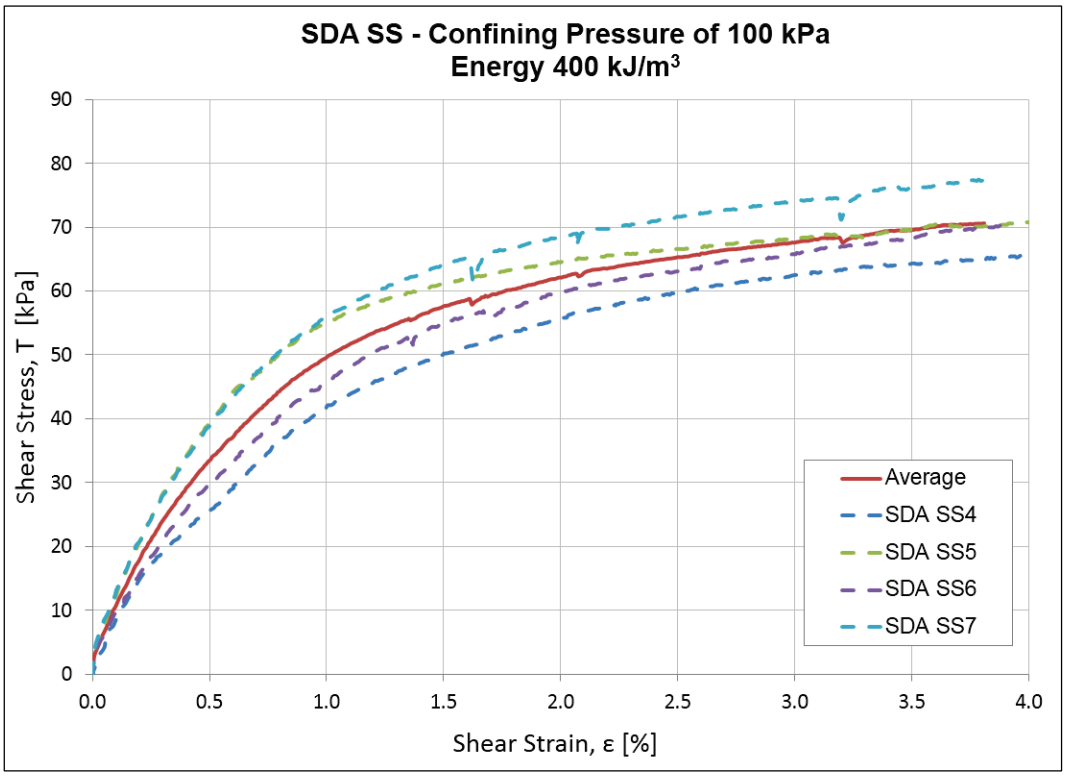

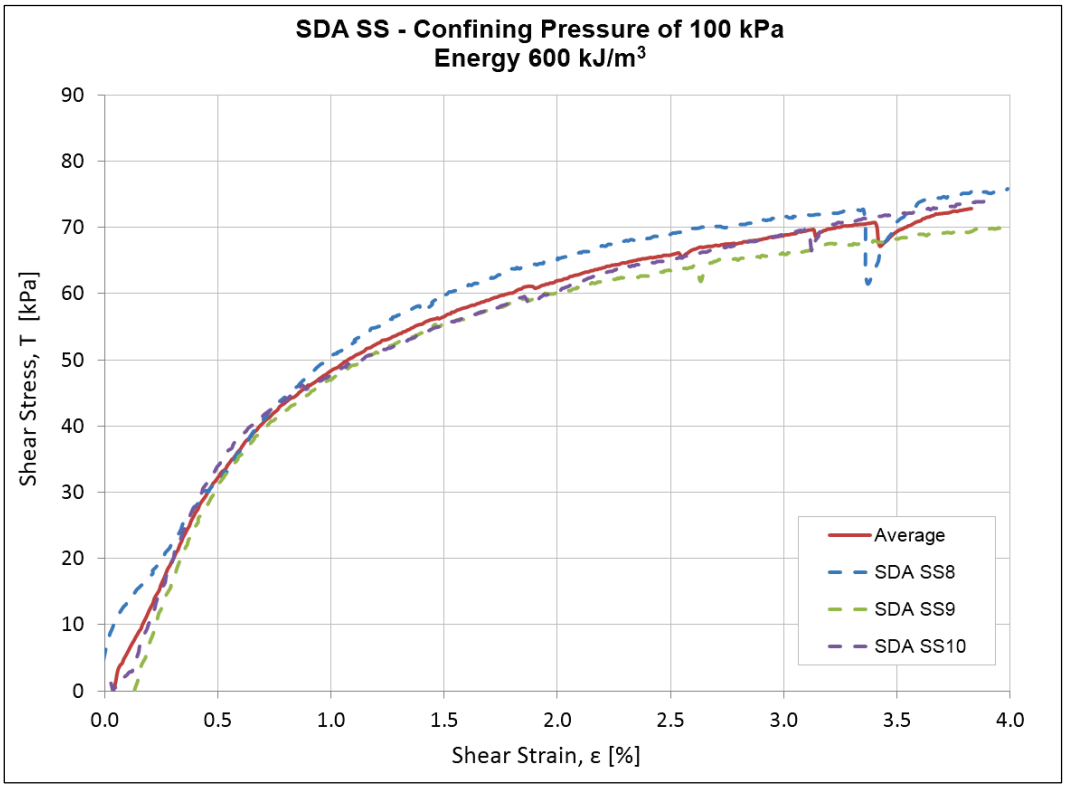
SDA SS - Confining Pressure of 100 kPa
Energy 600 kJ/m3
Shear Stress, T [kPa]
Shear Strain, ε [%]
Average
SDA SS8
SDA SS9
SDA SS10

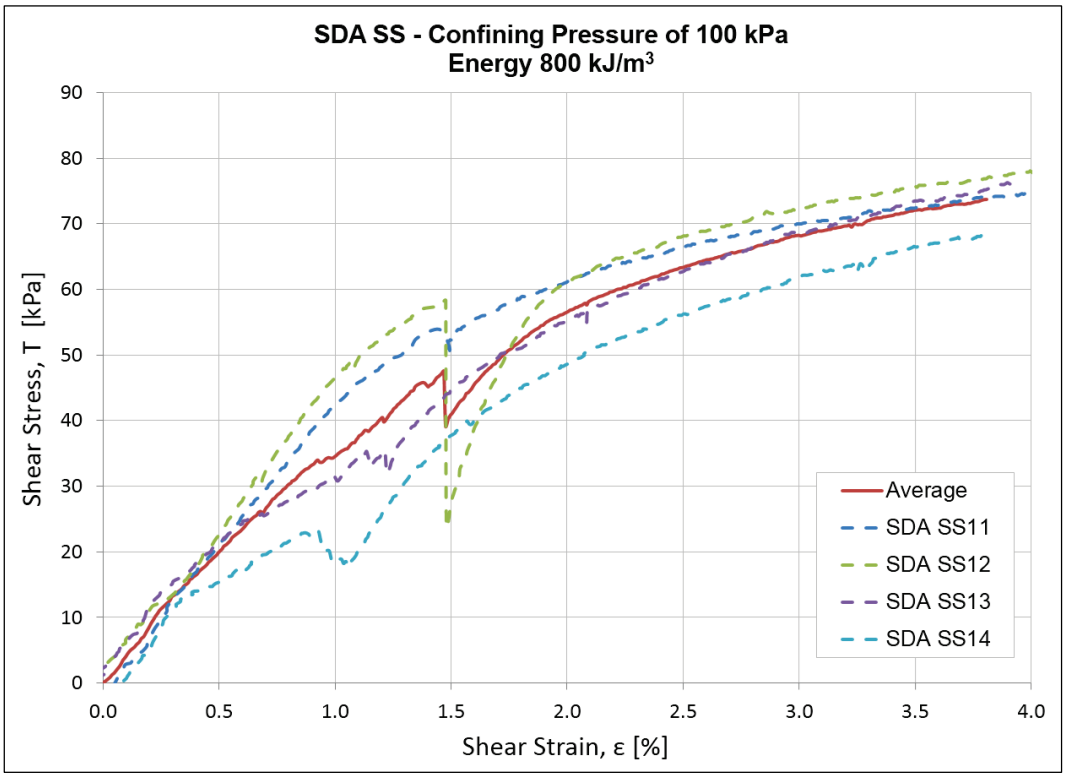
SDA SS - Confining Pressure of 100 kPa
Energy 800 kJ/m3
Shear Stress, T [kPa]
Shear Strain, ε [%]
Average
SDA SS11
SDA SS12
SDA SS13
SDA SS14

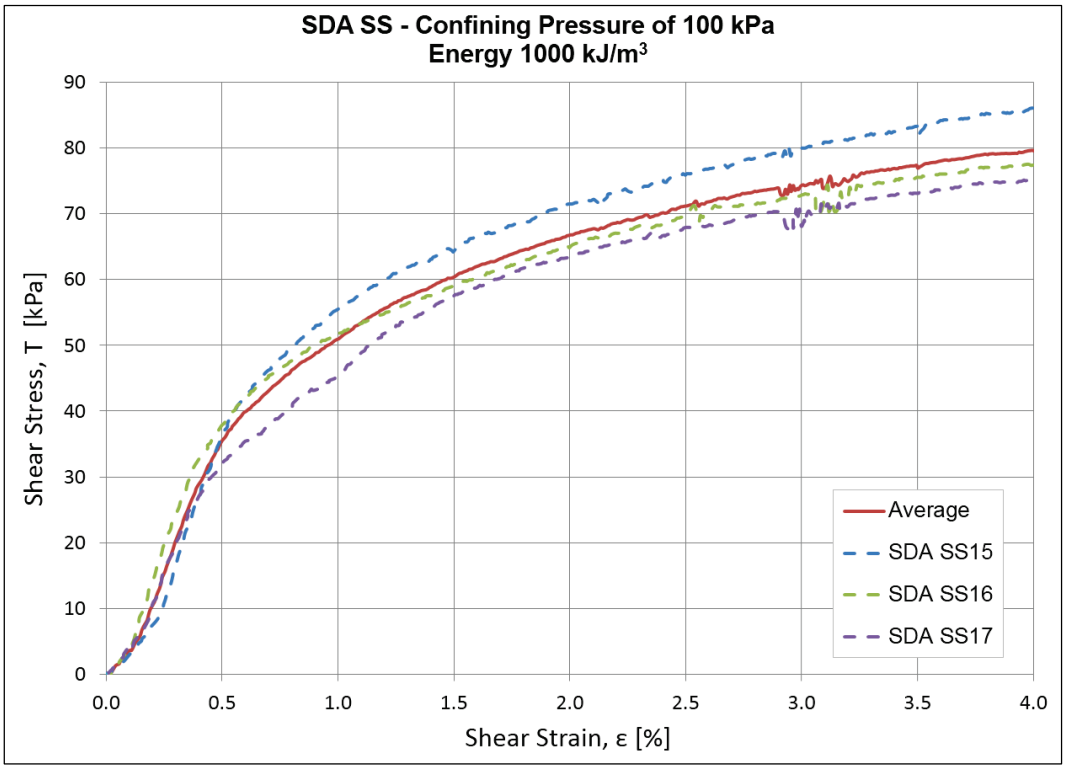
SDA SS - Confining Pressure of 100 kPa
Energy 1000 kJ/m3
Shear Stress, T [kPa]
Shear Strain, ε [%]
Average
SDA SS15
SDA SS16
SDA SS17

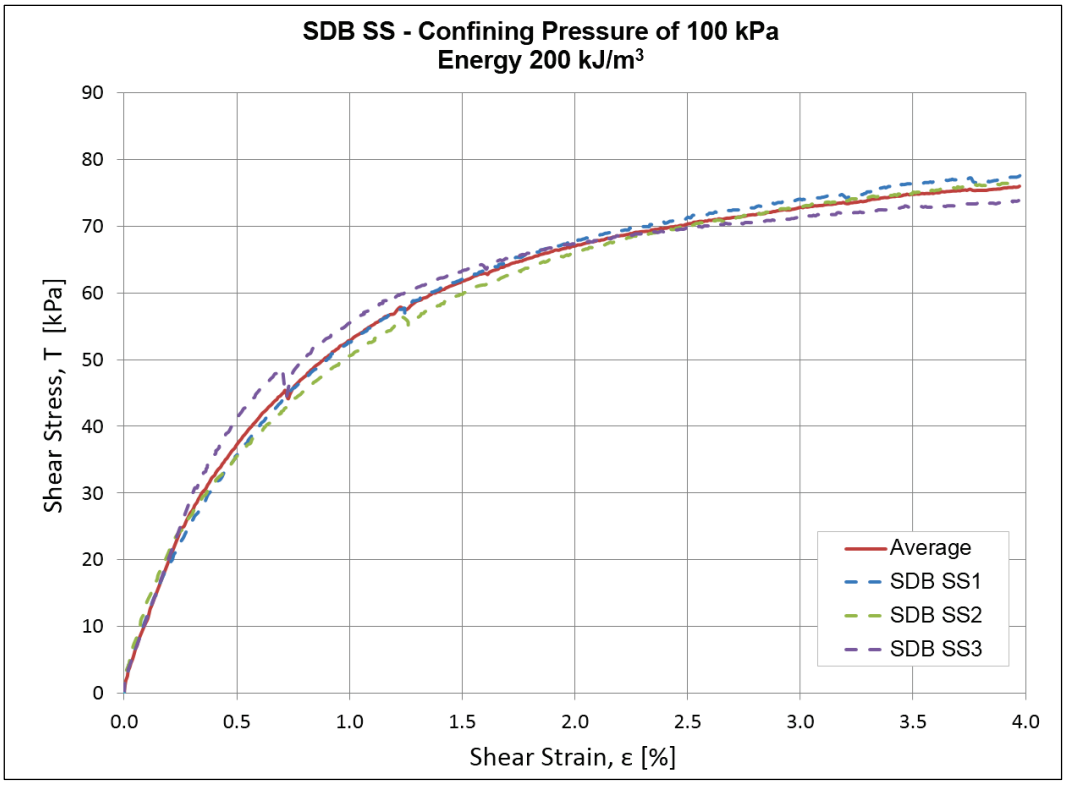
SDB SS - Confining Pressure of 100 kPa
Energy 200 kJ/m3
Shear Stress, T [kPa]
Shear Strain, ε [%]
Average
SDB SS1
SDB SS2
SDB SS3

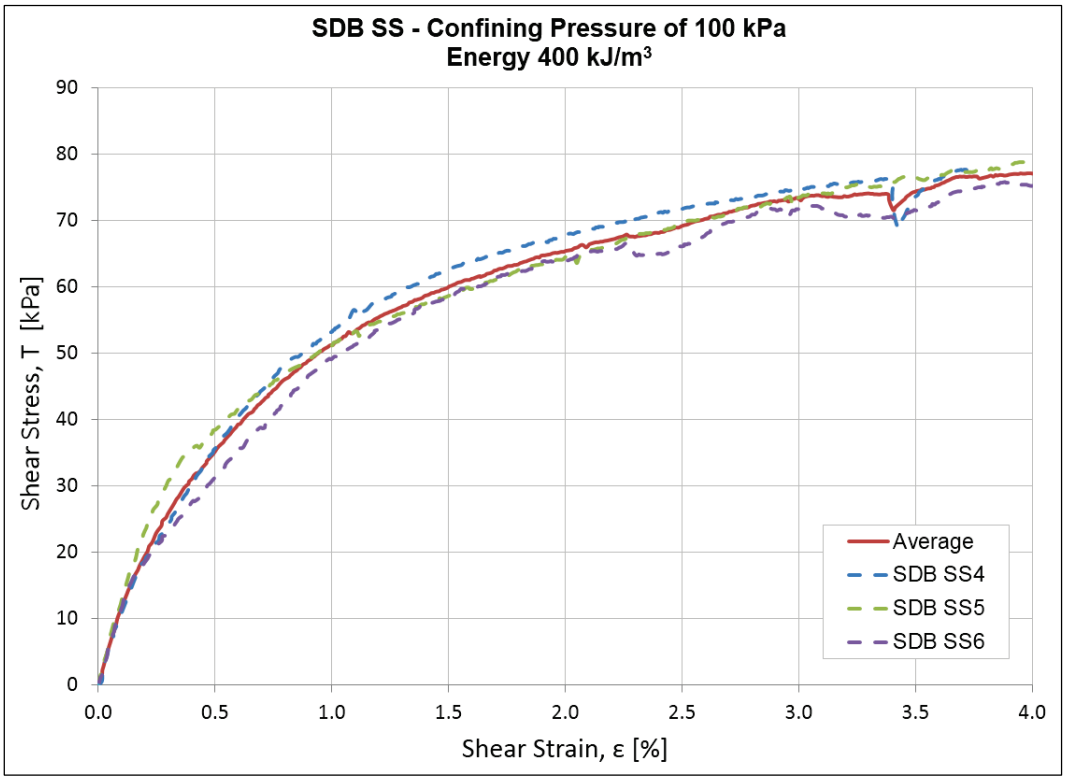
SDB SS - Confining Pressure of 100 kPa
Energy 400 kJ/m3
Shear Stress, T [kPa]
Shear Strain, ε [%]
Average
SDB SS4
SDB SS5
SDB SS6

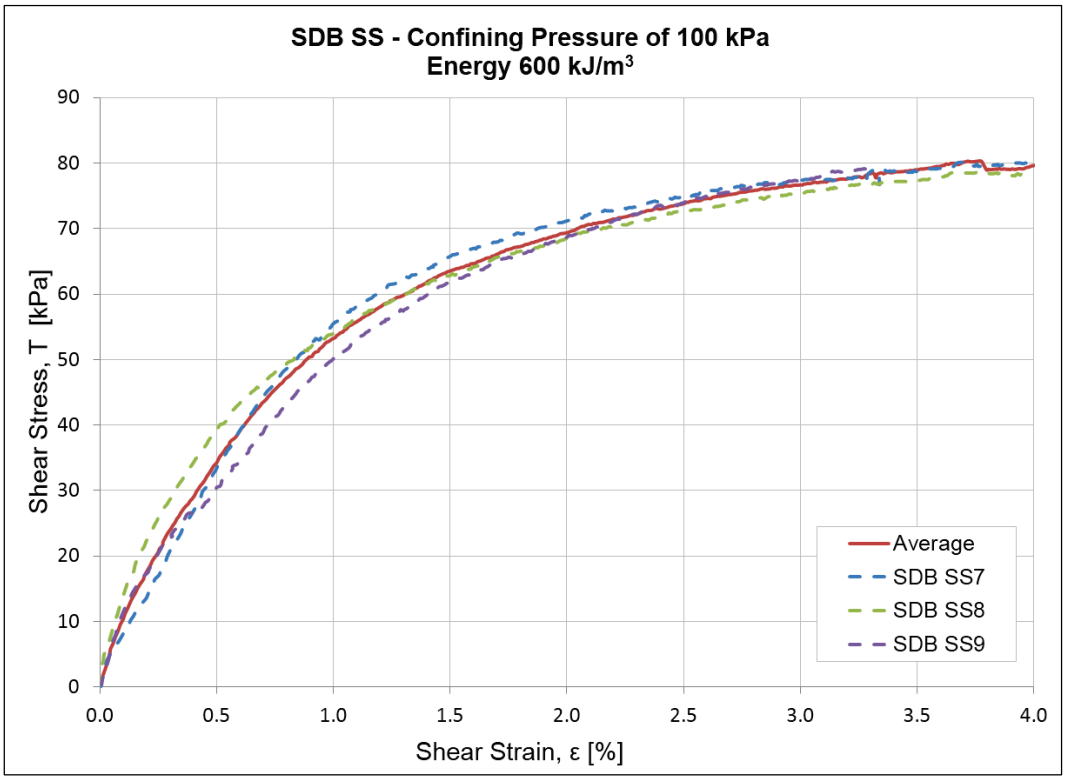
SDB SS - Confining Pressure of 100 kPa
Energy 600 kJ/m3
Shear Stress, T [kPa]
Shear Strain, ε [%]
Average
SDB SS7
SDB SS8
SDB SS9

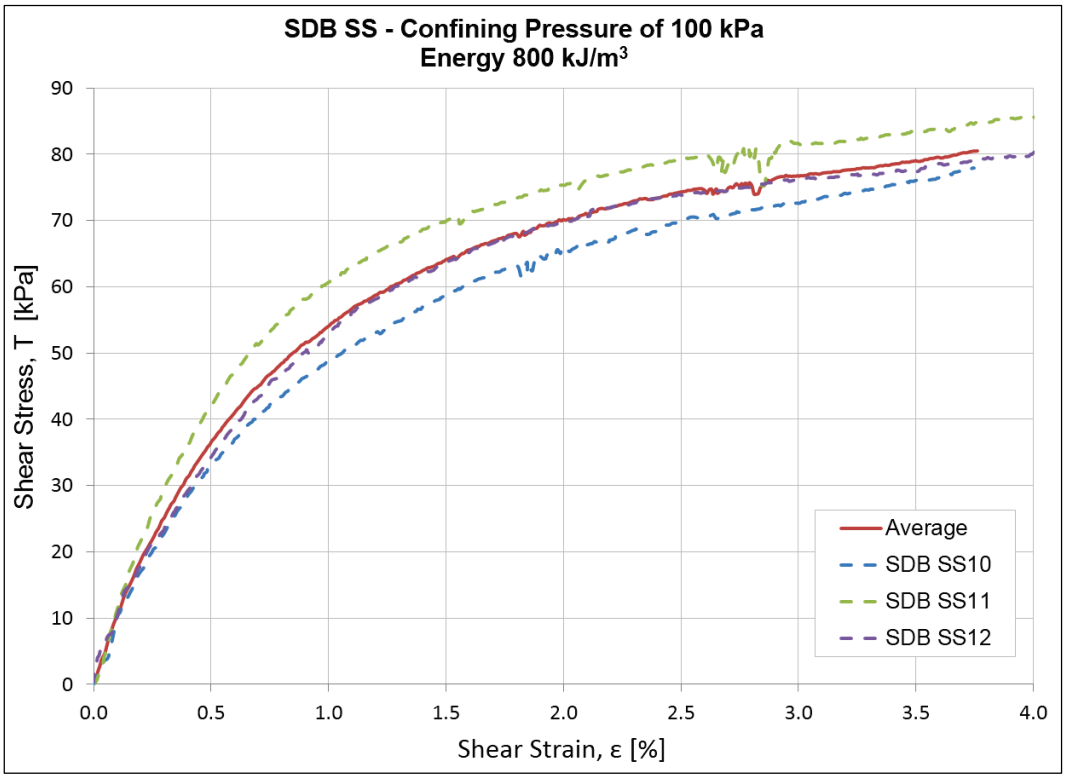
SDB SS - Confining Pressure of 100 kPa
Energy 800 kJ/m3
Shear Stress, T [kPa]
Shear Strain, ε [%]
Average
SDB SS10
SDB SS11
SDB SS12

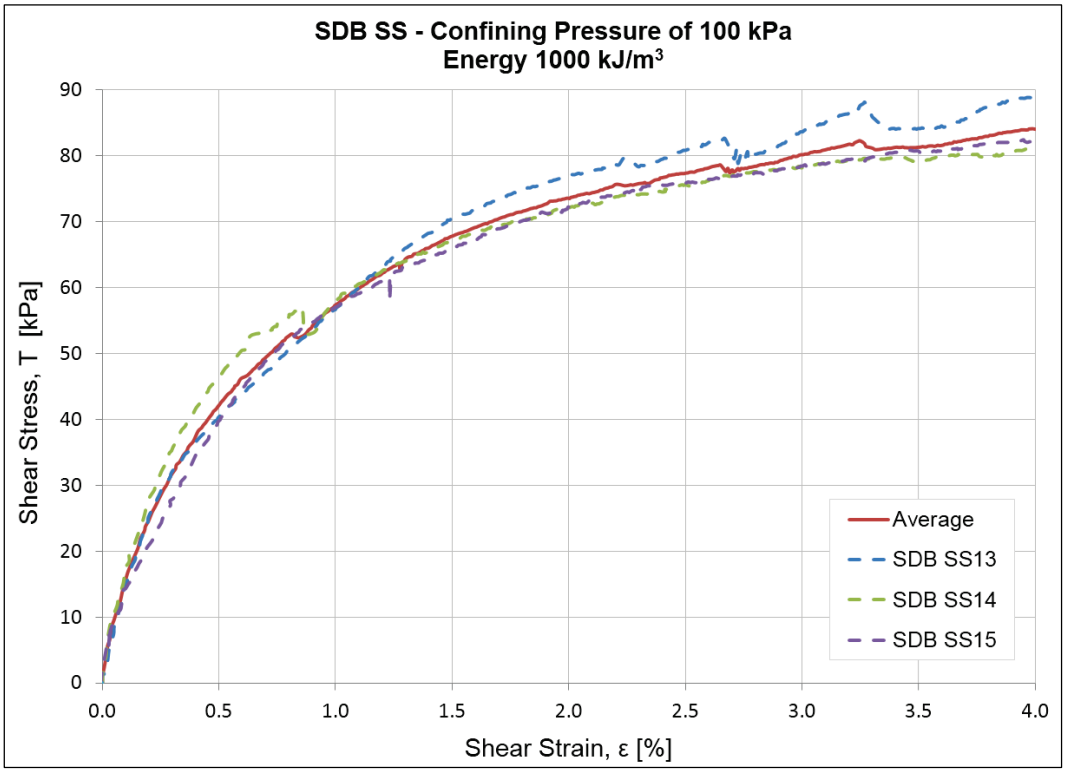
SDB SS - Confining Pressure of 100 kPa
Energy 1000 kJ/m3
Shear Stress, T [kPa]
Shear Strain, ε [%]
Average
SDB SS13
SDB SS14
SDB SS15

REPORT DOCUMENTATION PAGE

Form Approved
OMB No. 0704-0188

1. REPORT DATE (DD-MM-YYYY)	2. REPORT TYPE	3. DATES COVERED *(From - To)*
May 2016	Tech Report	

4. TITLE AND SUBTITLE

Protocol for Cohesionless Sample Preparation for Physical Experimentation

5a. CONTRACT NUMBER

5b. GRANT NUMBER

5c. PROGRAM ELEMENT NUMBER

6. AUTHOR(S)

Oliver-Denzil S. Taylor, Woodman W. Berry, Katherine E. Winters, Wesley R. Rowland, Mark D. Antwine, and Amy L. Cunningham

5d. PROJECT NUMBER

5e. TASK NUMBER

5f. WORK UNIT NUMBER

7. PERFORMING ORGANIZATION NAME(S) AND ADDRESS(ES)

Geotechnical and Structures Laboratory
U.S. Army Engineer Research and Development Center
3909 Halls Ferry Road
Vicksburg, MS 39180-6199

8. PERFORMING ORGANIZATION REPORT NUMBER

ERDC/GSL TR-16-11

9. SPONSORING / MONITORING AGENCY NAME(S) AND ADDRESS(ES)

U.S. Army Corps of Engineers

10. SPONSOR/MONITOR'S ACRONYM(S)

USACE

11. SPONSOR/MONITOR'S REPORT NUMBER(S)

12. DISTRIBUTION / AVAILABILITY STATEMENT

Approved for public release; distribution is unlimited.

13. SUPPLEMENTARY NOTES

13. ABSTRACT

The construction method and applied energy significantly influence sample behavior and strength characteristics; therefore, an energy-based sample reconstitution method is derived wherein uncertainties and laboratory scatter associated with soil fabric-behavior variance during sample preparation are mitigated. Samples of two different sands prepared using relative density methods resulted in different strengths at the point of failure; however, when prepared to the same normalized density, the same strength at the point of failure was observed. This suggests that normalized density could be a useful approach for laboratory investigation of cohesionless materials.

The procedure developed controls the three principal components of sample reconstitution, mass/type of material, quantity of water, and quantity/means of applied energy. All other properties, e.g., density, void ratio, etc., are products of sample preparation. Therefore, by controlling the three principal variables in sample preparation, high sample repeatability can be readily achieved wherein comparable analysis between different laboratory tests' results can be made by ensuring a comparable soil fabric prior to laboratory testing.

15. SUBJECT TERMS

Soil strength
Laboratory Testing Procedures
Generalized soil behavior

16. SECURITY CLASSIFICATION OF:			17. LIMITATION OF ABSTRACT	18. NUMBER OF PAGES	19a. NAME OF RESPONSIBLE PERSON
a. REPORT	b. ABSTRACT	c. THIS PAGE			19b. TELEPHONE NUMBER *(include area code)*
UNCLASSIFIED	UNCLASSIFIED	UNCLASSSIFIED		114	